The *Plasmodium falciparum* apicoplast cysteine desulfurase provides sulfur for both iron sulfur cluster assembly and tRNA modification

Russell P. Swift[†1,2+], Rubayet Elahi[†1,2], Krithika Rajaram[1,2], Hans B. Liu[1,2], Sean T. Prigge[1,2*]

[1] Department of Molecular Microbiology and Immunology, Johns Hopkins University, Baltimore, Maryland, United States of America

[2] The Johns Hopkins Malaria Research Institute, Baltimore, Maryland, United States of America

[+] Current address: Division of Biology and Biological Engineering, California Institute of Technology, Pasadena, California, United States of America

Contact information:

rswift@caltech.edu (RPS)

aelahi3@jhmi.edu (RE)

krajara1@jhu.edu (KR)

hliu82@jhmi.edu (HBL)

sprigge2@jhu.edu (STP)*

[†]Equal contribution

Correspondence should be addressed to **STP (sprigge2@jhu.edu)**

Abstract

Iron sulfur clusters (FeS) are ancient and ubiquitous protein cofactors that play fundamental roles in many aspects of cell biology. These cofactors cannot be scavenged or trafficked within a cell and thus must be synthesized in any subcellular compartment where they are required. We examined the FeS synthesis proteins found in the relict plastid organelle, called the apicoplast, of the human malaria parasite *Plasmodium falciparum.* Using a chemical bypass method, we deleted four of the FeS pathway proteins involved in sulfur acquisition and cluster assembly and demonstrated that they are all essential for parasite survival. However, the effect that these deletions had on the apicoplast organelle differed. Deletion of the cysteine desulfurase SufS led to disruption of the apicoplast organelle and loss of the organellar genome, whereas the other deletions did not affect organelle maintenance. Ultimately, we discovered that the requirement of SufS for organelle maintenance is not driven by its role in FeS biosynthesis, but rather, by its function in generating sulfur for use by MnmA, a tRNA modifying enzyme that we localized to the apicoplast. By complementing the activity of the parasite MnmA and SufS with a bacterial MnmA and its cognate cysteine desulfurase, we showed that the parasite SufS provides sulfur for both FeS biosynthesis and tRNA modification in the apicoplast. The dual role of parasite SufS is likely to be found in other plastid-containing organisms and highlights the central role of this enzyme in plastid biology.

Key words: *Plasmodium*, MnmA, SufS, iron-sulfur cluster, tRNA modification

Introduction

Malaria parasites contain a relict plastid organelle called the apicoplast that is required for its survival (Köhler et al., 1997; McFadden et al., 1996). The essentiality of this organelle and the unique biochemical pathways within, such as iron-sulfur cluster (FeS), and isoprenoid precursor biosynthetic pathways offers a potentially rich source of new antimalarial drug targets (Ellis et al., 2001; Jomaa et al., 1999; Seeber, 2002). Since its discovery, several inhibitors targeting these and other pathways have been described, supporting the assertion that this organelle represents a viable source of novel drug targets (Botté et al., 2012; Dahl & Rosenthal, 2008; Ke et al., 2014; Shears et al., 2015).

FeS serve as cofactors for an array of proteins across kingdoms and are involved in a myriad of biological functions, including electron transfer, sulfur donation, redox sensing, gene expression, and translation (Blahut et al., 2020; Przybyla-Toscano et al., 2018; Rouault, 2019). FeS cofactors are found in a variety of forms, most commonly in the rhombic 2Fe-2S or the cubic 4Fe-4S forms and are typically bound to proteins through covalent bonds with cysteine side chains (Beinert, 2000; Lill, 2009; Lu, 2018). In *Plasmodium falciparum*, FeS cofactors are formed within the apicoplast by the sulfur utilization factor pathway (SUF), for use by FeS-dependent proteins within the organelle (Charan et al., 2017; Gisselberg et al., 2013; Pala et al., 2018; Swift et al., 2022), while the mitochondrion houses the iron-sulfur cluster formation (ISC) pathway (Dellibovi-Ragheb et al., 2013; Gisselberg et al., 2013; Sadik et al., 2021). The ISC pathway generates FeS for use by FeS-dependent proteins within the mitochondrion, in addition to transferring a sulfur-containing moiety to the cytosolic iron-sulfur protein assembly (CIA) machinery for FeS generation and transfer to cytosolic and nuclear proteins (Dellibovi-Ragheb et al., 2013; Lill, 2009).

FeS biosynthesis is organized into three steps: sulfur acquisition, cluster assembly, and cluster transfer (**Figure 1A**). The SUF pathway employs the cysteine desulfurase (SufS) to mobilize sulfur from *L*-cysteine, resulting in a SufS-bound persulfide (Black & Santos, 2015b; Loiseau et al., 2003; Ollagnier-de-Choudens et al., 2003). SufE can enhance the cysteine desulfurase activity of SufS (Murthy et al., 2007; Outten et al., 2003; Pilon-Smits et al., 2002; Wollers et al., 2010; Ye et al., 2006) and is also able to accept sulfur atoms from SufS and transfer them to the $SufBC_2D$ FeS assembly complex (Saini et al., 2010). The $SufBC_2D$ complex serves as a scaffold for cluster formation with the ATPase activity of SufC being essential for the accumulation of iron from an unknown source (Bai et al., 2018; Hirabayashi et al., 2015; Saini et al., 2010). Subsequently, assembled clusters are transferred to downstream target apoproteins by transfer proteins such as SufA and NfuA (Chahal et al., 2009; Py et al., 2012).

In *Plasmodium*, all components of the SUF system are nuclear-encoded and trafficked to the apicoplast, except SufB, which is encoded by the ~35 kb apicoplast organellar genome (Wilson et al., 1996). The localization and activity of multiple components of the SUF pathway from *Plasmodium* spp. have been confirmed, including the cysteine desulfurase activity of SufS, its interaction with SufE and their localization to the apicoplast (Charan et al., 2014; Gisselberg et al., 2013). *In vitro* studies demonstrated the ATPase activity of SufC and complex formation by SufB, SufC, and SufD (Charan et al., 2017; Kumar et al., 2011). Similarly, the cluster transfer proteins SufA and NfuApi (an ortholog of NufA) were shown to bind FeS cofactors and transfer them to a model acceptor protein (Charan et al., 2017). In the apicoplast, the acceptor proteins are presumably IspG and IspH (enzymes in the isoprenoid precursor biosynthesis pathway), ferredoxin (Fd), LipA (lipoic acid synthase), and MiaB (tRNA methylthiotransferase) (Gisselberg et al., 2013; Ralph et al., 2004; Swift et al., 2022).

The SUF pathway appears to be required for the development of mosquito-stage parasites since conditional depletion of SufS blocks sporozoite maturation in *P. berghei* (Charan et al., 2017). The essentiality of SUF pathway proteins in blood-stage parasites is less clear since attempts to delete SufS, SufE, SufC, and SufD in *P. berghei*, were not successful (Haussig et al., 2014). SufA and NfuApi are individually dispensable in blood-stage *P. falciparum* and *P. berghei* (Haussig et al., 2013; Swift et al., 2022), but display synthetic lethality when both are deleted (Swift et al., 2022). These results and the toxic effects of a dominant-negative SufC mutant (Gisselberg et al., 2013) suggest that the SUF pathway is essential for blood-stage parasites.

Blood-stage *P. falciparum* parasites can survive without an apicoplast as long as sufficient isopentenyl pyrophosphate (IPP), a product of the apicoplast isoprenoid biosynthetic pathway, is exogenously provided to the parasite (Yeh & DeRisi, 2011). Since this discovery, the IPP chemical bypass system has been used to investigate the role and essentiality of numerous apicoplast-specific proteins and pathways, including the SUF pathway (Gisselberg et al., 2013) and FeS-dependent proteins in the apicoplast (Swift et al., 2022). In the work outlined here, we determined the roles of SUF pathway proteins in an apicoplast metabolic bypass parasite line containing a genetically-encoded isoprenoid precursor biosynthesis bypass pathway (Swift et al., 2020). We found that SUF proteins involved in sulfur acquisition (SufS and SufE) and cluster assembly (SufC and SufD) are all essential for parasite survival. Deletion of the cysteine desulfurase SufS, however, resulted in loss of the apicoplast organelle and its organellar genome whereas deletion of the other SUF proteins did not result in this phenotype. We hypothesized that SufS is also responsible for providing sulfur for use by MnmA, a tRNA modifying enzyme. We found that MnmA is located in the apicoplast and its loss results in the same apicoplast

disruption phenotype as observed for SufS. A series of complementation experiments using *Bacillus subtilis* MnmA and its cognate cysteine desulfurase demonstrated that SufS is required for both FeS synthesis and tRNA modification by MnmA, a novel paradigm that is likely to apply to other plastid-containing organisms.

Results

FeS assembly complex proteins SufC and SufD are essential for parasite survival, but are not required for apicoplast maintenance

In *P. falciparum,* FeS assembly is mediated by the $SufBC_2D$ complex (Charan et al., 2017). SufB is encoded by the apicoplast genome, while SufC (PF3D7_1413500) and SufD (PF3D7_1103400) are encoded by the nuclear genome. Dominant negative experiments with SufC suggested that the complex is essential for parasite survival (Gisselberg et al., 2013), however, gene deletions have not been successful in any malaria parasite species. To investigate the role of the FeS assembly complex, we targeted *sufC* and *sufD* in a metabolic bypass parasite line (PfMev) under continuous mevalonate supplementation (**Figure 1- figure supplement 1**). PfMev parasites synthesize IPP from exogenously provided mevalonate, enabling the disruption of genes encoding essential apicoplast-specific proteins (Swift et al., 2020). We confirmed the successful deletion of both *sufC* and *sufD* genes using genotyping PCR (**Figure 1B**). To determine whether the deletion of *sufC* or *sufD* resulted in apicoplast disruption, we attempted to amplify the apicoplast genome-encoded SufB from both the Δ*sufC* and Δ*sufD* parasite lines. Both parasite lines contained the *sufB* gene, indicating retention of the apicoplast genome (**Figure 1C**). We also observed intact apicoplast organelles, labeled by an apicoplast-localized super-folder green protein reporter (api-SFG) (Swift et al., 2020), in these parasite lines by live

epifluorescence microscopy (**Figure 1D**). Despite the presence of intact apicoplast organelles, both parasite lines required supplementation with exogenous mevalonate, demonstrating that SufC and SufD are essential proteins (**Figure 1E**). Taken together, these results show that SufC and SufD are essential for parasite survival, although neither protein is required for apicoplast maintenance.

Since SufC and SufD are essential, it is likely that the SufBC$_2$D complex is essential. Unfortunately, we cannot genetically modify the apicoplast genome-encoded SufB with any available experimental techniques, but we can simultaneously delete both SufC and SufD to remove the possibility of any type of complex forming with SufB. In *Escherichia coli*, pulldown assays demonstrated that different types of FeS assembly complexes can be formed (SufBC$_2$D and SufB$_2$C$_2$), which suggests that there may be some redundancy between complex proteins (Saini et al., 2010; Yuda et al., 2017). We generated Δ*sufC*/*sufD* double knockout parasites in the PfMev line, under continuous supplementation of mevalonate (**Figure 1F**). Consistent with the phenotypes of the Δ*sufC* and Δ*sufD* parasite lines, Δ*sufC*/*sufD* parasites were also found to have intact apicoplasts (**Figures 1G** and **1H**) and were dependent on exogenous mevalonate supplementation for survival (**Figure 1I**). Collectively, these findings demonstrate that while the FeS assembly complex is essential for parasite survival, it is not required for apicoplast maintenance.

SufS is required for apicoplast maintenance while SufE is not

We next investigated the sulfur acquisition steps of the SUF pathway upstream of SufC and SufD. In the apicoplast of *P. falciparum*, SufS (PF3D7_0716600), along with its partner SufE (PF3D7_0206100), mobilize sulfur from *L*-cysteine, with SufE transferring the sulfur to the

SufBC$_2$D complex (Gisselberg et al., 2013). The cysteine desulfurase activity of the *P. falciparum* SufS has been confirmed biochemically (Charan et al., 2014) and through complementation in *E. coli* (Gisselberg et al., 2013). It was also shown that the *P. falciparum* SufE enhances the cysteine desulfurase activity of SufS by up to ~17-fold in an *in vitro* biochemical assay (Charan et al., 2014). To disrupt sulfur acquisition in the SUF pathway, we generated deletions of both *sufS* and *sufE* in the PfMev line (**Figure 2A**). In Δ*sufE* parasites, the apicoplast remained intact as evidenced by successful PCR amplification of the *sufB* gene; however, we were unable to amplify this gene from Δ*sufS* parasites (**Figure 2B**). Consistent with the PCR results, we observed an intact apicoplast in Δ*sufE* parasites by live microscopy, while in Δ*sufS* parasites we observed multiple discrete api-SFG labeled vesicles - a hallmark of apicoplast organelle disruption (**Figure 2C**). Additionally, both parasite lines were dependent on mevalonate for survival (**Figure 2D**). Taken together, these results indicate that both SufE and SufS are required for parasite survival, but only SufS is required for apicoplast maintenance.

MnmA is essential for apicoplast maintenance

While SufS is required for apicoplast maintenance, none of the other SUF pathway proteins or any of the FeS-dependent proteins in the apicoplast are required for this process (Swift et al., 2022). This suggests that the reliance on sulfur for organelle maintenance is likely driven by a different sulfur-dependent pathway. Several biochemical pathways require sulfur, including those involved in the biosynthesis of thiamine, biotin, lipoic acid, molybdopterin, and thio-modifications of tRNA (Hidese et al., 2011; Leimkühler et al., 2017; Mihara & Esaki, 2002). Of these pathways, we found that the biosynthesis of lipoic acid and tRNA thio-modifications were the only ones that appeared to be present in *P. falciparum* with predicted

localization to the apicoplast (Ralph et al., 2004) (**Supplementary table 1**). In a recent study, we showed that lipoic acid synthesis is dispensable (Swift et al., 2022), however, tRNA thiolation has not been studied in malaria parasites. Based on sequence homology, *P. falciparum* parasites appear to contain several enzymes capable of catalyzing tRNA thiolation reactions, but only one appears to be a possible apicoplast protein. This protein (PF3D7_1019800) is currently annotated as a tRNA methyltransferase (Aurrecoechea et al., 2008), but it shares 30% sequence identity with an *E. coli* enzyme called MnmA (tRNA-specific 2-thiouridylase). MnmA inserts sulfur at carbon-2 (C2) of uridine at position 34 (s^2U34) of $tRNA^{Lys}_{UUU}$, $tRNA^{Glu}_{UUC}$, and $tRNA^{Gln}_{UUG}$ (Black & Santos, 2015a; Leimkühler et al., 2017; Shigi, 2014, 2018). *E. coli* MnmA receives sulfur from a series of five sulfur transfer proteins, TusA/B/C/D/E (Black & Santos, 2015a; Ikeuchi et al., 2006; Shigi, 2014), which ultimately acquire sulfur from the IscS cysteine desulfurase, but cannot obtain sulfur from the *E. coli* SufS (Bühning et al., 2017). It is not clear whether the apicoplast contains any orthologs of the Tus proteins, and the parasite IscS has already been localized to the mitochondrion instead of the apicoplast in malaria parasites (Gisselberg et al., 2013).

Multiple sequence alignments (MSA) of the putative *P. falciparum* MnmA (*Pf* MnmA) with orthologs from *E. coli*, *Bacillus subtilis,* and *Saccharomyces cerevisiae* reveal that it has a 421 aa N-terminal extension (**Figure 3- figure supplement 1**), which is predicted to contain an apicoplast transit peptide (Foth et al., 2003; Ralph et al., 2004). MSA also demonstrates that the *Pf* MnmA has conserved catalytic cysteines as well as a highly conserved ATP-binding PP-loop motif (SGGXDS) (**Figure 3A, Figure 3- figure supplement 1**) (Numata et al., 2006; Shigi et al., 2020). This PP-loop motif activates the C2 of nucleotide U34 of the target tRNA by adenylation in an ATP-dependent manner (Mueller, 2006; Numata et al., 2006). The first catalytic cysteine

receives sulfur generating an MnmA-persulfide, while the second catalytic cysteine releases the sulfur from the adduct and transfers it to the activated U34 (Čavužić & Liu, 2017; Shigi et al., 2020). Other pathogenic apicomplexans also seem to have an ortholog of MnmA with the conserved cysteines and domains (**Figure 3- figure supplement 2**) and a putative MnmA from *Toxoplasma gondii* has recently been described (Yang et al., 2022).

To validate the predicted apicoplast localization of the putative *Pf* MnmA, we generated a parasite line with two C-terminal FLAG tags in tandem appended to the endogenous *Pf*MnmA (**Figure 3B, 3C, 3D, Figure 3- figure supplement 3**). This parasite line, *mnmA*-flag, also contains an aptamer array in the 3' untranslated region (UTR) of *mnmA* to use with the TetR-DOZI system (Ganesan et al., 2016; Rajaram et al., 2020) for inducible control over protein production (**Figure 3B**). We showed that FLAG-tagged *Pf* MnmA colocalizes with the apicoplast marker protein, acyl carrier protein (ACP) by immunofluorescence (Manders' coefficient, M1 = 0.818, standard deviation = ± 0.187, n = 22), confirming *Pf* MnmA localization to the apicoplast (**Figure 3E**). We next attempted to knock down *Pf* MnmA using the TetR-DOZI system in the *mnmA*-flag parasite line (**Figure 3- figure supplement 4A**). We monitored parasite growth in control (aTc added) and knockdown (aTc removed) conditions over eight days. From day five onwards, the parasites showed a significant growth defect under the knockdown condition (**Figure 3F**). When parasites in the knockdown condition were supplemented with mevalonate (rescue), the parasites grew similarly to parasites under the control condition (**Figure 3F**), further confirming the apicoplast-associated activity of *Pf* MnmA. During the growth assay, we also assessed the apicoplast morphology of parasites under control and knockdown conditions via live epifluorescence microscopy every 48 h. We started to observe multiple discrete api-SFG labeled vesicles at day four following aTc removal (**Figure**

3G, Figure 3- figure supplement 4B), indicative of apicoplast disruption. At this point, about ~70% of parasites contained an intact apicoplast. By day eight, only ~25% of parasites had an intact apicoplast. Significant growth defects and disruption of the apicoplast following knock down of *Pf* MnmA suggests that *Pf* MnmA is essential for parasite survival and apicoplast maintenance. To further confirm these findings, we deleted the *mnmA* gene through Cas9-mediated genome editing in PfMev parasites under continuous mevalonate supplementation (**Figure 3I**). The deletion of *mnmA* resulted in apicoplast disruption, as evidenced by the inability to detect the apicoplast genome encoded *sufB* gene (**Figure 3J**) and the presence of multiple discrete vesicles labeled by api-SFG (**Figure 3K**). Additionally, Δ*mnmA* parasites were dependent on exogenous mevalonate supplementation for survival (**Figure 3L**). Overall, these results demonstrate that *Pf* MnmA is required for both apicoplast maintenance and parasite survival.

B. subtilis **MnmA and YrvO can be expressed in the** ***P. falciparum*** **apicoplast**

In *E. coli,* s^2U biosynthesis starts with the acquisition of sulfur from *L*-cysteine by the cysteine desulfurase IscS, which then relays the sulfur via the five proteins of the Tus system (TusABCDE) to MnmA (Black & Santos, 2015a; Ikeuchi et al., 2006; Outten et al., 2003; Shigi, 2014). MnmA then uses that sulfur to modify the target tRNAs at the U34 position in an ATP-dependent manner (Mueller, 2006; Numata et al., 2006). Not all bacteria contain IscS or the Tus system to relay sulfur to MnmA. In *B. subtilis* for example, a specialized cysteine desulfurase, YrvO, provides sulfur directly to MnmA (Black & Santos, 2015a). Although there are four different cysteine desulfurases (all four are SufS paralogs) present in *B. subtilis*, both *in vivo* complementation and *in vitro* biochemical studies established that YrvO is the sulfur source for

the s^2U modification catalyzed by MnmA (Black & Santos, 2015a). To clarify the role of MnmA in *P. falciparum,* we attempted to complement *Pf* MnmA with the *B. subtilis (Bs)* MnmA in $PfMev^{attB}$ parasites (Swift et al., 2021), through knock-in via mycobacteriophage integrase-mediated recombination (**Figure 4- figure supplement 1**) (Spalding et al., 2010). This parasite line is hereafter referred to as *bsmnmA*$^+$. *Bs* MnmA might not be functional in *P. falciparum* in the absence of its cognate cysteine desulfurase, *Bs* YrvO, as previously demonstrated in *E. coli* (Black & Santos, 2015a). To address this possibility, we also generated a parasite line expressing a *Bs* MnmA-YrvO fusion protein (*bsmnmA-yrvO*$^+$) (**Figure 4- figure supplement 2**) using the same knock-in method.

The *bsmnmA* and *bsmnmA-yrvO* expression cassettes encode a conditional localization domain (CLD) at the protein N-terminus for inducible control over protein localization (Roberts et al., 2019) and contain an mCherry tag on the C-terminus for visualization by live cell fluorescence (**Figure 4A**). The CLD directs the tagged protein to the apicoplast, but following the addition of the ligand, *Shield1*, the tagged protein is redirected to the parasitophorous vacuole (Roberts et al., 2019). An aptamer array was also included at the 3' UTR of these genes, for use with the TetR-DOZI system (Ganesan et al., 2016; Rajaram et al., 2020) (**Figure 4A**). We successfully generated both knock-in lines (**Figure 4B**). Live epifluorescence microscopy for both lines showed that *Bs* MnmA and *Bs* MnmA-YrvO proteins are trafficked to the apicoplast, as evidenced by the colocalization of the mCherry signal with the apicoplast api-SFG signal (**Figure 4C**; Manders' coefficient, M1 of *bsmnmA*$^+$ = 0.757, standard deviation = ± 0.155, n = 14; M1 of *bsmnmA-yrvO*$^+$ = 0.740, standard deviation = ± 0.142, n = 15). Taken together, these results show that *Bs* MnmA and *Bs* MnmA-YrvO can be expressed in the apicoplast of *P. falciparum*.

282

283 ***Bs* MnmA-YrvO fusion protein can complement the loss of parasite MnmA**

284 We used *bsmnmA-yrvO*$^{+}$ parasites to investigate whether loss of *Pf* MnmA can be
285 complemented by the *Bs* MnmA-YrvO fusion protein. We employed the same gRNA and repair
286 construct used in the experiment described in **Figure 3** to delete *pfmnmA* in the *bsmnmA-yrvO*$^{+}$
287 parasites. In repeated independent transfection experiments, we successfully generated *bsmnmA-*
288 *yrvO*$^{+}$ Δ*mnmA* parasites (**Figure 5A, Supplementary table 2**). These parasites were mevalonate
289 independent (**Figure 5B**) and possessed intact apicoplasts (**Figure 5C, 5D**), suggesting
290 complementation of *Pf* MnmA activity with *Bs* MnmA-YrvO fusion protein activity.
291 Additionally, the expression and apicoplast localization of *Bs* MnmA-YrvO fusion protein was
292 also confirmed via live epifluorescence microscopy (**Figure 5D**).
293 To demonstrate complementation of *Pf* MnmA with *Bs* MnmA-YrvO fusion protein more
294 conclusively, we next attempted to knock down *Bs* MnmA-YrvO in the *bsmnmA-yrvO*$^{+}$ Δ*mnmA*
295 parasite line by utilizing the TetR-DOZI and CLD systems (**Figure 4A**). We monitored the
296 growth of *bsmnmA-yrvO*$^{+}$ Δ*mnmA* parasites under permissive (aTc added, *Shield1* removed) and
297 non-permissive conditions (aTc removed, *Shield1* added) for eight days. Under the non-
298 permissive condition, the *bsmnmA-yrvO*$^{+}$ Δ*mnmA* parasites showed a significant growth defect
299 from day four onwards (**Figure 5E**). Live epifluorescence microscopy on day eight revealed that
300 parasites grown under the non-permissive condition exhibited a disrupted apicoplast phenotype
301 (**Figure 5F, Figure 5- figure supplement 1**). This conclusively shows that the *Bs* MnmA-YrvO
302 fusion protein is required to maintain the integrity of the apicoplast organelle after deletion of *Pf*
303 MnmA.

304

B. subtilis **MnmA alone can complement the loss of parasite MnmA**

The results from the previous section showed that *Pf* MnmA can be complemented by the *Bs* MnmA-YrvO fusion protein. However, whether *Bs* MnmA alone can complement *Pf* MnmA, without its cognate cysteine desulfurase, *Bs* YrvO, was not clear. To this end, we attempted to delete *pfmnmA* in the *bsmnmA*$^{+}$ parasite line. Only one out of four attempts to generate a *bsmnmA*$^{+}$ Δ*mnmA* line was successful (**Figure 6A, Supplementary table 2**). These parasites were mevalonate independent (**Figure 6B**) and possessed intact apicoplasts (**Figure 6C, 6D**), replicating the same phenotype as observed for *Bs* MnmA-YrvO complementation (**Figure 5B, 5C**, and **5D**). These results suggested that *Bs* MnmA alone was successful in complementing *Pf* MnmA. Next, we attempted to knock down *Bs* MnmA in the *bsmnmA*$^{+}$ Δ*mnmA* parasite line using the TetR-DOZI and CLD systems. We monitored the growth of *bsmnmA* $^{+}$ Δ*mnmA* parasites under permissive and non-permissive conditions for eight days. These parasites showed significant growth inhibition under the non-permissive condition from day three onwards (**Figure 6E**). Live epifluorescence microscopy of parasites cultured under the non-permissive condition showed a disrupted apicoplast on day eight (**Figure 6F, Figure 6- figure supplement 1**). These results conclusively show that complementation of Δ*mnmA* parasites with *Bs* MnmA can maintain the integrity of the organelle. These results also suggest that *Bs* MnmA is likely capable of receiving sulfur from the endogenous parasite cysteine desulfurase, SufS, which is critical for its function in the thiolation of target tRNAs.

P. falciparum **SufS provides sulfur for both FeS synthesis and tRNA thiolation**

Deletion of sufS resulted in a disrupted apicoplast mevalonate-dependent phenotype (**Figure 2**). However, deletion of other SUF pathway components (**Figure 1, 2)** resulted in an

intact apicoplast mevalonate-dependent phenotype. These findings led us to hypothesize that mevalonate-dependence results from loss of FeS cofactors needed for isoprenoid synthesis (Swift et al., 2022), while apicoplast disruption results from loss of sulfur needed for tRNA modification. By successfully complementing *Pf* MnmA with *Bs* MnmA we demonstrated that *Pf* MnmA has the same enzymatic activity as the well-characterized bacterial enzyme, and that this activity is essential for parasite survival and apicoplast maintenance (**Figure 5, 6**). However, the complementation experiments in **Figures 5** and **6** did not provide any direct evidence that *Pf* MnmA is reliant on sulfur generated from the endogenous SufS for use in tRNA modification. To probe whether SufS provides sulfur to *Pf* MnmA, we used the *bsmnmA-yrvO*$^{+}$ parasite line. In these parasites, we attempted to delete *sufS* with continuous supplementation of mevalonate. We expected to obtain a parasite line with intact apicoplasts and a mevalonate-dependent phenotype (**Figure 7A**), which would suggest that sulfur acquired by *Bs* YrvO is only transferred to MnmA but not to the components of the parasite SUF pathway. We were successful in generating the *bsmnmA-yrvO*$^{+}$ Δ*sufS* parasite line in the presence of mevalonate (**Figure 7B**). As anticipated, these parasites retained intact apicoplasts as confirmed by both PCR and live epifluorescence microscopy (**Figure 7C, 7D**). These parasites rely on mevalonate for growth (**Figure 7E**). Collectively, these results suggest that the parasite SufS provides sulfur for both the SUF pathway and MnmA-mediated tRNA modifications.

Discussion

A recent survey of *P. falciparum* apicoplast proteins found that five proteins are known or predicted to rely on FeS cofactors (Swift et al., 2022). Three of these proteins were found to be essential for the growth of blood-stage parasites due to their roles in supporting the MEP

isoprenoid precursor pathway (Akuh et al., 2022; Swift et al., 2022). These essential proteins could be deleted in PfMev parasites without a noticeable growth defect or loss of the apicoplast organelle as long as the cultures were supplemented with mevalonate. These results implied that the SUF pathway of FeS synthesis would also be essential for parasite growth and that deletion of SUF pathway proteins would not result in loss of the apicoplast. In general, this has proven to be the case with the deletion of SufE, SufC, and SufD. Deletion of SufS, however, led to apicoplast disruption and indicated that this enzyme plays another essential role in parasite biology. Similar to what we observed in *P. falciparum*, deletion of SufS in *T. gondii* also leads to loss of the apicoplast organelle and parasite death (Pamukcu et al., 2021). Conditional deletion of SufS in the murine malaria parasite *P. berghei* demonstrated that this enzyme is essential for the development of mosquito-stage parasites, although the status of the apicoplast was not reported in this study (Charan et al., 2017). Taken together, these studies suggest that SufS plays a central role in apicoplast biology in other parasite species and other stages of parasite development.

The phenotype of the SufC deletion line contrasts with a previous study using a dominant negative SufC mutant. *In vitro* studies showed that *P. falciparum* SufC participates in a $SufBC_2D$ complex that hydrolyzes ATP and can form FeS cofactors (Charan et al., 2017; Kumar et al., 2011). The ATPase activity of SufC is thought to provide energy to drive conformation changes to the entire $SufBC_2D$ complex required for iron binding and FeS assembly (Bai et al., 2018; Hirabayashi et al., 2015; Yuda et al., 2017). In *E. coli*, SufC and SufD are essential for SUF pathway activity and acquire iron for FeS assembly; loss of either protein results in reduced iron content in the complex (Saini et al., 2010) and the same may be true for the parasite proteins. We generated Δ*sufC*, Δ*sufD*, and Δ*sufC*/*sufD* lines and found that sufC and sufD are essential for parasite survival, but we did not observe an apicoplast disruption phenotype in these deletion

lines (**Figure 1**). This finding conflicted with previous results showing that expression of a SufC mutant (K140A) lacking ATPase activity functions as a dominant negative and leads to disruption of the apicoplast (Gisselberg et al., 2013). Several factors could be responsible for the apicoplast-disruption phenotype resulting from expression of SufC (K140A). In other organisms, the intact $SufBC_2D$ complex enhances SufS desulfurase activity (Hu, Kato, et al., 2017; Hu, Page, et al., 2017; Outten et al., 2003; Wollers et al., 2010) potentially leading to accumulation of toxic S^{-2} if non-functional SufC (K140A) blocks further sulfur utilization. Alternatively, dominant negative SufC could lead to dysfunctional iron homeostasis. ATP binding to SufC elicits a conformational change in the $SufBC_2D$ complex, exposing sites required for iron binding and enabling the formation of nascent clusters (Bai et al., 2018; Hirabayashi et al., 2015; Yuda et al., 2017). The dominant negative mutant SufC should be able to bind ATP, but not hydrolyze it, locking the $SufBC_2D$ complex in an open position and exposing these sites to the environment. Exposure and release of iron could lead to oxidative damage and loss of the organelle.

Gene deletion studies exposed different roles for the two proteins (SufE and SufS) involved in sulfur acquisition. We found that both SufE and SufS are required for parasite survival, however, only SufS is required for apicoplast maintenance (**Figure 2, 8A, 8B, 8C**). These phenotypes make sense if SufE is required for FeS synthesis but not for tRNA thiolation. In other organisms, SufE has been shown to be capable of enhancing the cysteine desulfurase activity of SufS (Murthy et al., 2007; Outten et al., 2003; Pilon-Smits et al., 2002; Wollers et al., 2010; Ye et al., 2006) and this appears to be the case with the *P. falciparum* proteins with ~17-fold rate enhancement reported (Charan et al., 2014). SufE proteins also facilitate the transfer of sulfur to the $SufBC_2D$ complex, but SufS enzymes can often transfer sulfur directly to the

complex as is presumably the case in organisms lacking SufE (Huet et al., 2005). The requirement for SufE in *P. falciparum* suggests that either SufS desulfurase activity or SufS sulfur transfer activity (to the $SufBC_2D$ complex) is too low in the absence of SufE to support FeS synthesis. The fact that SufE is not required for apicoplast maintenance (and presumably tRNA thiolation) further suggests that SufS desulfurase activity in the absence of SufE is adequate for tRNA thiolation and that SufS may transfer sulfur directly to MnmA.

A recent study in the asexual blood-stage of *P. falciparum* reported 28 different tRNA modifications, including s^2U and mcm^5s^2U (Ng et al., 2018). The s^2U modification of tRNA is ubiquitous and critical for a number of biological functions related to protein translation as demonstrated in other organisms, including the recognition of wobble codons (Urbonavičius et al., 2001), tRNA ribosome binding (Ashraf et al., 1999), reading frame maintenance (Black & Santos, 2015a), and the reduction of +1 and +2 frameshifts (Black & Santos, 2015a; Urbonavičius et al., 2001). To investigate the biological function of *P. falciparum* MnmA, we complemented parasites lacking endogenous MnmA by expressing the well-studied MnmA homolog from *B. subtillis* (*Bs* MnmA) with and without its cognate cysteine desulfurase (*Bs* YrvO) partner in the apicoplast. The role of *Bs* MnmA in the s^2U modification of target tRNAs has been demonstrated by both genetic and biochemical analysis (Black & Santos, 2015a). *Bs* MnmA successfully complemented loss of *P. falciparum* MnmA and resulted in parasites that did not require mevalonate for survival. Subsequent knock down of the complemented *Bs* MnmA resulted in disruption of the apicoplast, demonstrating that MnmA activity and the s^2U tRNA modification are essential for apicoplast maintenance and parasite survival (**Figure 5, 6, 8E, 8F**). These results also establish the biological function of *Plasmodium* MnmA in the thiolation of target tRNAs in the apicoplast. Loss of tRNA thiolation presumably disrupts the translation of

420 essential proteins encoded by the apicoplast genome, ultimately causing the disruption and loss
421 of the organelle.

422 For our complementation experiments, we needed multiple attempts to generate a single
423 *bsmnmA*$^{+}$ Δ*mnmA* line while every attempt to generate *bsmnmA-yrvO*$^{+}$ Δ*mnmA* parasites was
424 successful (**Supplementary table 2**). This is perhaps because the parasite SufS is not very
425 efficient in providing sulfur to *Bs* MnmA (**Figure 8E**). By contrast, *Bs* YrvO can effectively
426 transfer sulfur to *Bs* MnmA in *bsmnmA-yrvO*$^{+}$ Δ*mnmA* parasites (**Figure 8F**). Despite our
427 difficulties in obtaining Δ*mnmA* parasites in the *bsmnmA*$^{+}$ background, we did not observe a
428 statistically significant growth difference between *bsmnmA*$^{+}$ Δ*mnmA* and *bsmnmA-yrvO*$^{+}$ Δ*mnmA*
429 parasite lines (**Figure 6- figure supplement 2**). The specificity of interaction between *Bs* MnmA
430 and desulfurase partners makes sense considering the specificity observed in *B. subtilis*. Even
431 though *B. subtilis* produces four SufS paralogs, only YrvO appears to function with *Bs* MnmA
432 (Black & Santos, 2015a) and both proteins are essential for bacterial growth (Kobayashi et al.,
433 2003).

434 To show that parasite MnmA receives sulfur from the endogenous cysteine desulfurase,
435 SufS, we deleted SufS in the *bsmnmA-yrvO*$^{+}$ line. This deletion resulted in parasites that were
436 reliant on mevalonate for survival but contained an intact apicoplast (**Figure 7**). Mevalonate
437 dependency in *bsmnmA-yrvO*$^{+}$ Δ*sufS* parasites can be explained by the likely lack of interaction
438 between *Bs* YrvO and other SUF pathway proteins. If *Bs* YrvO cannot transfer sulfur to SufE or
439 to the SufBC$_2$D complex directly, FeS cofactors will not be synthesized in the apicoplast. Recent
440 results show that lack of FeS cofactors generated by the SUF pathway prevents essential
441 isoprenoid precursor synthesis leading to parasite death in absence of an exogenous source of
442 isoprenoid precursors (Swift et al., 2022). Presumably, the apicoplast remains intact in the

443 *bsmnmA-yrvO*$^{+}$ Δ*sufS* line because *Bs* YrvO and *Bs* MnmA (and *Pf* MnmA) function together to
444 produce essential tRNA s^2U modifications (**Figure 7, 8G**). Taken together, these results show
445 that the parasite SufS provides sulfur for both FeS biosynthesis and the MnmA-mediated s^2U
446 modification of target tRNAs in the parasite apicoplast, both of which are required for parasite
447 survival (**Figure 8 A, C**). Although loss of FeS biosynthesis is not required for apicoplast
448 maintenance, tRNA modification is. Thus, deletion of SufS results in loss of FeS biosynthesis
449 and tRNA modification in the apicoplast, culminating in apicoplast disruption and parasite death
450 (**Figure 8H**).

451 The dual activity of *P. falciparum* SufS and its direct interaction with MnmA are not
452 typical features of SufS desulfurases. In *E. coli*, IscS is required for MnmA-mediated tRNA
453 thiolation and the role of SufS is confined exclusively to FeS biosynthesis (Bühning et al., 2017).
454 Thiolation of tRNA in *E. coli* is also an indirect process involving the five proteins of the Tus
455 system to transfer sulfur from the desulfurase to MnmA (Black & Santos, 2015a; Ikeuchi et al.,
456 2006; Shigi, 2014, 2018). Similarly, the cysteine desulfurase of *S. cerevisiae* (called Nfs1) is an
457 IscS homolog and accomplishes the same feat through four sulfur transferases (Nakai et al.,
458 2004; Shigi, 2018). While we cannot rule out the possible presence of intermediate sulfur
459 transferases in *P. falciparum*, homology searches failed to detect them. The tRNA thiolation
460 mechanism found in *B. subtilis* is most similar to what we have observed in *P. falciparum*; a
461 SufS paralog (YrvO) transfers sulfur directly to MnmA (Black & Santos, 2015a). The unique
462 feature of the *P. falciparum* system is that SufS has dual activity and is essential for two
463 metabolic pathways, while *B. subtilis* YrvO is dedicated to tRNA thiolation (Black & Santos,
464 2015a).

In this work and a previous publication (Swift et al., 2022) we defined the roles of the five known FeS-dependent proteins and six of the seven proteins involved in the SUF FeS synthesis pathway (SufB was not studied because we do not have a way to target the apicoplast genome). The combined information supports a model in which SufS is needed for both FeS biosynthesis and tRNA thiolation in the apicoplast. In blood-stage parasites, the SUF pathway is required solely for providing FeS cofactors to enable isoprenoid precursor synthesis, but FeS cofactors should also be required for lipoic acid and fatty acid biosynthesis in mosquito-stage and liver-stage parasites (Akuh et al., 2022; Shears et al., 2015). All stages of parasite development may require tRNA modifications due to the role they play in codon recognition (Urbonavičius et al., 2001) which may have elevated importance in the apicoplast due to the unusually small number of only 24 tRNAs (Wilson et al., 1996). The dual roles of SufS may be a feature of the apicoplasts found in other pathogens such as *T. gondii*. Deletion of *T. gondii* SufS or MnmA results in apicoplast defects and parasite death (Pamukcu et al., 2021; Yang et al., 2022). Overall, the work presented here reveals a novel metabolic paradigm and exposes new vulnerabilities in malaria parasites that may extend to other related apicomplexan parasites.

Experimental procedures

P. falciparum parental parasite lines

For generating the knockout and knock-in lines we used two different parental lines: PfMev (Swift et al., 2020) and PfMev^{attB} (Swift et al., 2021). Both parasite lines can generate isoprenoid precursors from an engineered cytosolic mevalonate-dependent pathway (Swift et al., 2020; Swift et al., 2021). In the presence of mevalonate, these parasite lines can replicate normally even in the absence of an intact apicoplast. The PfMev^{attB} parasite line has an attB site

in the P230p locus (Swift et al., 2021). In both parasite lines, the apicoplast is labeled by the super-folder green fluorescent protein (api-SFG) which has been codon-modified for expression in *P. falciparum* (Roberts et al., 2019). The api-SFG reporter contains the signal and transit peptide (first 55 amino acids) of the *P. falciparum* acyl-carrier protein (ACP) appended to the N-terminal end of SFG to direct trafficking to the apicoplast (Swift et al., 2020; Swift et al., 2021).

P. falciparum culture

Asexual stage *P. falciparum* parasites were cultured in human O^+ erythrocytes at 2% hematocrit in RPMI 1640 medium with *L*-glutamine (USBiological, MA, USA). The RPMI 1640 medium was supplemented with 20 mM HEPES, 0.2% sodium bicarbonate, 12.5 µg/mL hypoxanthine, 5 g/L Albumax II (Life Technologies, CA, USA), and 25 µg/mL gentamicin. Cultures were incubated at 37°C and maintained in 25 cm^2 gassed flasks (94% N_2, 3% O_2, and 3% CO_2).

Generation of _P. falciparum_ plasmid constructs for gene deletion

We employed Cas9-mediated gene editing to delete genes of interest (**Figure 1- figure supplement 1**). For gene deletion, the pRS repair plasmid (Swift et al., 2020) in combination with the pUF1-Cas9 plasmid (Ghorbal et al., 2014) were used. Alternatively, the pRSng (Swift et al., 2020) or pRSng(BSD) repair plasmid (Swift et al., 2022) in combination with the pCasG-LacZ plasmid (Rajaram et al., 2020) were used for targeted gene deletion. The plasmids used for generation of the gene deletion lines are listed in **Supplementary table 3**.

To generate deletion constructs, ~300-500 bp homology arms (HA) were amplified from *P. falciparum* NF54 genomic DNA with HA1 and HA2 forward and reverse primers

511 (**Supplementary table 4**). The HA1 and HA2 amplicons were inserted into the *NotI* and
512 *NgoMIV* restriction sites, respectively, of the repair plasmids by In-Fusion (Clontech
513 Laboratories, CA, USA) ligation independent cloning (LIC). The gRNA sequences
514 (**Supplementary table 4)** were inserted as annealed oligonucleotides into the *BsaI* sites of
515 pCasG-LacZ plasmids by LIC to generate pCasG-GOI plasmid or into the pRS plasmid. All the
516 plasmids were sequenced to confirm sequence fidelity. All the restriction enzymes used in this
517 section were sourced from New England Biolabs Inc, MA, USA.
518
519 **Generation of plasmid constructs for knockdown and epitope tagging of *Pf* MnmA**
520 To generate the knockdown construct of the endogenous *Pf* MnmA, we created the pKD-
521 *mnmA*-2xFLAG-10xapt plasmid. This plasmid also allowed us to tag *Pf* MnmA C-terminally
522 with 2xFLAG. To make this plasmid, ~ 300-400 bp HA1 and HA2 of the *pfmnmA* gene were
523 PCR amplified with MnmAKD.HA1F + MnmAKD.HA1R and MnmAKD.HA2F +
524 MnmAKD.HA2R, respectively from *P. falciparum* NF54 genomic DNA, (**Supplementary table**
525 **4**). These HA PCR fragments were fused together to generate a combined HA2-HA1 fragment
526 with MnmAKD.HA2F and MnmAKD.HA1R in an additional PCR step. The HA2 and HA1
527 fragments in the combined HA2-HA1 fragment are separated by two *EcoRV* sites to facilitate
528 linearization of the plasmid. The HA2-HA1 fragment was inserted into the *AscI* and *AatII* sites of
529 the pKD-2xFLAG-10xapt plasmid to generate the pKD-*mnmA*-2xFLAG-10xapt plasmid by LIC.
530 The pKD-2xFLAG-10xapt plasmid was generated by replacing the 3xHA tag of the pKD
531 plasmid reported elsewhere (Rajaram et al., 2020). To replace the 3xHA tag with the 2xFLAG
532 tag, the FLAG tag sequence was synthesized as oligonucleotides (**Supplementary table 4**),
533 annealed, and then inserted into the *AatII* and *PspMOI* sites of the pKD plasmid. Prior to

534 transfection, the pKD-*mnmA*-2xFLAG-10xapt plasmid was linearized with *EcoRV*. The
535 MnmA.KD gRNA sequence (**Supplementary table 4)** was inserted as annealed oligonucleotides
536 into the *BsaI* sites of the pCasG-LacZ plasmid by LIC to generate the pCasG-*mnmA*KD plasmid.
537
538 **Generation of plasmid constructs for *B. subtilis mnmA* and *mnmA-yrvO* knock-in**
539 To generate the *bsmnmA* knock-in plasmid, we amplified the *bsmnmA* gene from *B.*
540 *subtilis* genomic DNA with the following primer pair: MnmA.BspEI.InF.F and
541 MnmA.BsiWI.InF.R. The amplified product was used to replace the *Ec*DPCK locus from the
542 pCLD-*Ec*DPCK-mCherry-apt (Swift et al., 2021) plasmid using the *BspEI* and *BsiWI* cloning
543 sites to generate pCLD-*bsmnmA*-mCherry-apt. For enhanced stability of the aptamer system, we
544 replaced the existing 10x-aptamer array (apt) with a redesigned 10x-aptamer array (10xapt) that
545 prevents aptamer loss (Rajaram et al., 2020). First, the 10xapt DNA was amplified with the
546 MY.Apt.PspOMI.F and MY.Apt.XmaI.R primer pair from a pKD plasmid (Rajaram et al.,
547 2020). The apt locus was removed from the pCLD-*bsmnmA*-mCherry-apt plasmid by digestion
548 with *PspOMI* and *XmaI*, followed by insertion of the 10xapt PCR product using the same cloning
549 sites by LIC resulting in pCLD-*bsmnmA*-mCherry-10xapt plasmid. The fidelity of the *Bs mnmA*
550 and 10xapt sequence of the pCLD-*bsmnmA*-mCherry-10xapt was confirmed by sequencing.
551 In *B. subtilis*, the genes *mnmA* and *yrvO* are 31 bp apart from each other and are co-
552 transcribed (Black & Santos, 2015a). Hence, we decided to generate the pCLD-*bsmnmA-yrvO*-
553 mCherry-10xapt plasmid with *bsmnmA* and *bsyrvO* genes fused in one cassette with a 15 bp
554 linker. To make the fusion gene, we first amplified *mnmA* with MnmA.BspEI.InF.F and
555 MnmA.Link.R, and *yrvO* with YrvO.Link.F and YrvO.BsiWI.InF.R primer pairs. These two
556 PCR products were stitched together by PCR amplification (*bsmnmA-yrvO,* **Figure 4- figure**

557 **supplement 2**) using the primer pair MnmA.BspEI.InF.F and YrvO.BsiWI.InF.R. The *bsmnmA-*
558 *yrvO* fragment was inserted into the pCLD-*bsmnmA*-mCherry-10xapt plasmid, previously
559 digested with *BspEI* and *BsiWI*, using LIC. The resulting plasmid, pCLD-*bsmnmA-yrvO-*
560 mCherry-10xapt was sequenced to confirm the sequence fidelity of *bsmnmA-yrvO*. All the
561 primers are listed in **Supplementary table 4** and all the restriction enzymes were purchased
562 from New England Biolabs Inc, MA, USA.
563
564 **Parasite transfections**
565 To generate the Δ*sufC,* Δ*sufD*, Δ*sufE,* Δ*sufS*, and Δ*mnmA* transgenic lines, PfMev
566 parasites were transfected with the respective plasmids using previously described transfection
567 methods (Spalding et al., 2010). Briefly, 75 µg of both gRNA containing pUF1-CasG or pCasG
568 plasmids and corresponding pRS or pRSng repair plasmids (**Supplementary table 3**) were
569 electroporated into 400 µL of red blood cells (RBCs) by low-voltage electroporation. The
570 transfected RBCs were mixed with 2.5 mL of synchronized schizont stage PfMev parasites and
571 were cultured in complete medium with 50 µM mevalonate (Racemic mevalonolactone, Sigma-
572 Aldrich, MO, USA). After 48 h, 1.5 µM DSM1 (BEI resources, VA, USA), 2.5 nM WR99210
573 (Jacobus pharmaceuticals, NJ, USA), and 50 µM mevalonate were added to select for the
574 transfectants over the course of seven days. After seven days, the cultures were maintained in
575 complete medium with 50 µM mevalonate until parasites appeared in the culture. Once the
576 parasites appeared, the cultures were maintained in complete medium with 2.5 nM WR99210
577 and 50 µM mevalonate.
578 For generating the Δ*sufC/sufD* line, RBCs were transfected with the pCasG-*sufC* and
579 pRSng(BSD)-*sufC* plasmids as described above. Synchronized Δ*sufD* parasites were added to the

transfected RBCs and cultured in medium with 50 µM mevalonate. The transfectants were selected with 2.5 µg/mL blasticidin (Corning Inc, NY, USA), 1.5 µM DSM1, 2.5 nM WR99210, and 50 µM mevalonate, after which the culture was maintained in complete medium containing 2.5 nM WR99210, and 50 µM mevalonate until parasites appeared. Upon parasite appearance, the culture was maintained in complete medium with 2.5 µg/mL blasticidin, 2.5 nM WR99210, and 50 µM mevalonate.

For generation of the *mnmA*-flag parasite lines, the linearized pKD-*mnmA*-2xFLAG-10xapt and pCasG-*mnmA*KD plasmids were co-transfected into RBCs as mentioned above. Following transfection, these RBCs were mixed with PfMev parasites and selected with 2.5 µg/mL blasticidin and 1.5 µM DSM1 along with 0.5 µM anhydrous tetracycline (aTc, Cayman Chemical, MI, USA) for seven days. After initial selection for seven days, this culture was grown in complete medium with aTc until parasite reappearance. Upon parasite reappearance, the culture was switched to and maintained in complete medium containing 2.5 µg/mL blasticidin and 0.5 µM aTc.

To generate the *bsmnmA*$^{+}$ and *bsmnmA-yrvO*$^{+}$ transgenic parasite lines, either the pCLD-*bsmnmA*-mCherry-10xapt or pCLD-*bsmnmA-yrvO*-mCherry-10xapt plasmids were co-transfected into RBCs with the pINT plasmid (Nkrumah et al., 2006) encoding the mycobacteriophage integrase (this integrase mediates attP/attB integration into the target genome locus). Transfected RBCs were mixed with PfMev^{attB} parasites (Swift et al., 2021) and cultured with 2.5 µg/mL blasticidin and 0.50 µM aTc for seven days. After seven days, these cultures were grown in complete medium with aTc until parasites were observed, at which point the cultures were maintained in complete medium containing 2.5 µg/mL blasticidin and 0.50 µM aTc.

603 The *bsmnmA*$^{+}$ Δ*mnmA*, *bsmnmA-yrvO*$^{+}$ Δ*mnmA*, and *bsmnmA-yrvO*$^{+}$ Δ*sufS* transgenic
604 parasite lines were generated with the same Cas9 and pRSng repair plasmids that were used to
605 generate the Δ*mnmA*, and Δ*sufS* transgenic lines. For *bsmnmA*$^{+}$ Δ*mnmA*, *bsmnmA-yrvO*$^{+}$ Δ*mnmA*,
606 and *bsmnmA-yrvO*$^{+}$ Δ*sufS*, medium supplemented with 1.5 µM DSM1, 2.5 nM WR99210, 1.25
607 µg/mL blasticidin, and 0.50 µM aTc was used for the initial seven days of selection, after which
608 the cultures were switched to growth medium containing blasticidin and aTc. Upon parasite
609 appearance, all cultures were maintained in medium containing WR99210, blasticidin, and aTc.
610 The *bsmnmA-yrvO*$^{+}$ Δ*sufS* transgenic parasite line was supplemented with 50 µM mevalonate in
611 addition to WR99210, blasticidin, and aTc. The *bsmnmA*$^{+}$ Δ*mnmA* line was difficult to generate
612 with only one successful line out of four attempts. Between two and eight parasite lines from
613 independent transfections were obtained for all other gene deletions (**Supplementary table 2**).
614
615 **Confirmation of gene knockout, C-terminal tagging, and gene knock-in**
616 Lysates from parasite cultures were prepared from the transgenic parasite lines by
617 incubating at 90 °C for 5 min. These lysates were used as the template for all genotype
618 confirmation PCRs. For confirmation of gene knockouts, the 5'- and 3'-end of the disrupted (Δ5'
619 and Δ3', respectively) and native gene loci (5' and 3', respectively) were amplified with
620 corresponding primers (**Supplementary table 4**). Expected amplicons for confirmation PCRs
621 are provided in **Figure 1- figure supplement 1C**. To confirm the successful C-terminal tagging
622 of MnmA and insertion of the aptamer array at the 3'UTR of MnmA, the 5'- and 3'-end of
623 modified genes (Δ5' and Δ3', respectively) and the native gene locus (C) were amplified with
624 corresponding primers. The expected amplicon sizes for these PCR products are provided in
625 **Figure 3- figure supplement 3B**. For gene knock-in confirmation, corresponding primers

(**Supplementary table 4**) were used to amplify the recombinant attL and attR loci for integration of the knocked-in gene and the unaltered attB locus as a control. The anticipated PCR amplicon sizes for knock-in confirmation PCRs can be found in **Figure 4- figure supplement 1B**. Parental lines as indicated were used as a control for these reactions.

Immunoblot

Asynchronous parasite cultures were washed three times with cold-complete medium. The cultures were treated with 0.15% (wt/vol) saponin in cold phosphate-buffered saline (PBS; pH 7.4) for 10 min on ice for permeabilization of the RBC and parasitophorous vacuolar membranes. Saponin-isolated parasites were centrifuged at 1940 g for 10 min at 4 °C and washed three times with cold-PBS. These parasites were used immediately or were snap frozen in liquid N_2 and saved at -80 °C for later use.

Saponin-isolated parasites were resuspended in 1x NuPAGE LDS sample buffer (Thermo Fisher Scientific, MA, USA) containing 2% β-mercaptoethanol and boiled for 5 min. Proteins were resolved on 4-12% gradient reducing gels and transferred to nitrocellulose membranes. The membranes were blocked with 5% milk in PBS containing 0.1% Tween 20 (Milk/PBST) for 1 h at room temperature and incubated overnight at 4 °C with mouse anti-FLAG monoclonal antibody (Catalogue no. F3165, Millipore Sigma, MO, USA) diluted 1:1000 in Milk/PBST. The membrane was then incubated for 1 h at room temperature with sheep anti-mouse horseradish peroxidase (HRP)-conjugated antibody (Catalogue no. GENA931, Millipore Sigma, MO, USA) diluted 1:10000 in Milk/PBST. Chemiluminescent signal was developed with SuperSignal West Pico chemiluminescent substrate (Thermo Fisher Scientific, MA, USA) according to the manufacturer's protocol and detected on autoradiography film. For loading controls, the

membrane was stripped of antibodies with 200 mM glycine (pH 2.0) for 5 min at room temperature. After blocking the membrane with 5% Milk/PBST, the membrane was re-probed with 1:25000 anti-Aldolase mouse monoclonal antibody (from David J. Sullivan, Johns Hopkins Bloomberg School of Public Health) and 1:10000 sheep anti-mouse HRP-conjugated antibody, using the methods described above.

Confirmation of apicoplast genome loss

The apicoplast-encoded *sufB* gene (PF3D7_API04700) was used as a proxy for the presence of the apicoplast genome and was amplified by PCR with a primer pair listed in **Supplementary table 4**. As controls, genes from the nuclear genome (*ldh*, PF3D7_1324900) and the mitochondrial genome (*cox1*, PF3D7_MIT02100) were amplified with corresponding primer pairs (**Supplementary table 4**). Parasite lysates of the parental line were used as positive controls for apicoplast genome detection. The anticipated amplicon sizes are 520 bp, 581 bp, and 761 bp for *ldh*, *sufB* and *cox1*, respectively.

Immunofluorescence assays and live cell microscopy

For immunofluorescence assays, *mnmA*-flag parasites were fixed and permeabilized as described previously (Gallagher et al., 2011). Briefly, infected RBCs from 250 µL of culture were harvested by centrifugation and resuspended in 30 µL of 4% electron microscopy (EM) grade paraformaldehyde and 0.0075% EM grade glutaraldehyde in PBS (pH 7.4) for 30 min at room temperature. Fixed cells were then permeabilized with 0.1% Triton X-100 in PBS for 10 min and then treated with 0.1 mg/mL of sodium borohydride ($NaBH_4$) in PBS for 10 min to reduce free aldehyde groups. After a 2 h blocking step with 3% bovine serum albumin (BSA) in

672 PBS, cells were incubated overnight at 4 °C with 1:500 rabbit anti-ACP antibody (Gallagher &
673 Prigge, 2010) and 1:500 mouse anti-FLAG antibody (Catalogue no. F3165, Millipore Sigma,
674 MO, USA). The cells were washed with PBS three times and then incubated for 2 h with 1:1000
675 goat anti-mouse Alexa 488 (Catalogue no. A11029, Invitrogen, CA, USA) and 1:1000 goat anti-
676 rabbit Alexa 59 (Catalogue no. A11037, Invitrogen, CA, USA) secondary antibodies in PBS with
677 3% BSA. After three washes with PBS, the cells were mounted on coverslips with ProLong Gold
678 4′, 6-diamidino-2-phenylindole (DAPI) antifade reagent (Life Technologies, CA, USA) and
679 sealed with nail polish.
680 For live cell imaging of the Δ*sufC,* Δ*sufD*, Δ*sufE,* Δ*sufS*, Δ*mnmA*, and Δ*sufC/sufD*
681 transgenic lines, 100 µL of asynchronous parasites were incubated with 1 µg/mL DAPI
682 (Invitrogen, CA, USA) and 30 nM MitoTracker CMX-Ros (Invitrogen, CA, USA) for 30
683 minutes at 37 °C. The stained cells were then washed three times with complete medium and
684 incubated for 5 minutes at 37 °C after each wash. After the final wash, the cells were
685 resuspended in 20 µL of complete medium, placed on a slide and sealed under a cover slip with
686 wax. For live cell imaging of the *bsmnmA*$^+$*, bsmnmA-yrvO*$^+$*, bsmnmA*$^+$ Δ*mnmA*, *bsmnmA-yrvO*$^+$
687 Δ*mnmA*, and *bsmnmA-yrvO*$^+$ Δ*sufS* parasite lines, cells were stained with 1 µg/mL DAPI only.
688 All images were taken with a Zeiss AxioImager M2 microscope (Carl Zeiss Microscopy,
689 LLC, NY, USA) equipped with a Hamamatsu ORCA-R2 camera (Hamamatsu Photonics,
690 Hamamatsu, Japan) using a 100x/1.4 NA lens. A series of images were taken spanning 5 µm
691 along the z-plane with 0.2 µm spacing. An iterative restoration algorithm using the Volocity
692 software (PerkinElmer, MA, USA) was used to deconvolve the images to report a single image
693 in the z-plane.

694 The degree of colocalization between the red channel (anti-ACP or mCherry) and green
695 channel (anti-FLAG or api-SFG) signals was determined with Volocity software. The fluorescent
696 intensity thresholds were set using the region of interest (ROI) tool using Volocity. To set the
697 thresholds, the fluorescence intensity of a region of the cell with no staining for either signal
698 (background) was used. To measure the degree of colocalization, the Manders' coefficient (M1)
699 (Manders et al., 1993)was determined. M1 is defined as the percentage of total pixels from the
700 test channel (anti-FLAG, mCherry) that overlaps with the percentage of total pixels from the
701 organellar marker channel (anti-ACP, api-SFG). A value of M1=1 denotes perfect colocalization,
702 while M1=0 denotes no colocalization (Manders et al., 1993). Mean M1 (±standard deviation)
703 values were obtained by analyzing multiple images from at least two independent biological
704 replicates.
705
706 **Parasite growth assay**
707 Parasite growth was monitored using an Attune Nxt Flow Cytometer (Thermo Fisher
708 Scientific, MA, USA) as previously described (Swift et al., 2020; Tewari et al., 2022). For
709 determining the growth dependence on mevalonate, cultures were seeded in the presence or
710 absence of 50 µM mevalonate at 0.5% parasitemia and 2% hematocrit in a total volume of 250
711 µL, in quadruplicate for each condition. Parasite growth was monitored every 24 h over four
712 days following SYBR green I (Invitrogen, CA, USA) staining. For the growth curves shown in
713 **Figure 3F**, the parasites were cultured in the presence of 0.5 µM aTc (control), absence of aTc
714 (knockdown), or with 50 µM mevalonate supplementation (rescue). For growth assays presented
715 in **Figures 5E** and **6E**, parasites were grown in the presence of 0.5 µM aTc and absence of
716 *Shield1* (Aobious Inc, MA, USA) (permissive condition) or in the absence of aTc and presence

of 0.5 µM *Shield1* (nonpermissive condition). In all the experiments presented in **Figures 3F**, **5E**, and **6E**, parasite growth was monitored over eight days. On day four, the cultures were diluted 1:10. Data from two independent biological replicates (each in quadruplicate) of the indicated parasite lines were analyzed using a two-way ANOVA with a Sidak-Bonferroni correction in Prism V8.4 (GraphPad Software, CA, USA).

Acknowledgements

We express our gratitude to Patricia C. Dos Santos (Wake Forest University) for insights on *B. subtilis* MnmA and YrvO. We also extend our thanks to David J. Sullivan (Johns Hopkins Bloomberg School of Public Health) for the anti-Aldolase mouse monoclonal antibody and Erin D. Goley (Johns Hopkins University School of Medicine) for providing *B. subtilis*.

This work was supported by the National Institutes of Health R01 AI125534 (STP) and R21 AI101589 (STP), the Johns Hopkins Malaria Research Institute, and the Bloomberg Philanthropies. RE was supported by Johns Hopkins Malaria Research Institute postdoctoral fellowship. KR was supported by NIH training grant T32AI007417. The funders had no role in study design, data collection and analysis, decision to publish, or preparation of the manuscript.

Author contributions

RPS, RE, and STP arranged the figures and wrote the manuscript, with input from all listed coauthors. STP coordinated this work. RPS, RE, KR, and HBL carried out the experiments displayed in this manuscript. All authors contributed to revision of the manuscript.

Conflict of interests

The authors declare that they have no conflict of interest.

Figure Legends

Figure 1. Apicoplast FeS assembly is not essential for apicoplast maintenance

(A) FeS assembly in the *Plasmodium falciparum* apicoplast. In the sulfur acquisition step, SufS, liberates sulfur from cysteine (Cys), resulting in a bound persulfide. SufE transfers sulfur from SufS to SufB of the $SufBC_2D$ FeS assembly complex. SufA and NfuApi receive FeS cofactors from the $SufBC_2D$ complex and transfer them to downstream FeS-dependent proteins. The proteins investigated in this study are colored blue. Ala, alanine; Fe, iron. **(B)** Genotyping PCR confirming deletion of *sufC* (top panel) and Δ*sufD* (bottom panel). **(C)** Successful amplification *sufB* (lane A) gene in the Δ*sufC* (left panel) and Δ*sufD* (right panel) parasites indicates the presence of the apicoplast genome. **(D)** Representative epifluorescence microscopy images of Δ*sufC* (top panel) and Δ*sufD* (bottom panel) parasites show a single intact apicoplast. **(E)** Mevalonate (Mev)-dependent growth of Δ*sufC* (top panel) and Δ*sufD* (bottom panel) parasites over four days. **(F)** Genotyping PCR confirms deletion of both *sufC* (top panel) and *sufD* (bottom panel) in Δ*sufC/sufD* double knockout parasites. **(G)** Successful amplification of *sufB* (lane A) demonstrates intact apicoplast in Δ*sufC/sufD* parasites. **(H)** Representative epifluorescence microscopy images of Δ*sufC/sufD* parasites shows an apicoplast with typical intact morphology. **(I)** Mevalonate (Mev)-dependent growth of Δ*sufC/sufD* parasites over four days.

In panels (B) and (F), successful gene deletion is demonstrated by the presence of PCR products for the Δ5' and Δ3' loci, but not the unmodified loci (5' and 3') loci found in the PfMev (parental) line. Expected PCR amplicon sizes are in **Figure 1- figure supplement 1(C)**. In (C) and (G), PCR detection of the *ldh*, *sufB*, and *cox1* genes of the parasite nuclear (N), apicoplast (A), and mitochondrial (M) genomes, respectively, were attempted from transgenic as well as PfMev (parental) parasite lines. In (D) and (H), the api-SFG protein (green) labels apicoplast, MitoTracker (red) stains the mitochondrion, and nuclear DNA is stained with DAPI (blue). Each image shows a field representing 10 µm x 10 µm. For panels (E) and (I), asynchronous parasites were cultured with or without 50 µM Mev and parasitemia was monitored every 24 h via flow cytometry. Data points shows daily mean parasitemia ± standard error of the mean (SEM) from two independent biological replicates, each with four technical replicates. DNA markers in (B), (C), (D), and (G) are in kilobases (kb).

Figure 1- figure supplement 1. Generation and characterization of knockout parasite lines **(A)** Schematic illustration of a double crossover homologous recombination event between the native locus of gene of interest (GOI) and the repair plasmid with two homology (HA) arms. The Cas9-endonuclease promotes a double-stranded break in the native locus while the HAs from the repair plasmid recombine through a double crossover recombination event resulting in the generation of the recombinant locus ("modified locus"). Individual segments are not to scale. The positions and directions of the primers (red arrow) used for confirmation of gene knockout are indicated. Primer sequences are available in **Supplementary file 1- table 4**. **(B)** Table showing the primer pairs and the template used for each PCR reaction. **(C)** Table showing the expected amplicon sizes for the genotyping PCR reactions shown in **Figures 1(B)**, **1(F)**, **2(A)**, **3(I)**, **5(A)**, **6(A)**, **and 7(B)**.

Figure 1- source data 1. Uncropped agarose gel images of PCR analyses presented in **Figures 1(B)**, **1(C)**, **1(F)**, **and 1(G)**.

Figure 1- source data 2. Growth assay parasitemia counts for Δ*sufC* (top table) and Δ*sufD* (bottom table) used for **Figure 1(E)**.

Figure 1- source data 3. Growth assay parasitemia counts for Δ*sufC/sufD* used for **Figure 1(I)**.

Figure 2. Apicoplast cysteine desulfurase, SufS is essential for apicoplast maintenance **(A)** Genotyping PCR confirming deletion of *sufE* (top panel) or *sufS* (bottom panel) in PfMev parasites. In both Δ*sufE* and Δ*sufS* parasite lines, gene deletions were validated by the presence of PCR products for the Δ5' and Δ3' loci, but not for the unmodified loci (5' and 3') found in the PfMev (parental) line. Genotyping PCR reactions and expected amplicon sizes are described in **Figure 1- figure supplement 1**. **(B)** Attempted PCR amplification of *ldh*, *sufB*, and *cox1* genes of the parasite nuclear (N), apicoplast (A), and mitochondrial (M) genomes, respectively, from the Δ*sufE,* Δ*sufS,* and PfMev (parental) parasites. Successful amplification of *sufB* in the Δ*sufE* (top panel) parasites indicates the presence of the apicoplast genome, while failure to amplify this gene in Δ*sufS* parasites (bottom panel) indicates loss of the apicoplast genome. **(C)** Representative epifluorescence microscopy images of Δ*sufE* (top panel) and Δ*sufS* (bottom panel) parasites. In the Δ*sufE* parasites, a single intact apicoplast is seen. Whereas in Δ*sufS* multiple discrete vesicles were seen, indicating disruption of the apicoplast organelle. The api-

SFG protein (green) labels the apicoplast, MitoTracker (red) stains the mitochondrion, and nuclear DNA is stained with DAPI (blue). Each image is a field representing 10 µm x 10 µm. **(D)** Mevalonate (Mev)- dependent growth of Δ*sufE* (top panel) and Δ*sufS* (bottom panel) parasites. Asynchronous parasites from each line were cultured with or without 50 µM Mev and parasitemia was monitored every 24 h by flow cytometry for four days. Data points showing daily mean parasitemia ± SEM from two independent biological replicates, each with four technical replicates.

In panels (A) and (B), DNA markers are in kilobases (kb).

Figure 2- source data 1. Uncropped agarose gel images of PCR analyses presented in **Figures 2(A)** and **2(B)**.

Figure 2- source data 2. Growth assay parasitemia counts for Δ*sufE* (top table) and Δ*sufS* (bottom table) used for **Figure 2(D)**.

Figure 3. *Plasmodium falciparum* MnmA is essential for apicoplast maintenance and parasite survival

(A) Snapshots from the multiple sequence alignment of MnmA orthologs from *P. falciparum* (*Pf* MnmA, PlasmoDB ID: PF3D7_1019800), *Saccharomyces cerevisae* (*Sc* Mtu1, Uniprot ID: Q12093), *Escherichia coli* MnmA (*Ec* MnmA, Uniprot ID: P25745), and *Bacillus subtilis* (*Bs* MnmA, Uniprot ID: O35020) showing the conserved sequence motifs in the catalytic domains. The complete alignment is shown in **Figure 3- figure supplement 1**. The PP-loop signature motif SGGXDS shown in teal and the D-type signature motif C----DXXC-----C in bright green. The red asterisks (*) indicate catalytic cysteines. **(B)** Expected modified locus following introduction of 2xFLAG at 3'-end of *pfmnmA* and 10xAptamer in the 3'UTR. **(C)** Genotyping of *mnmA*-flag parasites confirms plasmid integration as evidenced by the presence of PCR amplicons for the recombinant Δ5' and Δ3' loci but not for the unmodified locus (C), as compared to the PfMev (parental) line. Expected PCR amplicon sizes are provided in **Figure 3- figure supplement 3(B)**. **(D)** Immunoblot of saponin-isolated PfMev (parental, P) and *mnmA*-flag (tagged, T) parasite lysates with anti-FLAG antibody (top panel). Anticipated molecular weight for the tagged protein is 120 kDa. Anti-Aldolase immunoblot shows relative loading

levels (bottom panel). Protein markers are in kilodaltons (kDa). The uncropped version is shown in **Figure 3- figure supplement 3(C)**. **(E)** Representative immunofluorescence microscopy images show *Pf* MnmA-2xFLAG (green) colocalization with the apicoplast marker ACP (acyl carrier protein, red). Manders' coefficient (M1, green in red) quantifies the degree of colocalization. **(F)** Anhydrous tetracycline (aTc)-dependent growth of *mnmA*-flag parasites. Asynchronous parasites were grown with 0.5 µM aTc (control), without 0.5 µM aTc (knockdown), or with 50 µM mevalonate (Mev, rescue). Parasitemia was monitored via flow cytometry every 24 h for eight days. On day four, parasite cultures were diluted 1:10. Data points show daily mean parasitemia ± SEM from two independent biological replicates, each with four technical replicates; two-way ANOVA (Sidak-Bonferroni method), *** $p<0.001$. **(G)** Representative epifluorescence microscopy images of day four samples of *mnmA*-flag parasites grown in control (aTc added) and knockdown (aTc removed) conditions from the experiment shown in (F). Under control conditions, the apicoplast remains intact; under knockdown conditions, multiple discrete vesicles are seen, demonstrating a disrupted apicoplast. The full image panel is shown in **Figure 3- figure supplement 4(B)**. **(H)** Graph showing the percentage of *mnmA*-flag parasites with an intact apicoplast when grown in control (aTc added) and knockdown (aTc removed) conditions in the experiment shown in (F). Live epifluorescence microscopy images were taken every 48 h and apicoplast morphology (intact or disrupted) was determined based on apicoplast-localized api-SFG. Error bars represent standard deviation from at least 18 images taken for each time point and growth condition from two independent experiments. **(I)** Genotyping PCR confirming *mnmA* deletion in Δ*mnmA* parasites. In the Δ*mnmA* parasite line, gene deletion was validated by the presence of PCR products for the Δ5' and Δ3' loci, but not for the unmodified loci (5' and 3') found in the PfMev (parental) line. Genotyping PCR reactions and expected amplicon sizes are described in **Figure 1- figure supplement 1**. **(J)** Attempted PCR amplification of *ldh*, *sufB*, and *cox1* genes of the parasite nuclear (N), apicoplast (A), and mitochondrial (M) genomes, respectively, from the Δ*mnmA* and PfMev (parental) parasites. Lack of a PCR amplicon for *sufB* in the Δ*mnmA* parasite line suggests loss of the apicoplast genome. **(K)** Representative epifluorescence microscopy images of Δ*mnmA* parasites. Multiple discrete vesicles are seen, demonstrating a disrupted apicoplast. **(L)** Mevalonate (Mev)-dependent growth of the Δ*mnmA* parasites. Asynchronous parasites were cultured with or without 50 µM Mev for four days. Parasitemia was monitored every 24 h by

865 flow cytometry. Data points show daily mean parasitemia ± SEM from two independent
866 biological replicates, each with four technical replicates.
867
868 In Panels (G) and (K), api-SFG protein (green) labels the apicoplast, the mitochondrion is stained
869 with MitoTracker (red), and nuclear DNA is stained with DAPI (blue). In (E), (G) and (K), each
870 image depicts a field of 10 µm x 10 µm. In (C), (I) and (J), DNA markers are in kilobases (kb).
871
872 **Figure 3- figure supplement 1. Multiple sequence alignment (MSA) of MnmA orthologs**
873 MSA of MnmA orthologs from *P. falciparum* (*Pf* MnmA, PlasmoDB ID: PF3D7_1019800), *S.*
874 *cerevisae* (*Sc* Mtu1, Uniprot ID: Q12093), *E. coli* MnmA (*Ec* MnmA, Uniprot ID: P25745), and
875 *B. subtilis* (*Bs* MnmA, Uniprot ID: O35020) showing the conserved sequence motifs in the
876 catalytic domains. The PP-loop signature motif SGGXDS is underlined in teal and the D-type
877 signature motif C----DXXC-----C is underlined in bright green. The red asterisks (*) indicate
878 catalytic cysteines. The ClustalW program from Geneious Prime (version 2019.2.1, Geneious
879 Biologics, CA, USA) was used to align these sequences (https://www.geneious.com).
880
881 **Figure 3- figure supplement 2. Multiple sequence alignment (MSA) of MnmA orthologs**
882 **from pathogenic apicomplexans**
883 MSA of MnmA orthologs from *P. falciparum* (PlasmoDB ID: PF3D7_1019800), *Babesia*
884 *microti* (PiroplasmaDB ID: BMR1_03g03155), *Theileria annulata* (PiroplasmaDB ID:
885 TA12620), *Toxoplasma gondii* (ToxoDB ID: TGME49_309110), and *Eimeria tenella* (ToxoDB
886 ID: ETH_00027940) showing the conserved sequence motifs in the catalytic domains. The PP-
887 loop signature motif SGGXDS is underlined in teal and the D-type signature motif C----DXXC--
888 ---C is underlined in bright green. The red asterisks (*) indicate catalytic cysteines. The ClustalW
889 program from Geneious Prime (version 2019.2.1, Geneious Biologics, CA, USA) was used to
890 align these sequences (https://www.geneious.com).
891
892 **Figure 3- figure supplement 3. Generation of the MnmA localization/knockdown construct**
893 **(A)** Schematic showing the insertion of 2x-FLAG at the 3' end and aptamers in the 3'UTR of
894 *pfmnmA*. The pKD-*mnmA*-2xFLAG-10xapt plasmid was linearized with *EcoRV* digestion. The
895 homology arms (HA) on the plasmid corresponding to the native *mnmA* locus are shown,

indicating how homologous recombination occurs. Primer positions for insertion confirmation PCR are shown with red arrows. Primer sequences are available in **Supplementary file 1- table 4**. Individual segments are not to scale. HA, homology arm; cds, coding sequence; UTR, untranslated region; hBSD, codon-harmonized blasticidin deaminase. **(B)** Table showing the anticipated amplicon sizes for insertion confirmation PCRs shown in **Figure 3(C)**. **(C)** Full panel of immunoblot shown in **Figure 3(D)**. Immunodetection of saponin-isolated PfMev (parental, P) and *mnmA*-flag (tagged, T) parasite lysates. These lysates were probed with an anti-FLAG antibody (top panel). The anticipated molecular weight for the tagged protein is 120 kDa. These lysates were also probed with an anti-Aldolase antibody to show relative loading levels (bottom panel). Protein markers are in kilodaltons (kDa).

Figure 3- figure supplement 4. Effect of aTc removal on *Pf* MnmA in the *mnmA*-flag line
(A) Immunodetection of *mnmA*-flag in lysates of saponin-isolated parasites. Parasites were grown under nonpermissive conditions (aTc removed) with samples collected daily for Western blot. MnmA-2xFLAG protein was detected with anti-FLAG antibody (top panel). The blot was washed and reprobed with an anti-Aldolase antibody to show relative loading levels (bottom panel). Protein markers are in kilodaltons (kDa). **(B)** Live epifluorescence microscopy of day zero, two, four, six, and eight samples from non-permissive growth conditions for the *mnmA*-flag parasite line. From day four onwards, multiple discrete vesicles were observed instead of a the single intact apicoplast organelle observed prior to day four. The api-SFG protein (green) marks the apicoplast, the mitochondrion is labeled by MitoTracker (red), and nuclear DNA is stained with DAPI (blue). Representative images are shown. Each image depicts a field of 10 µm x 10 µm.

Figure 3- source data 1. Uncropped agarose gel images of PCR analyses presented in **Figures 3(C)**, **3(I)**, and **3(J)**.
Figure 3- source data 2. Growth assay parasitemia counts used for **Figure 3(F)**. The yellow highlighted row represents the expected parasitemia count after 1:10 dilution of day 4 parasites.
Figure 3- source data 3. Counts of intact apicoplasts presented in **Figure 3(H)**.
Figure 3- source data 4. Growth assay parasitemia counts for Δ*mnmA* used for **Figure 3(L)**.

Figure 3- figure supplement 3- source data 1. Full immunoblot shown in **Figure 3- figure supplement 3(C)**.

Figure 3- figure supplement 4- source data 1. Full immunoblot shown in **Figure 3- figure supplement 4(A)**.

Figure 4. *Bacillus subtilis* MnmA and MnmA-YrvO can be expressed in the parasite apicoplast

(A) Schematics illustrating the expected gene product in the *bsmnmA*$^{+}$ and *bsmnmA-yrvO*$^{+}$ parasite lines following successful genetic modification. **(B)** Amplification of the attL and attR regions from *bsmnmA*$^{+}$ and *bsmnmA-yrvO*$^{+}$ transgenic parasites indicates successful plasmid integration in both lines. Amplification of the attB region from the PfMev^{attB} parasite line (parental) was used as a control. DNA markers are in kilobases (kb). Expected PCR amplicon sizes are provided in **Figure 4- figure supplement 1(B)**. **(C)** Representative epifluorescence microscopy images of *bsmnmA*$^{+}$ (top panel) and *bsmnmA-yrvO*$^{+}$ (bottom panel) transgenic parasites. The *bsmnmA* and *bsmnmA-yrvO* fusion protein contains a C-terminal mCherry tag (red) and colocalizes with the apicoplast api-SFG marker (green). The nuclear DNA is stained with DAPI (blue). The degree of colocalization of the *bsmnmA* or *bsmnmA-yrvO* fusion proteins with the api-SFG apicoplast marker are shown in the merge images and the Manders' coefficients (M1; red in green) are provided. Each image depicts a field of 10 µm x 10 µm.

Figure 4- figure supplement 1. Generation and characterization of parasite lines expressing *Bacillus subtilis* MnmA and MnmA-YrvO

(A) Schematic illustration showing insertion of the pCLD-*bs*GOI-mCherry-10xapt plasmids into the attB locus of PfMev^{attB} parasites. The TetR-DOZI inducible system regulator and harmonized blasticidin-*S*-deaminase (hBSD) are separated by a T2A viral skip peptide. The CLD-*bs*GOI-mCherry-10xapt and TetR-DOZI-2A-hBSD cassettes are expressed under a single bidirectional promoter. This plasmid was co-transfected with the pINT plasmid, which expresses integrase for catalyzing attB/attP integration. Primer pairs (in red) for PCR amplification of the attB region of the parental line and the recombinant attL and attR regions are shown. Primer sequences are available in **Supplementary file 1- table 4**. *bs*GOI, *B. subtillis* genes of interest: *mnmA* or

mnmA-yrvO fusion. **(B)** Table showing the anticipated amplicon sizes for insertion confirmation PCR reactions shown in **Figure 4(B)**.

Figure 4- figure supplement 2. The engineered sequence encoding the *B. subtilis* MnmA-YrvO fusion protein

The two genes were linked with a 15 bp linker (red font) and was used for generation of pCLD-*bsmnmA-yrvO*-mCherry-10xapt plasmid. Highlighted in grey is the sequence for the *B. subtilis mnmA*, with the sequence for the *B. subtilis yrvO* highlighted in yellow.

Figure 4- source data 1. Uncropped agarose gel images of PCR analyses presented in **Figure 4(B)**.

Figure 5. *Bacillus subtilis* MnmA-YrvO fusion protein can complement *Plasmodium falciparum* MnmA

(A) Genotyping PCR confirms *mnmA* deletion in *bsmnmA-yrvO*$^{+}$ Δ*mnmA* parasites. Successful deletion was validated by the presence of PCR amplicons for the Δ5' and Δ3' loci, but not for the unmodified loci (5' and 3') found in the *bsmnmA-yrvO*$^{+}$ (parental) parasites. Genotyping PCR reactions and expected amplicon sizes are described in **Figure 1- figure supplement 1**. **(B)** Mevalonate (Mev)-independent growth of *bsmnmA-yrvO*$^{+}$ Δ*mnmA* parasites. Asynchronous parasites were grown with or without 50 µM Mev. Every 24 h parasitemia was monitored by flow cytometry for four days. Data points show daily mean parasitemia ± SEM from two independent biological replicates, each with four technical replicates; n.s., non-significant, two-way ANOVA (Sidak-Bonferroni method), $p>0.05$. **(C)** Attempted PCR amplification of *ldh*, *sufB*, and *cox1* genes of the parasite nuclear (N), apicoplast (A), and mitochondrial (M) genomes, respectively, from *bsmnmA-yrvO*$^{+}$ Δ*mnmA* and *bsmnmA-yrvO*$^{+}$ (parental) parasites. Successful amplification of *sufB* in *bsmnmA-yrvO*$^{+}$ Δ*mnmA* parasites indicates the presence of the apicoplast genome. **(D)** Representative epifluorescence microscopy images of *bsmnmA-yrvO*$^{+}$ Δ*mnmA* parasites showing an intact apicoplast. **(E)** Growth of the *bsmnmA-yrvO*$^{+}$ Δ*mnmA* parasites. Asynchronous parasites were grown under permissive (with 0.5 µM aTc and without 0.5 µM *Shield1*), or non-permissive (without 0.5 µM aTc and with 0.5 µM *Shield1*) conditions. Parasitemia was monitored via flow cytometry every 24 h for eight days. On day four, parasite

cultures were diluted 1:10. Data points showing daily mean parasitemia ± SEM from two independent biological replicates, each with four technical replicates; two-way ANOVA (Sidak-Bonferroni method), * $p<0.05$. **(F)** Representative epifluorescence microscopy images of day eight *bsmnmA-yrvO*$^{+}$ Δ*mnmA* parasites from (E). The apicoplast remains intact under permissive conditions, whereas multiple discrete vesicles were observed under non-permissive conditions. The *Bs* MnmA-YrvO-mCherry (red) is only visible under permissive conditions. The full image panel is available in **Figure 5- figure supplement 1**.

In (D) and (F), the *Bs* MnmA-YrvO fusion protein contains a C-terminal mCherry fluorescent protein (red). Api-SFG protein (green) labels the apicoplast, and nuclear DNA is stained with DAPI (blue). Each image depicts a field of 10 µm x 10 µm. In (A) and (C), DNA markers are in kilobases (kb).

Figure 5- figure supplement 1. Live epifluorescence microscopy of day eight samples from permissive and non-permissive growth conditions for *bsmnmA-yrvO*$^{+}$Δ*mnmA*

The apicoplast remained intact under permissive conditions, while multiple discrete vesicles were observed under non-permissive conditions, indicative of a disrupted apicoplast organelle. The *Bs* mnmA-YrvO fusion protein contains a C-terminal mCherry fluorescent protein tag (red) which is only visible under permissive conditions. The api-SFG protein (green) labels the apicoplast, and nuclear DNA is stained with DAPI (blue). Representative images are shown. Each image depicts a field of 10 µm x 10 µm.

Figure 5- source data 1. Uncropped agarose gel images of PCR analyses presented in **Figures 5(A)** and **5(C)**.

Figure 5- source data 2. Growth assay parasitemia counts for *bsmnmA-yrvO*$^{+}$ΔmnmA used for **Figure 5(B)**.

Figure 5- source data 3. Growth assay parasitemia counts for *bsmnmA-yrvO*$^{+}$ΔmnmA used for **Figure 5(E)**. The yellow highlighted row represents the expected parasitemia count after 1:10 dilution of day 4 parasites.

Figure 6. *Bacillus subtilis* MnmA can complement loss of *Plasmodium falciparum* MnmA

(A) Genotyping PCR confirms *mnmA* deletion in *bsmnmA*$^{+}$ Δ*mnmA* parasites, as evidenced by the presence of PCR amplicons for the Δ5' and Δ3' loci, but not for the unmodified loci (5' and 3') found in the *bsmnmA*$^{+}$ (parental) parasites. Genotyping PCR reactions and expected amplicon sizes are described in **Figure 1- figure supplement 1**. **(B)** Mevalonate (Mev)-independent growth of *bsmnmA*$^{+}$ Δ*mnmA* parasites. Asynchronous parasites were grown with or without 50 µM Mev and parasitemia was monitored every 24 h by flow cytometry for four days. Data points represent daily mean parasitemia ± SEM from two independent biological replicates, each with four technical replicates; n.s., non-significant, two-way ANOVA (Sidak-Bonferroni method), $p>0.05$. **(C)** PCR detection of *ldh*, *sufB*, and *cox1* genes of the parasite nuclear (N), apicoplast (A), and mitochondrial (M) genomes, respectively, in *bsmnmA*$^{+}$ Δ*mnmA* and *bsmnmA*$^{+}$ (parental) parasites. Successful amplification of *sufB* in the *bsmnmA*$^{+}$ Δ*mnmA* parasites indicates the presence of the apicoplast genome. **(D)** Representative epifluorescence microscopy images of *bsmnmA*$^{+}$ Δ*mnmA* parasites shows an intact apicoplast. **(E)** Asynchronous *bsmnmA*$^{+}$ Δ*mnmA* parasites were grown under permissive (with 0.5 µM aTc and without 0.5 µM *Shield1*), or non-permissive (without 0.5 µM aTc and with 0.5 µM *Shield1*) conditions. Parasitemia was monitored via flow cytometry every 24 h for eight days. On day four, parasite cultures were diluted 1:10. Data points represent daily mean parasitemia ± SEM from two independent biological replicates, each with four technical replicates; n.s., non-significant, two-way ANOVA (Sidak-Bonferroni method), * $p<0.05$. **(F)** Representative epifluorescence microscopy images of day eight *bsmnmA*$^{+}$ Δ*mnmA* parasites from (E). The apicoplast remained intact under permissive conditions, while multiple discrete vesicles were observed under non-permissive conditions, indicative of a disrupted apicoplast organelle. The *Bs* MnmA -mCherry (red) is only visible under permissive conditions. The full image is available in **Figure 6- figure supplement 1**.

In (D) and (F), The Bs MnmA protein is tagged C-terminally with mCherry (red), api-SFG protein (green) labels the apicoplast, and nuclear DNA is stained with DAPI (blue). Each image depicts a field of 10 µm x 10 µm. In (A) and (C), DNA markers are in kilobases (kb).

Figure 6- figure supplement 1. Live epifluorescence microscopy of day eight samples from permissive and non-permissive growth conditions for *bsmnmA* $^{+}$Δ*mnmA* parasites

The apicoplast remained intact under permissive conditions, while multiple discrete vesicles were observed under non-permissive conditions, indicative of a disrupted apicoplast organelle. The *Bs* MnmA protein contains a C-terminal mCherry fluorescent protein tag (red) which is only visible under permissive conditions. The api-SFG protein (green) labels the apicoplast, and nuclear DNA is stained with DAPI (blue). Representative images are shown. Each image depicts a field of 10 µm x 10 µm.

Figure 6- figure supplement 2. Growth comparison between the *bsmnmA*$^{+}$ Δ*mnmA* parasite line and *bsmnmA-yrvO*$^{+}$ Δ*mnmA* parasite line

Asynchronous parasites were grown in complete medium with 0.5 µM aTc for eight days. Parasite growth was monitored via flow cytometry every 24 h. On day four, parasite cultures were diluted 1:10. Data presented are from two independent biological replicates, each with four technical replicates, error bars represent the standard error of the mean; n.s., non-significant, two-way ANOVA (Sidak-Bonferroni method), $p>0.05$.

Figure 6- source data 1. Uncropped agarose gel images of PCR analyses presented in **Figures 6(A)** and **6(C)**.

Figure 6- source data 2. Growth assay parasitemia counts for *bsmnmA*$^{+}$ΔmnmA used for **Figure 6(B)**.

Figure 6- source data 3. Growth assay parasitemia counts for *bsmnmA*$^{+}$ΔmnmA used for **Figure 6(E)**. The yellow highlighted row represents the expected parasitemia count after 1:10 dilution of day 4 parasites.

Figure 6- figure supplement 2- source data 1. Growth assay parasitemia counts used for **Figure 6 - figure supplement 2**. All parasites were cultured in presence of anhydrotetracycline (aTc). The yellow highlighted row represents the expected parasitemia count after 1:10 dilution of day 4 parasites.

Figure 7. *Plasmodium falciparum* SufS provides sulfur for both the SUF pathway and MnmA-catalyzed tRNA thiolation

(A) The expected outcome of *sufS* deletion in *bsmnmA-yrvO*$^{+}$ parasites is explained in the schematic. In absence of parasite SufS, sulfur for FeS biosynthesis is unavailable resulting in no FeS synthesis. Since, the IPP precursor biosynthesis pathway contains FeS-dependent enzymes, this pathway cannot function, rendering parasites reliant on exogenous mevalonate (mev) to survive. Sulfur liberated by *Bs* YrvO is sufficient for the MnmA-mediated s^2U tRNA modification and efficient protein translation. **(B)** Genotyping PCR confirms deletion of *sufS* in *bsmnmA-yrvO*$^{+}$ Δ*sufS* parasites. Successful deletion was validated by the presence of PCR amplicons for the Δ5' and Δ3' loci, but not for the unmodified loci (5' and 3') found in the *bsmnmA-yrvO*$^{+}$ (parental) parasites. Genotyping PCR reactions and expected amplicon sizes are described in **Figure 1- figure supplement 1**. **(C)** Attempted PCR amplification of *ldh*, *sufB*, and *cox1* genes from the parasite nuclear (N), apicoplast (A), mitochondrial (M) genomes, respectively, in *bsmnmA-yrvO*$^{+}$ Δ*sufS* and *bsmnmA-yrvO*$^{+}$ (parental) parasites. Successful amplification of *sufB* in the *bsmnmA-yrvO*$^{+}$ Δ*sufS* parasite line indicates the presence of the apicoplast genome. **(D)** Representative epifluorescence microscopy images of the *bsmnmA-yrvO*$^{+}$ Δ*sufS* parasite line expressing api-SFG protein (green) and the *Bs* MnmA-YrvO-mCherry (red). The nuclear DNA is stained with DAPI (blue). A single intact apicoplast was seen in this parasite. Each image depicts a field of 10 µm x 10 µm. **(E)** Mevalonate (mev)-dependent growth of *bsmnmA-yrvO*$^{+}$ Δ*sufS* parasites. Asynchronous were cultured with or without 50 µM Mev for four days. Flow cytometry was used to monitor parasitemia every 24 h. Data points represent daily mean parasitemia ± SEM from two independent biological replicates, each with four technical replicates.

In panels (B) and (C), DNA markers are in kilobases (kb).

Figure 7- source data 1. Uncropped agarose gel images of PCR analyses presented in **Figures 7(B)** and **7(C)**.

Figure 7- source data 2. Growth assay parasitemia counts for *bsmnmA-yrvO*$^{+}$ Δ*sufS* used for **Figure 7(E)**.

Figure 8. Dual role of SufS in the *P. falciparum* apicoplast

(A) Dual role of SufS in FeS synthesis and s^2U modification of tRNAs in the apicoplast of *P. falciparum*. **(B)** In Δ*sufE* parasites, deletion of *sufE* results in a mevalonate (Mev)-dependent phenotype with an intact apicoplast. This phenotype is likely caused by the deletion of SufE resulting in the loss of FeS biosynthesis. **(C)** In Δ*sufS* parasites, disruption of both FeS biosynthesis and MnmA-dependent tRNA thiolation results in a mevalonate (Mev)-dependent phenotype with a disrupted apicoplast. **(D)** In Δ*mnmA* parasites, deletion of *mnmA* results in a mevalonate (Mev)-dependent phenotype with a disrupted apicoplast. Deletion of MnmA likely causes tRNA thiolation defect leading to translational aberration and ultimately apicoplast disruption. **(E)** In *bsmnmA-yrvO*$^+$ Δ*mnmA* parasites, both SufS and *Bs* YrvO have cysteine desulfurase activity that transfers sulfur to *Bs* MnmA in the absence of the endogenous parasite MnmA. **(F)** In *bsmnmA*$^+$ Δ*mnmA* parasites, *Bs* MnmA complements the loss of the endogenous parasite MnmA. The possibility that SufS can transfer sulfur to *Bs* MnmA is represented by the dotted arrow. **(G)** In *bsmnmA-yrvO*$^+$ Δ*sufS* parasites, *Bs* YrvO can transfer sulfur to *Bs* MnmA and/or parasite MnmA, but not to SufE and the FeS biosynthesis pathway. In this scenario, parasites would have intact apicoplasts due to proper tRNA thiolation but would be mevalonate-dependent due to loss of FeS biosynthesis. **(H)** Events leading to parasite death because of loss of SufS activity in the apicoplast. In panels, (A)-(G), Cys, cysteine; Ala, alanine.

References

Akuh, O.-A., Elahi, R., Prigge, S. T., & Seeber, F. (2022). The ferredoxin redox system – an essential electron distributing hub in the apicoplast of Apicomplexa. *Trends Parasitol, 38*(10), 868-881. https://doi.org/https://doi.org/10.1016/j.pt.2022.08.002

Ashraf, S. S., Sochacka, E., Cain, R., Guenther, R., Malkiewicz, A., & Agris, P. F. (1999). Single atom modification (O → S) of tRNA confers ribosome binding. *RNA, 5*(2), 188-194. https://doi.org/10.1017/S1355838299981529

Aurrecoechea, C., Brestelli, J., Brunk, B. P., Dommer, J., Fischer, S., Gajria, B., Gao, X., Gingle, A., Grant, G., Harb, O. S., Heiges, M., Innamorato, F., Iodice, J., Kissinger, J. C., Kraemer, E., Li, W., Miller, J. A., Nayak, V., Pennington, C., Pinney, D. F., Roos, D. S., Ross, C., Stoeckert, C. J., Jr., Treatman, C., & Wang, H. (2008). PlasmoDB: a functional genomic database for malaria parasites. *Nucleic Acids Res, 37*(suppl_1), D539-D543. https://doi.org/10.1093/nar/gkn814

Bai, Y., Chen, T., Happe, T., Lu, Y., & Sawyer, A. (2018). Iron–sulphur cluster biogenesis via the SUF pathway. *Metallomics, 10*(8), 1038-1052. https://doi.org/10.1039/c8mt00150b

Beinert, H. (2000). Iron-sulfur proteins: ancient structures, still full of surprises. *J Biol Inorg Chem, 5*(1), 2-15. https://doi.org/10.1007/s007750050002

Black, K. A., & Santos, P. C. D. (2015a). Abbreviated pathway for biosynthesis of 2-Thiouridine in *Bacillus subtilis*. *J Bacteriol, 197*(11), 1952-1962. https://doi.org/doi:10.1128/JB.02625-14

Black, K. A., & Santos, P. C. D. (2015b). Shared-intermediates in the biosynthesis of thio-cofactors: Mechanism and functions of cysteine desulfurases and sulfur acceptors. *Biochim Et Biophys Acta (BBA)-Mol Cell Res, 1853*(6), 1470-1480. https://doi.org/https://doi.org/10.1016/j.bbamcr.2014.10.018

Blahut, M., Sanchez, E., Fisher, C. E., & Outten, F. W. (2020). Fe-S cluster biogenesis by the bacterial Suf pathway. *Biochim Et Biophys Acta (BBA)-Mol Cell Res, 1867*(11), 118829. https://doi.org/https://doi.org/10.1016/j.bbamcr.2020.118829

Botté, C. Y., Dubar, F., McFadden, G. I., Maréchal, E., & Biot, C. (2012). *Plasmodium falciparum* apicoplast drugs: targets or off-Targets? *Chem Rev, 112*(3), 1269-1283. https://doi.org/10.1021/cr200258w

Bühning, M., Valleriani, A., & Leimkühler, S. (2017). The role of SufS is restricted to Fe–S cluster biosynthesis in *Escherichia coli*. *Biochemistry, 56*(14), 1987-2000. https://doi.org/10.1021/acs.biochem.7b00040

Čavužić, M., & Liu, Y. (2017). Biosynthesis of Sulfur-containing tRNA modifications: a comparison of bacterial, archaeal, and eukaryotic pathways. *Biomolecules, 7*(1), 27. https://www.mdpi.com/2218-273X/7/1/27

Chahal, H. K., Dai, Y., Saini, A., Ayala-Castro, C., & Outten, F. W. (2009). The SufBCD Fe−S scaffold complex interacts with SufA for Fe−S Cluster transfer. *Biochemistry, 48*(44), 10644-10653. https://doi.org/10.1021/bi901518y

Charan, M., Choudhary, H. H., Singh, N., Sadik, M., Siddiqi, M. I., Mishra, S., & Habib, S. (2017). [Fe–S] cluster assembly in the apicoplast and its indispensability in mosquito stages of the malaria parasite. *FEBS J, 284*(16), 2629-2648. https://doi.org/https://doi.org/10.1111/febs.14159

Charan, M., Singh, N., Kumar, B., Srivastava, K., Siddiqi, M. I., & Habib, S. (2014). Sulfur mobilization for Fe-S cluster assembly by the essential SUF pathway in the *Plasmodium falciparum* apicoplast and its inhibition. *Antimicrob Agents Chemother, 58*(6), 3389-3398. https://doi.org/doi:10.1128/AAC.02711-13

Dahl, E. L., & Rosenthal, P. J. (2008). Apicoplast translation, transcription and genome replication: targets for antimalarial antibiotics. *Trends Parasitol, 24*(6), 279-284. https://doi.org/https://doi.org/10.1016/j.pt.2008.03.007

Dellibovi-Ragheb, T. A., Gisselberg, J. E., & Prigge, S. T. (2013). Parasites FeS up: iron-sulfur cluster biogenesis in eukaryotic pathogens. *PLoS Pathog, 9*(4), e1003227. https://doi.org/10.1371/journal.ppat.1003227

Ellis, K. E. S., Clough, B., Saldanha, J. W., & Wilson, R. J. M. (2001). Nifs and Sufs in malaria. *Mol Microbiol, 41*(5), 973-981. https://doi.org/https://doi.org/10.1046/j.1365-2958.2001.02588.x

Foth, B. J., Ralph, S. A., Tonkin, C. J., Struck, N. S., Fraunholz, M., Roos, D. S., Cowman, A. F., & McFadden, G. I. (2003). Dissecting apicoplast targeting in the malaria marasite *Plasmodium falciparum*. *Science, 299*(5607), 705-708. https://doi.org/doi:10.1126/science.1078599

Gallagher, J. R., Matthews, K. A., & Prigge, S. T. (2011). *Plasmodium falciparum* apicoplast transit peptides are unstructured *in vitro* and during apicoplast import. *Traffic, 12*(9), 1124-1138. https://doi.org/https://doi.org/10.1111/j.1600-0854.2011.01232.x

Gallagher, J. R., & Prigge, S. T. (2010). *Plasmodium falciparum* acyl carrier protein crystal structures in disulfide-linked and reduced states and their prevalence during blood stage growth. *Proteins: Structure, Function, and Bioinformatics, 78*(3), 575-588. https://doi.org/https://doi.org/10.1002/prot.22582

Ganesan, S. M., Falla, A., Goldfless, S. J., Nasamu, A. S., & Niles, J. C. (2016). Synthetic RNA–protein modules integrated with native translation mechanisms to control gene expression in malaria parasites. *Nat Commun, 7*(1), 10727. https://doi.org/10.1038/ncomms10727

1237 Ghorbal, M., Gorman, M., Macpherson, C. R., Martins, R. M., Scherf, A., & Lopez-Rubio, J.-J.
1238 (2014). Genome editing in the human malaria parasite *Plasmodium falciparum* using the
1239 CRISPR-Cas9 system. *Nat Biotechnol, 32*(8), 819-821. https://doi.org/10.1038/nbt.2925
1240
1241 Gisselberg, J. E., Dellibovi-Ragheb, T. A., Matthews, K. A., Bosch, G., & Prigge, S. T. (2013).
1242 The Suf iron-sulfur cluster synthesis pathway is required for apicoplast maintenance in
1243 malaria parasites. *PLoS Pathog, 9*(9), e1003655.
1244 https://doi.org/10.1371/journal.ppat.1003655
1245
1246 Haussig, J. M., Matuschewski, K., & Kooij, T. W. A. (2013). Experimental genetics of
1247 *Plasmodium berghei* NFU in the apicoplast iron-sulfur cluster biogenesis pathway. *PLOS*
1248 *ONE, 8*(6), e67269. https://doi.org/10.1371/journal.pone.0067269
1249
1250 Haussig, J. M., Matuschewski, K., & Kooij, T. W. A. (2014). Identification of vital and
1251 dispensable sulfur utilization factors in the *Plasmodium* apicoplast. *PLOS ONE, 9*(2),
1252 e89718. https://doi.org/10.1371/journal.pone.0089718
1253
1254 Hidese, R., Mihara, H., & Esaki, N. (2011). Bacterial cysteine desulfurases: versatile key players
1255 in biosynthetic pathways of sulfur-containing biofactors. *Appl Microbiol Biotechnol,*
1256 *91*(1), 47-61. https://doi.org/10.1007/s00253-011-3336-x
1257
1258 Hirabayashi, K., Yuda, E., Tanaka, N., Katayama, S., Iwasaki, K., Matsumoto, T., Kurisu, G.,
1259 Outten, F. W., Fukuyama, K., Takahashi, Y., & Wada, K. (2015). Functional dynamics
1260 revealed by the structure of the SufBCD complex, a novel ATP-binding cassette (ABC)
1261 protein that serves as a scaffold for iron-sulfur cluster biogenesis. *J Biol Chem, 290*(50),
1262 29717-29731. https://doi.org/10.1074/jbc.M115.680934
1263
1264 Hu, X., Kato, Y., Sumida, A., Tanaka, A., & Tanaka, R. (2017). The $SUFBC_2D$ complex is
1265 required for the biogenesis of all major classes of plastid Fe-S proteins. *Plant J, 90*(2),
1266 235-248. https://doi.org/https://doi.org/10.1111/tpj.13483
1267
1268 Hu, X., Page, M. T., Sumida, A., Tanaka, A., Terry, M. J., & Tanaka, R. (2017). The iron–sulfur
1269 cluster biosynthesis protein SUFB is required for chlorophyll synthesis, but not
1270 phytochrome signaling. *Plant J, 89*(6), 1184-1194.
1271 https://doi.org/https://doi.org/10.1111/tpj.13455
1272
1273 Huet, G., Daffé, M., & Saves, I. (2005). Identification of the *Mycobacterium tuberculosis* SUF
1274 machinery as the exclusive mycobacterial system of [Fe-S] cluster assembly: evidence
1275 for Its implication in the pathogen's survival. *J Bacteriol, 187*(17), 6137-6146.
1276 https://doi.org/doi:10.1128/JB.187.17.6137-6146.2005
1277
1278 Ikeuchi, Y., Shigi, N., Kato, J.-i., Nishimura, A., & Suzuki, T. (2006). Mechanistic insights into
1279 sulfur relay by multiple sulfur mediators involved in Thiouridine biosynthesis at tRNA
1280 wobble positions. *Mol Cell, 21*(1), 97-108.
1281 https://doi.org/https://doi.org/10.1016/j.molcel.2005.11.001
1282

Jomaa, H., Wiesner, J., Sanderbrand, S., Altincicek, B., Weidemeyer, C., Hintz, M., Türbachova, I., Eberl, M., Zeidler, J., Lichtenthaler, H. K., Soldati, D., & Beck, E. (1999). Inhibitors of the nonmevalonate pathway of isoprenoid biosynthesis as antimalarial drugs. *Science, 285*(5433), 1573-1576. https://doi.org/doi:10.1126/science.285.5433.1573

Ke, H., Sigala, P. A., Miura, K., Morrisey, J. M., Mather, M. W., Crowley, J. R., Henderson, J. P., Goldberg, D. E., Long, C. A., & Vaidya, A. B. (2014). The heme biosynthesis pathway is essential for *Plasmodium falciparum* development in mosquito stage but not in blood stages. *J Biol Chem, 289*(50), 34827-34837. https://doi.org/https://doi.org/10.1074/jbc.M114.615831

Kobayashi, K., Ehrlich, S. D., Albertini, A., Amati, G., Andersen, K. K., Arnaud, M., Asai, K., Ashikaga, S., Aymerich, S., Bessieres, P., Boland, F., Brignell, S. C., Bron, S., Bunai, K., Chapuis, J., Christiansen, L. C., Danchin, A., Débarbouillé, M., Dervyn, E., Deuerling, E., Devine, K., Devine, S. K., Dreesen, O., Errington, J., Fillinger, S., Foster, S. J., Fujita, Y., Galizzi, A., Gardan, R., Eschevins, C., Fukushima, T., Haga, K., Harwood, C. R., Hecker, M., Hosoya, D., Hullo, M. F., Kakeshita, H., Karamata, D., Kasahara, Y., Kawamura, F., Koga, K., Koski, P., Kuwana, R., Imamura, D., Ishimaru, M., Ishikawa, S., Ishio, I., Le Coq, D., Masson, A., Mauël, C., Meima, R., Mellado, R. P., Moir, A., Moriya, S., Nagakawa, E., Nanamiya, H., Nakai, S., Nygaard, P., Ogura, M., Ohanan, T., O'Reilly, M., O'Rourke, M., Pragai, Z., Pooley, H. M., Rapoport, G., Rawlins, J. P., Rivas, L. A., Rivolta, C., Sadaie, A., Sadaie, Y., Sarvas, M., Sato, T., Saxild, H. H., Scanlan, E., Schumann, W., Seegers, J. F. M. L., Sekiguchi, J., Sekowska, A., Séror, S. J., Simon, M., Stragier, P., Studer, R., Takamatsu, H., Tanaka, T., Takeuchi, M., Thomaides, H. B., Vagner, V., van Dijl, J. M., Watabe, K., Wipat, A., Yamamoto, H., Yamamoto, M., Yamamoto, Y., Yamane, K., Yata, K., Yoshida, K., Yoshikawa, H., Zuber, U., & Ogasawara, N. (2003). Essential *Bacillus subtilis* genes. *Proc Natl Acad Sci U S A, 100*(8), 4678-4683. https://doi.org/doi:10.1073/pnas.0730515100

Köhler, S., Delwiche, C. F., Denny, P. W., Tilney, L. G., Webster, P., Wilson, R. J. M., Palmer, J. D., & Roos, D. S. (1997). A plastid of probable green algal origin in apicomplexan parasites. *Science, 275*(5305), 1485-1489. https://doi.org/doi:10.1126/science.275.5305.1485

Kumar, B., Chaubey, S., Shah, P., Tanveer, A., Charan, M., Siddiqi, M. I., & Habib, S. (2011). Interaction between sulphur mobilisation proteins SufB and SufC: evidence for an iron–sulphur cluster biogenesis pathway in the apicoplast of *Plasmodium falciparum*. *Int J Parasitol, 41*(9), 991-999. https://doi.org/https://doi.org/10.1016/j.ijpara.2011.05.006

Leimkühler, S., Bühning, M., & Beilschmidt, L. (2017). Shared sulfur mobilization routes for tRNA Thiolation and Molybdenum cofactor biosynthesis in prokaryotes and eukaryotes. *Biomolecules, 7*(1), 5. https://www.mdpi.com/2218-273X/7/1/5

Lill, R. (2009). Function and biogenesis of iron–sulphur proteins. *Nature, 460*(7257), 831-838. https://doi.org/10.1038/nature08301

Loiseau, L., Ollagnier-de-Choudens, S., Nachin, L., Fontecave, M., & Barras, F. (2003). Biogenesis of Fe-S cluster by the bacterial Suf System: SufS and SufE form a new type of cysteine desulfurase. *J Biol Chem, 278*(40), 38352-38359. https://doi.org/https://doi.org/10.1074/jbc.M305953200

Lu, Y. (2018). Assembly and transfer of iron–sulfur clusters in the plastid. *Front Plant Sci, 9*. https://doi.org/10.3389/fpls.2018.00336

Manders, E. M. M., Verbeek, F. J., & Aten, J. A. (1993). Measurement of co-localization of objects in dual-colour confocal images. *J Microsc, 169*(3), 375-382. https://doi.org/https://doi.org/10.1111/j.1365-2818.1993.tb03313.x

McFadden, G. I., Reith, M. E., Munholland, J., & Lang-Unnasch, N. (1996). Plastid in human parasites. *Nature, 381*(6582), 482-482. https://doi.org/10.1038/381482a0

Mihara, H., & Esaki, N. (2002). Bacterial cysteine desulfurases: their function and mechanisms. *Appl Microbiol Biotechnol, 60*(1), 12-23. https://doi.org/10.1007/s00253-002-1107-4

Mueller, E. G. (2006). Trafficking in persulfides: delivering sulfur in biosynthetic pathways. *Nat Chem Biol, 2*(4), 185-194. https://doi.org/10.1038/nchembio779

Murthy, U. M. N., Ollagnier-de-Choudens, S., Sanakis, Y., Abdel-Ghany, S. E., Rousset, C., Ye, H., Fontecave, M., Pilon-Smits, E. A. H., & Pilon, M. (2007). Characterization of *Arabidopsis thaliana* SufE2 and SufE3: functions in chloroplast iron-sulfur cluster assembly and NAD synthesis. *J Biol Chem, 282*(25), 18254-18264. https://doi.org/https://doi.org/10.1074/jbc.M701428200

Nakai, Y., Umeda, N., Suzuki, T., Nakai, M., Hayashi, H., Watanabe, K., & Kagamiyama, H. (2004). Yeast Nfs1p is involved in Thio-modification of both mitochondrial and cytoplasmic tRNAs. *J Biol Chem, 279*(13), 12363-12368. https://doi.org/https://doi.org/10.1074/jbc.M312448200

Ng, C. S., Sinha, A., Aniweh, Y., Nah, Q., Babu, I. R., Gu, C., Chionh, Y. H., Dedon, P. C., & Preiser, P. R. (2018). tRNA epitranscriptomics and biased codon are linked to proteome expression in *Plasmodium falciparum*. *Mol Syst Biol, 14*(10), e8009. https://doi.org/https://doi.org/10.15252/msb.20178009

Nkrumah, L. J., Muhle, R. A., Moura, P. A., Ghosh, P., Hatfull, G. F., Jacobs, W. R., & Fidock, D. A. (2006). Efficient site-specific integration in *Plasmodium falciparum* chromosomes mediated by mycobacteriophage Bxb1 integrase. *Nat Methods, 3*(8), 615-621. https://doi.org/10.1038/nmeth904

Numata, T., Ikeuchi, Y., Fukai, S., Suzuki, T., & Nureki, O. (2006). Snapshots of tRNA sulphuration via an adenylated intermediate. *Nature, 442*(7101), 419-424. https://doi.org/10.1038/nature04896

1375 Ollagnier-de-Choudens, S., Lascoux, D., Loiseau, L., Barras, F., Forest, E., & Fontecave, M.
1376 (2003). Mechanistic studies of the SufS–SufE cysteine desulfurase: evidence for sulfur
1377 transfer from SufS to SufE. *FEBS Lett, 555*(2), 263-267.
1378 https://doi.org/https://doi.org/10.1016/S0014-5793(03)01244-4
1379
1380 Outten, F. W., Wood, M. J., Muñoz, F. M., & Storz, G. (2003). The SufE protein and the
1381 SufBCD complex enhance SufS cysteine desulfurase activity as part of a sulfur transfer
1382 pathway for Fe-S cluster assembly in *Escherichia coli*. *J Biol Chem, 278*(46), 45713-
1383 45719. https://doi.org/https://doi.org/10.1074/jbc.M308004200
1384
1385 Pala, Z. R., Saxena, V., Saggu, G. S., & Garg, S. (2018). Recent advances in the [Fe–S] cluster
1386 biogenesis (SUF) pathway functional in the apicoplast of *Plasmodium*. *Trends Parasitol,*
1387 *34*(9), 800-809. https://doi.org/https://doi.org/10.1016/j.pt.2018.05.010
1388
1389 Pamukcu, S., Cerutti, A., Bordat, Y., Hem, S., Rofidal, V., & Besteiro, S. (2021). Differential
1390 contribution of two organelles of endosymbiotic origin to iron-sulfur cluster synthesis
1391 and overall fitness in *Toxoplasma*. *PLoS Pathog, 17*(11), e1010096.
1392 https://doi.org/10.1371/journal.ppat.1010096
1393
1394 Pilon-Smits, E. A. H., Garifullina, G. F., Abdel-Ghany, S., Kato, S.-I., Mihara, H., Hale, K. L.,
1395 Burkhead, J. L., Esaki, N., Kurihara, T., & Pilon, M. (2002). Characterization of a NifS-
1396 like chloroplast protein from *Arabidopsis*. Implications for its role in sulfur and selenium
1397 metabolism. *Plant Physiol, 130*(3), 1309-1318. https://doi.org/10.1104/pp.102.010280
1398
1399 Przybyla-Toscano, J., Roland, M., Gaymard, F., Couturier, J., & Rouhier, N. (2018). Roles and
1400 maturation of iron–sulfur proteins in plastids. *J Biol Inorg Chem, 23*(4), 545-566.
1401 https://doi.org/10.1007/s00775-018-1532-1
1402
1403 Py, B., Gerez, C., Angelini, S., Planel, R., Vinella, D., Loiseau, L., Talla, E., Brochier-Armanet,
1404 C., Garcia Serres, R., Latour, J.-M., Ollagnier-de Choudens, S., Fontecave, M., & Barras,
1405 F. (2012). Molecular organization, biochemical function, cellular role and evolution of
1406 NfuA, an atypical Fe-S carrier. *Mol Microbiol, 86*(1), 155-171.
1407 https://doi.org/https://doi.org/10.1111/j.1365-2958.2012.08181.x
1408
1409 Rajaram, K., Liu, H. B., & Prigge, S. T. (2020). Redesigned TetR-Aptamer system to control
1410 gene expression in *Plasmodium falciparum*. *mSphere, 5*(4), e00457-00420.
1411 https://doi.org/doi:10.1128/mSphere.00457-20
1412
1413 Ralph, S. A., van Dooren, G. G., Waller, R. F., Crawford, M. J., Fraunholz, M. J., Foth, B. J.,
1414 Tonkin, C. J., Roos, D. S., & McFadden, G. I. (2004). Metabolic maps and functions of
1415 the Plasmodium falciparum apicoplast. *Nat Rev Microbiol, 2*(3), 203-216.
1416 https://doi.org/10.1038/nrmicro843
1417
1418 Roberts, A. D., Nair, S. C., Guerra, A. J., & Prigge, S. T. (2019). Development of a conditional
1419 localization approach to control apicoplast protein trafficking in malaria parasites.
1420 *Traffic, 20*(8), 571-582. https://doi.org/https://doi.org/10.1111/tra.12656

Rouault, T. A. (2019). The indispensable role of mammalian iron sulfur proteins in function and regulation of multiple diverse metabolic pathways. *BioMetals, 32*(3), 343-353. https://doi.org/10.1007/s10534-019-00191-7

Sadik, M., Afsar, M., Ramachandran, R., & Habib, S. (2021). [Fe–S] biogenesis and unusual assembly of the ISC scaffold complex in the *Plasmodium falciparum* mitochondrion. *Mol Microbiol, 116*(2), 606-623. https://doi.org/https://doi.org/10.1111/mmi.14735

Saini, A., Mapolelo, D. T., Chahal, H. K., Johnson, M. K., & Outten, F. W. (2010). SufD and SufC ATPase activity are required for iron acquisition during *in vivo* Fe-S cluster formation on SufB. *Biochemistry, 49*(43), 9402-9412. https://doi.org/10.1021/bi1011546

Seeber, F. (2002). Biogenesis of iron–sulphur clusters in amitochondriate and apicomplexan protists. *Int J Parasitol, 32*(10), 1207-1217. https://doi.org/https://doi.org/10.1016/S0020-7519(02)00022-X

Shears, M. J., Botté, C. Y., & McFadden, G. I. (2015). Fatty acid metabolism in the *Plasmodium* apicoplast: drugs, doubts and knockouts. *Mol Biochem Parasitol, 199*(1), 34-50. https://doi.org/https://doi.org/10.1016/j.molbiopara.2015.03.004

Shigi, N. (2014). Biosynthesis and functions of sulfur modifications in tRNA. *Front Genet, 5*. https://doi.org/10.3389/fgene.2014.00067

Shigi, N. (2018). Recent advances in our understanding of the biosynthesis of sulfur modifications in tRNAs. *Front Microbiol, 9*. https://doi.org/10.3389/fmicb.2018.02679

Shigi, N., Horitani, M., Miyauchi, K., Suzuki, T., & Kuroki, M. (2020). An ancient type of MnmA protein is an iron–sulfur cluster-dependent sulfurtransferase for tRNA anticodons. *RNA, 26*(3), 240-250. https://doi.org/10.1261/rna.072066.119

Spalding, M. D., Allary, M., Gallagher, J. R., & Prigge, S. T. (2010). Validation of a modified method for Bxb1 mycobacteriophage integrase-mediated recombination in *Plasmodium falciparum* by localization of the H-protein of the glycine cleavage complex to the mitochondrion. *Mol Biochem Parasitol, 172*(2), 156-160. https://doi.org/https://doi.org/10.1016/j.molbiopara.2010.04.005

Swift, R. P., Rajaram, K., Elahi, R., Liu, H. B., & Prigge, S. T. (2022). Roles of ferredoxin-dependent proteins in the apicoplast of *Plasmodium falciparum* parasites. *mBio, 13*(1), e03023-03021. https://doi.org/doi:10.1128/mbio.03023-21

Swift, R. P., Rajaram, K., Liu, H. B., Dziedzic, A., Jedlicka, A. E., Roberts, A. D., Matthews, K. A., Jhun, H., Bumpus, N. N., Tewari, S. G., Wallqvist, A., & Prigge, S. T. (2020). A mevalonate bypass system facilitates elucidation of plastid biology in malaria parasites. *PLoS Pathog, 16*(2), e1008316. https://doi.org/10.1371/journal.ppat.1008316

Swift, R. P., Rajaram, K., Liu, H. B., & Prigge, S. T. (2021). Dephospho-CoA kinase, a nuclear-encoded apicoplast protein, remains active and essential after *Plasmodium falciparum* apicoplast disruption. *EMBO J, 40*(16), e107247. https://doi.org/https://doi.org/10.15252/embj.2020107247

Tewari, S. G., Kwan, B., Elahi, R., Rajaram, K., Reifman, J., Prigge, S. T., Vaidya, A. B., & Wallqvist, A. (2022). Metabolic adjustments of blood-stage *Plasmodium falciparum* in response to sublethal pyrazoleamide exposure. *Sci Rep, 12*(1), 1167. https://doi.org/10.1038/s41598-022-04985-7

Urbonavičius, J., Qian, Q., Durand, J. M. B., Hagervall, T. G., & Björk, G. R. (2001). Improvement of reading frame maintenance is a common function for several tRNA modifications. *EMBO J, 20*(17), 4863-4873. https://doi.org/https://doi.org/10.1093/emboj/20.17.4863

Wilson, R. J. M., Denny, P. W., Preiser, P. R., Rangachari, K., Roberts, K., Roy, A., Whyte, A., Strath, M., Moore, D. J., Moore, P. W., & Williamson, D. H. (1996). Complete gene map of the plastid-like DNA of the malaria parasite *Plasmodium falciparum*. *J Mol Biol, 261*(2), 155-172. https://doi.org/https://doi.org/10.1006/jmbi.1996.0449

Wollers, S., Layer, G., Garcia-Serres, R., Signor, L., Clemancey, M., Latour, J.-M., Fontecave, M., & Ollagnier de Choudens, S. (2010). Iron-sulfur (Fe-S) cluster assembly: the SufBCD complex is a new type of Fe-S scaffold with a falvin redox cofactor. *J Biol Chem, 285*(30), 23331-23341. https://doi.org/https://doi.org/10.1074/jbc.M110.127449

Yang, Y., Lin, M., Chen, X., Zhao, X., Chen, L., Zhao, M., Yao, C., Sheng, K., Yang, Y., Ma, G., & Du, A. (2022). The first apicoplast tRNA thiouridylase plays a vital role in the growth of *Toxoplasma gondii*. *Front Cell Infect Microbiol, 12*. https://doi.org/10.3389/fcimb.2022.947039

Ye, H., Abdel-Ghany, S. E., Anderson, T. D., Pilon-Smits, E. A. H., & Pilon, M. (2006). CpSufE activates the cysteine desulfurase CpNifS for chloroplastic Fe-S cluster formation. *J Biol Chem, 281*(13), 8958-8969. https://doi.org/https://doi.org/10.1074/jbc.M512737200

Yeh, E., & DeRisi, J. L. (2011). Chemical rescue of malaria parasites lacking an apicoplast defines organelle function in blood-stage *Plasmodium falciparum*. *PLoS Biol, 9*(8), e1001138. https://doi.org/10.1371/journal.pbio.1001138

Yuda, E., Tanaka, N., Fujishiro, T., Yokoyama, N., Hirabayashi, K., Fukuyama, K., Wada, K., & Takahashi, Y. (2017). Mapping the key residues of SufB and SufD essential for biosynthesis of iron-sulfur clusters. *Sci Rep, 7*(1), 9387. https://doi.org/10.1038/s41598-017-09846-2

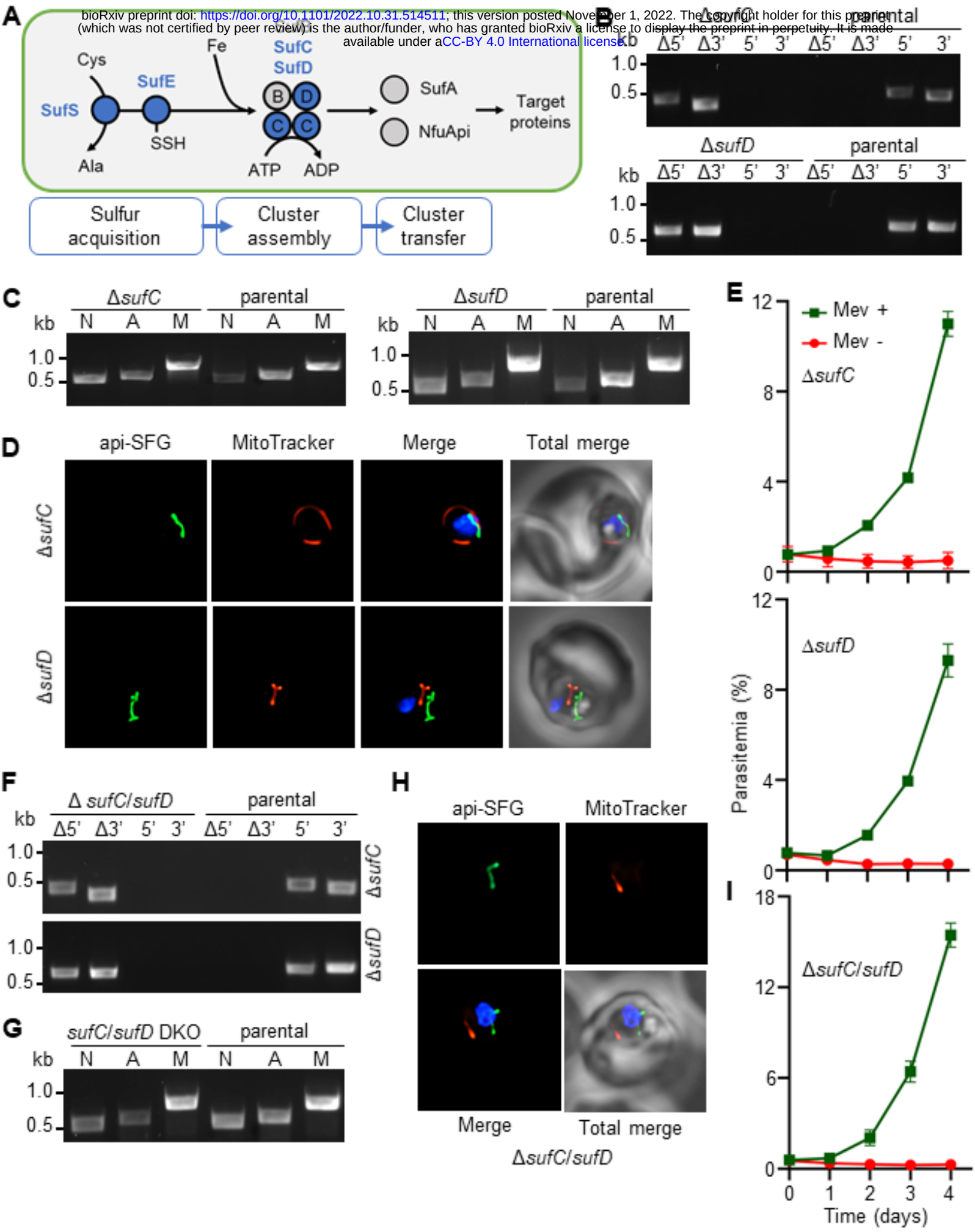

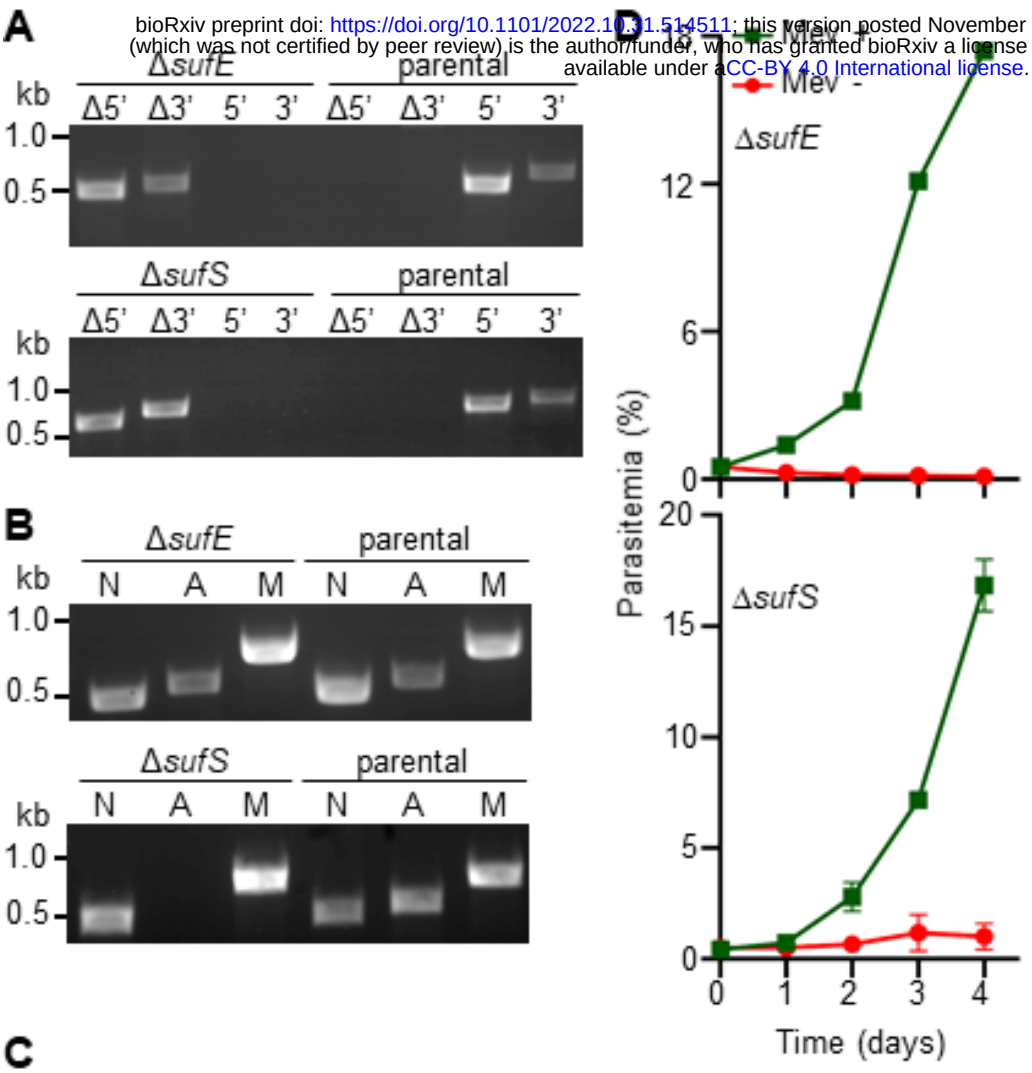

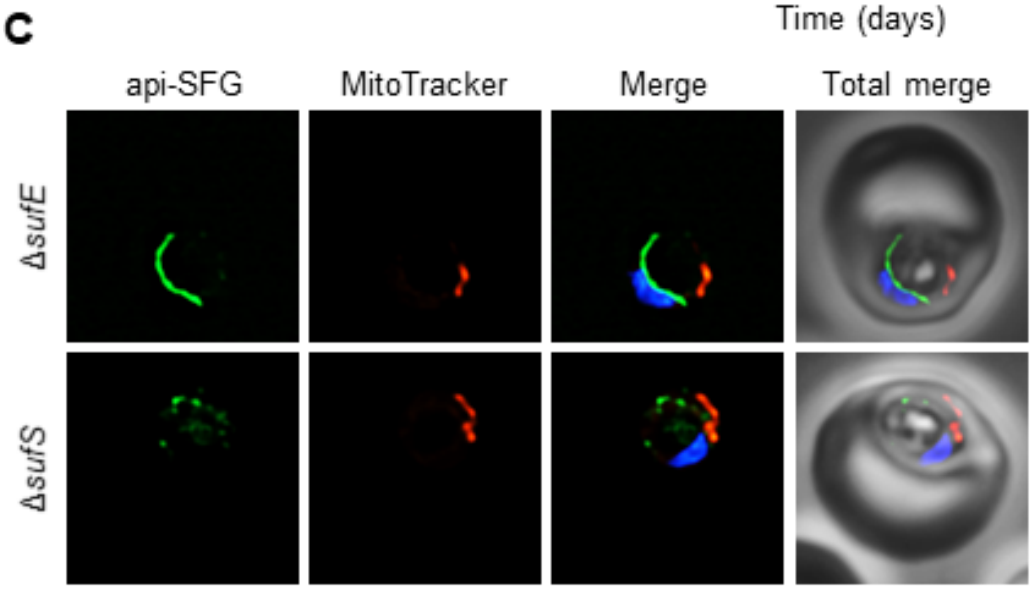

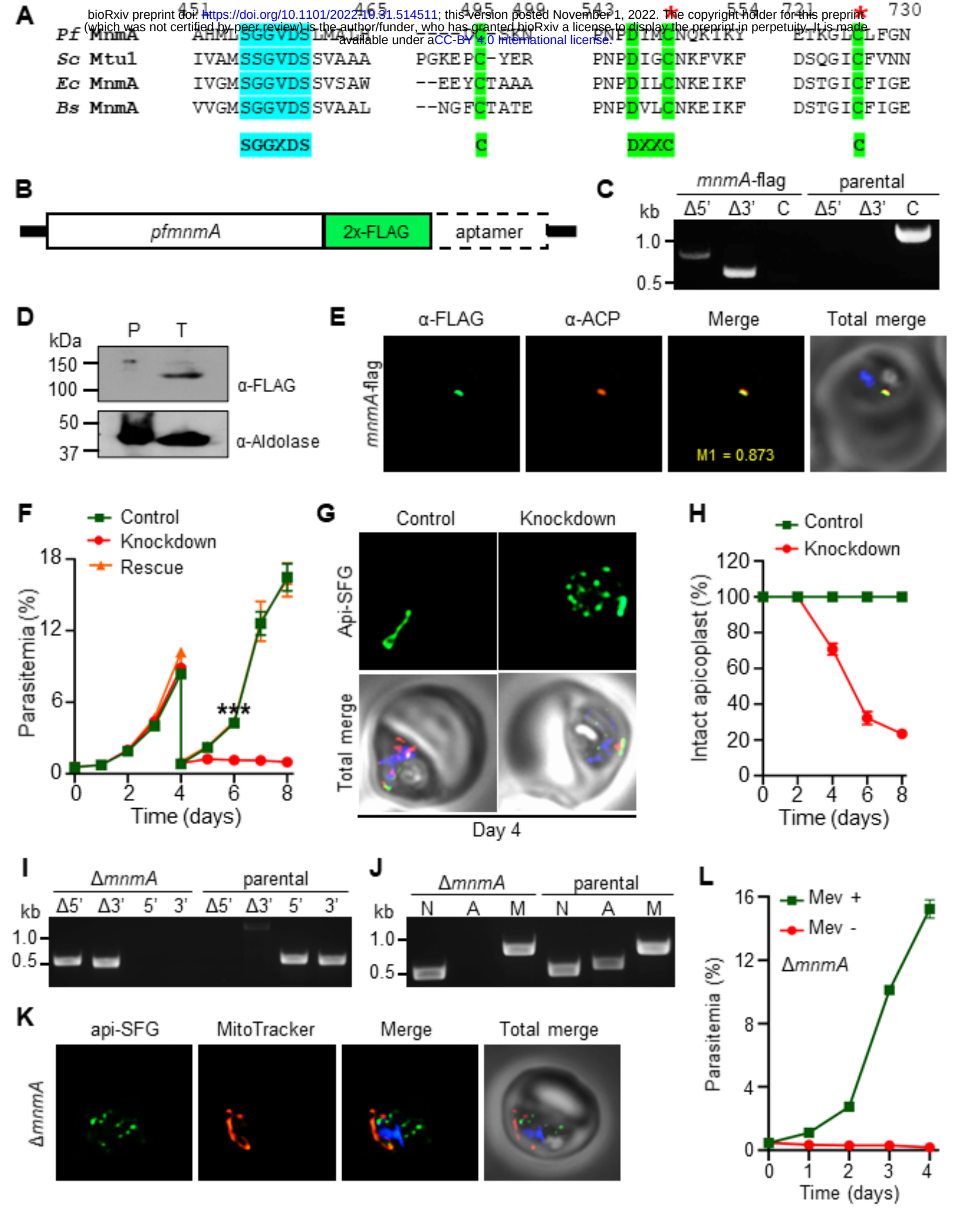

A

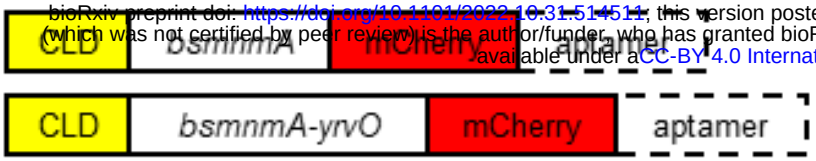

B

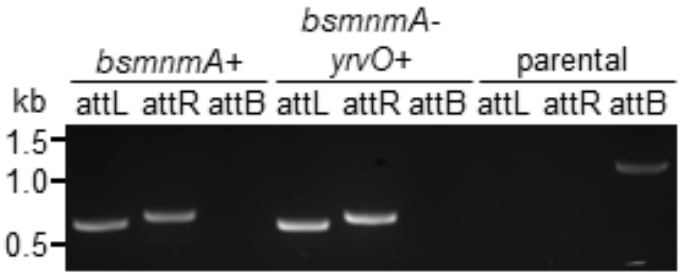

C

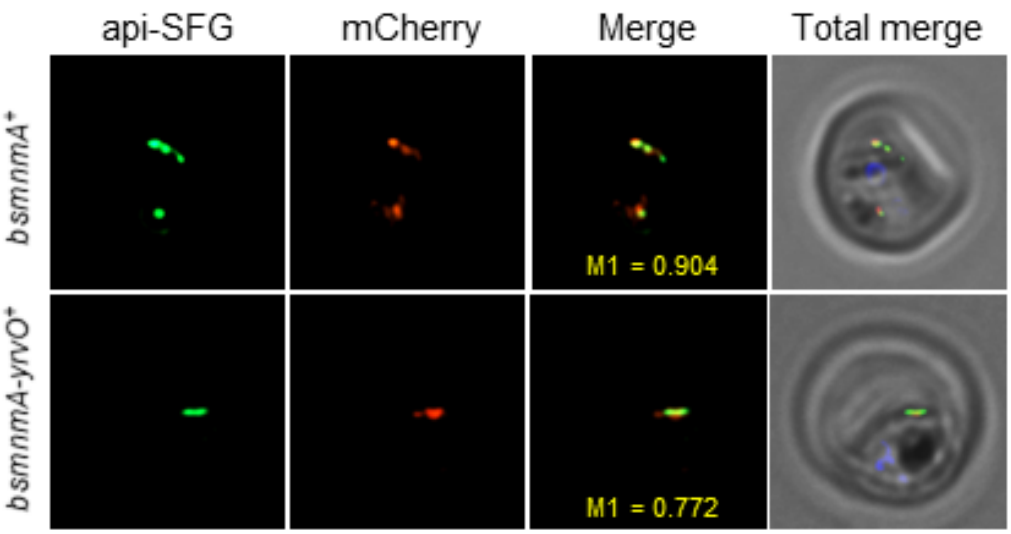

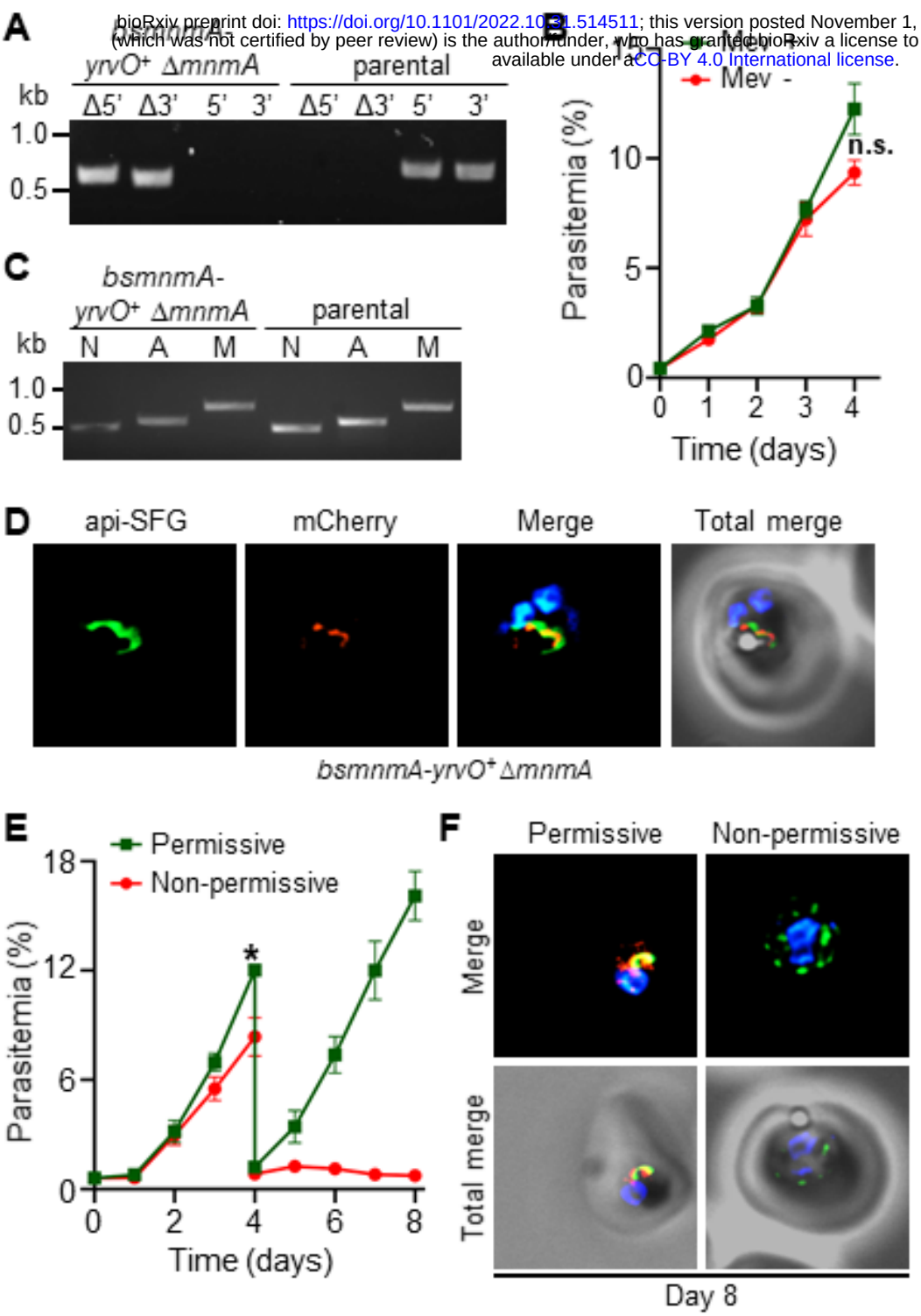

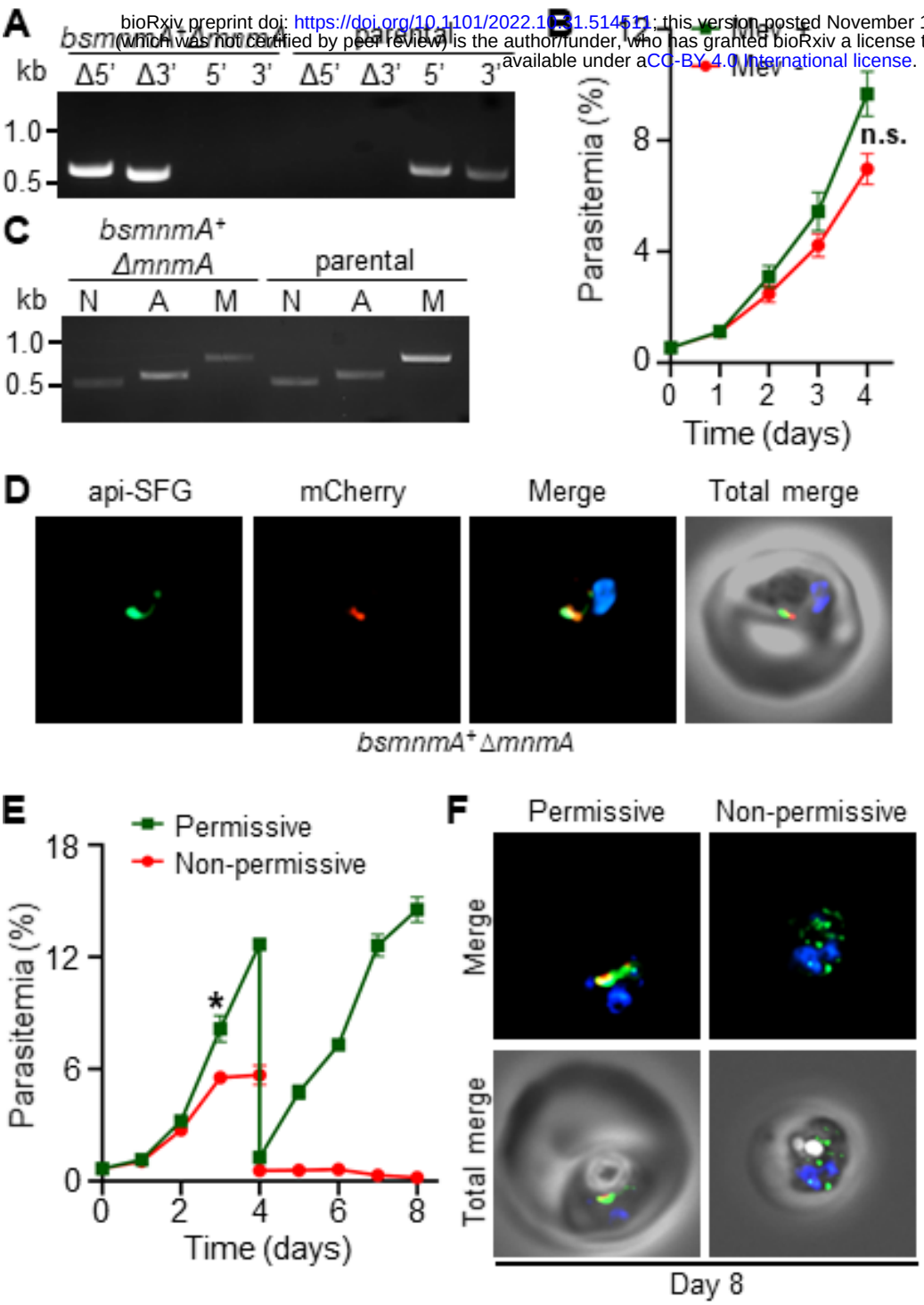

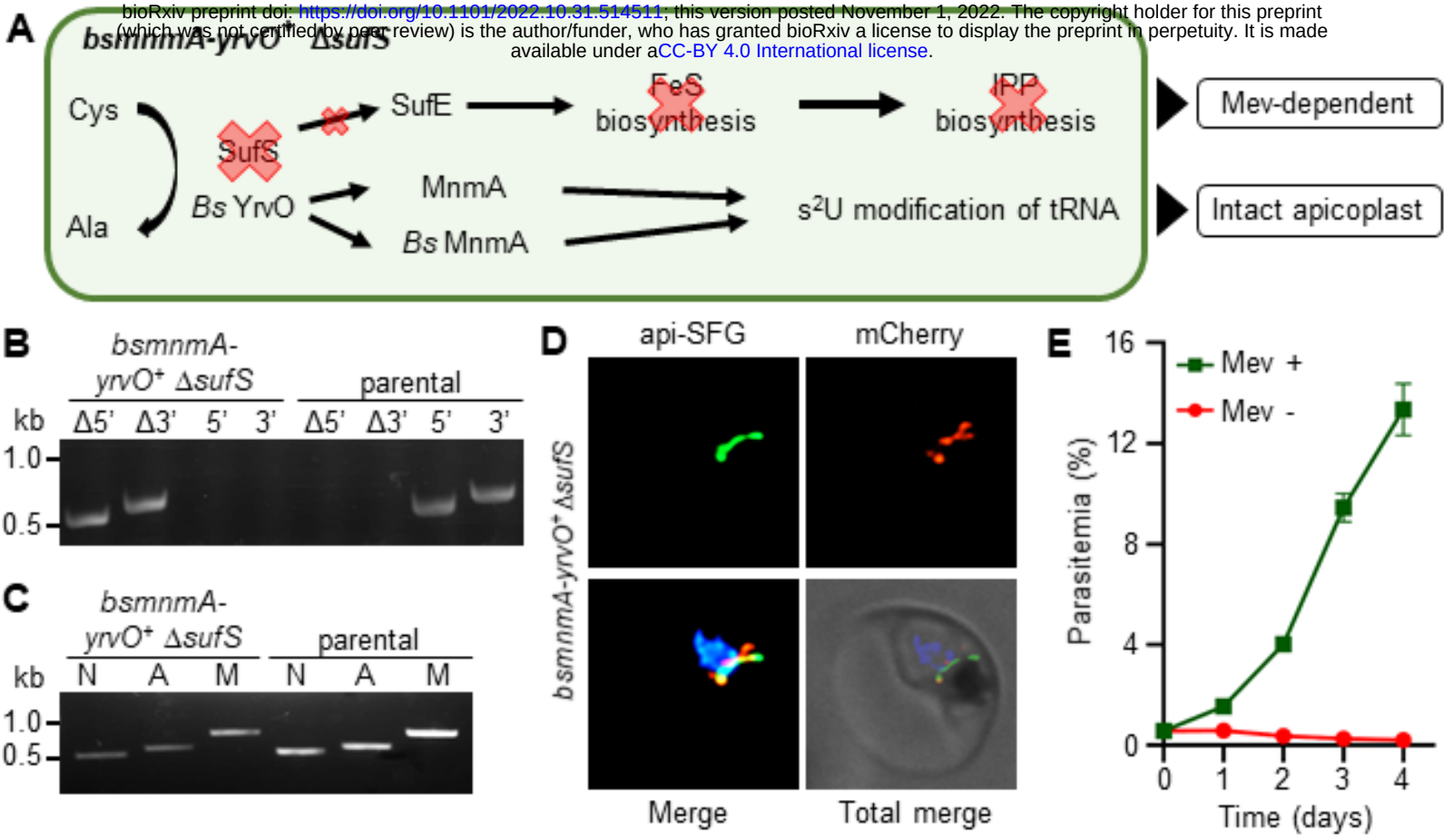

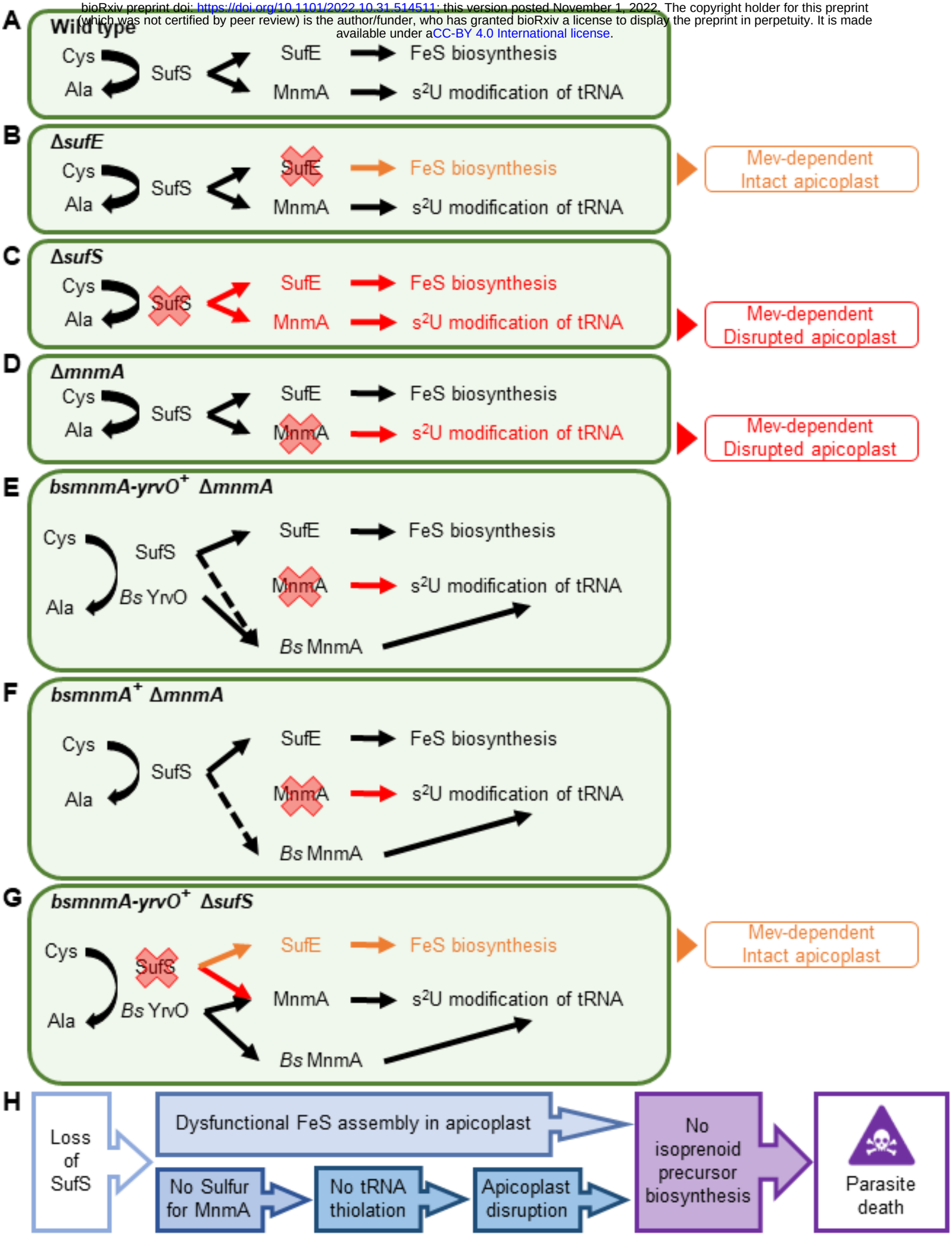

A

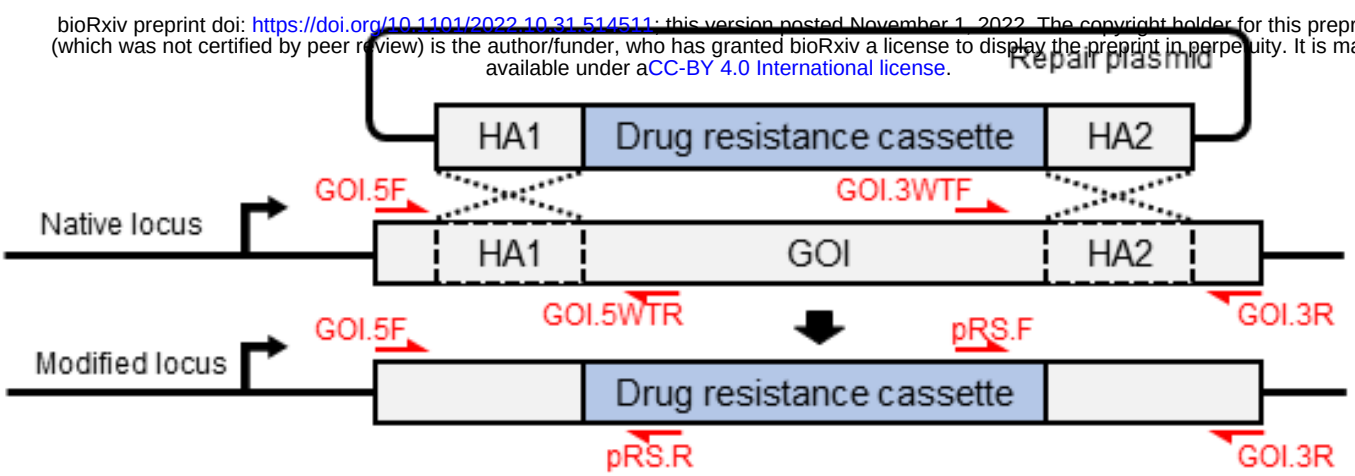

B

PCR reaction	Primer combination		Parasite line
	Forward	Reverse	
Δ5'	GOI.5F	pRS.R	Gene knockout lines
Δ3'	pRS.F	GOI.3R	
5'	GOI.5F	GOI.5WTR	
3'	GOI.3WTF	GOI.3R	
Δ5'	GOI.5F	pRS.R	PfMev (parental)
Δ3'	pRS.F	GOI.3R	
5'	GOI.5F	GOI.5WTR	
3'	GOI.3WTF	GOI.3R	

C

	Anticipated amplicon sizes (bp)			
Gene of interest	Δ5'	Δ3'	5'	3'
sufC	467	389	486	457
sufD	593	582	636	649
sufE	490	543	556	656
sufS	584	677	691	754
mnmA	605	577	626	617

Figure 1- figure supplement 1

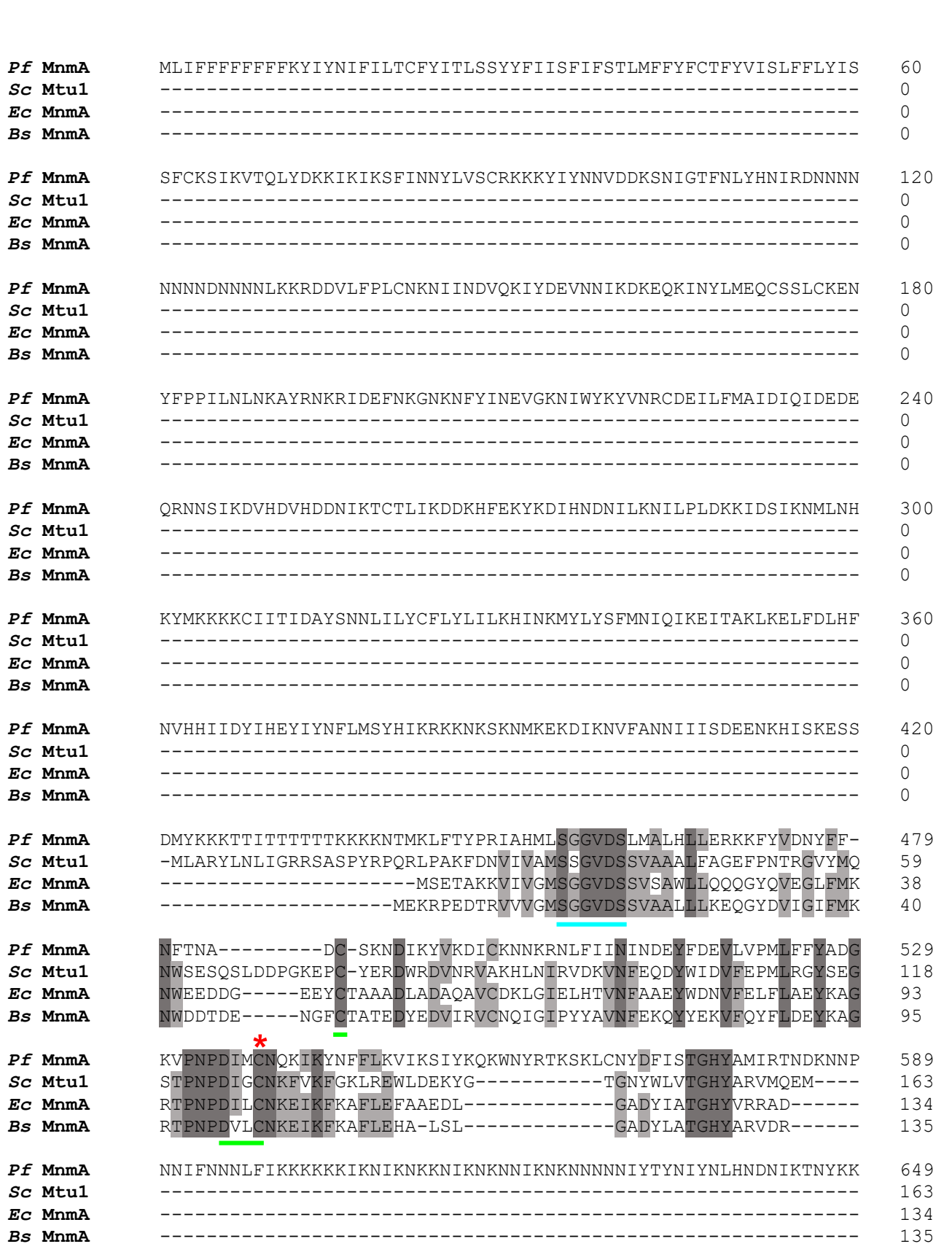
Pf MnmA MLIFFFFFFFFKYIYNIFILTCFYITLSSYYFIISFIFSTLMFFYFCTFYVISLFFLYIS 60
Sc Mtu1 ---------- 0
Ec MnmA ---------- 0
Bs MnmA ---------- 0
Pf MnmA SFCKSIKVTQLYDKKIKIKSFINNYLVSCRKKKYIYNNVDDKSNIGTFNLYHNIRDNNNN 120
Sc Mtu1 ---------- 0
Ec MnmA ---------- 0
Bs MnmA ---------- 0
Pf MnmA NNNNDNNNNLKKRDDVLFPLCNKNIINDVQKIYDEVNNIKDKEQKINYLMEQCSSLCKEN 180
Sc Mtu1 ---------- 0
Ec MnmA ---------- 0
Bs MnmA ---------- 0
Pf MnmA YFPPILNLNKAYRNKRIDEFNKGNKNFYINEVGKNIWYKYVNRCDEILFMAIDIQIDEDE 240
Sc Mtu1 ---------- 0
Ec MnmA ---------- 0
Bs MnmA ---------- 0
Pf MnmA QRNNSIKDVHDVHDDNIKTCTLIKDDKHFEKYKDIHNDNILKNILPLDKKIDSIKNMLNH 300
Sc Mtu1 ---------- 0
Ec MnmA ---------- 0
Bs MnmA ---------- 0
Pf MnmA KYMKKKKCIITIDAYSNNLILYCFLYLILKHINKMYLYSFMNIQIKEITAKLKELFDLHF 360
Sc Mtu1 ---------- 0
Ec MnmA ---------- 0
Bs MnmA ---------- 0
Pf MnmA NVHHIIDYIHEYIYNFLMSYHIKRKKNKSKNMKEKDIKNVFANNIIISDEENKHISKESS 420
Sc Mtu1 ---------- 0
Ec MnmA ---------- 0
Bs MnmA ---------- 0
Pf MnmA DMYKKKTTITTTTTTKKKKNTMKLFTYPRIAHMLSGGVDSLMALHLLERKKFYVDNYFF- 479
Sc Mtu1 -MLARYLNLIGRRSASPYRPQRLPAKFDNVIVAMSSGVDSSVAAALFAGEFPNTRGVYMQ 59
Ec MnmA ----------MSETAKKVIVGMSGGVDSSVSAWLLQQQGYQVEGLFMK 38
Bs MnmA ----------MEKRPEDTRVVVGMSGGVDSSVAALLLKEQGYDVIGIFMK 40
Pf MnmA NFTNA---------DC-SKNDIKYVKDICKNNKRNLFIININDEYFDEVLVPMLFFYADG 529
Sc Mtu1 NWSESQSLDDPGKEPC-YERDWRDVNRVAKHLNIRVDKVNFEQDYWIDVFEPMLRGYSEG 118
Ec MnmA NWEEDDG-----EEYCTAAADLADAQAVCDKLGIELHTVNFAAEYWDNVFELFLAEYKAG 93
Bs MnmA NWDDTDE-----NGFCTATEDYEDVIRVCNQIGIPYYAVNFEKQYYEKVFQYFLDEYKAG 95
Pf MnmA KVPNPDIMCNQKIKYNFFLKVIKSIYKQKWNYRTKSKLCNYDFISTGHYAMIRTNDKNNP 589
Sc Mtu1 STPNPDIGCNKFVKFGKLREWLDEKYG----------TGNYWLVTGHYARVMQEM---- 163
Ec MnmA RTPNPDILCNKEIKFKAFLEFAAEDL----------GADYIATGHYVRRAD------ 134
Bs MnmA RTPNPDVLCNKEIKFKAFLEHA-LSL----------GADYLATGHYARVDR------ 135
Pf MnmA NNIFNNNLFIKKKKKKIKNIKNKKNIKNKNNIKNKNNNNNIYTYNIYNLHNDNIKTNYKK 649
Sc Mtu1 ---------- 163
Ec MnmA ---------- 134
Bs MnmA ---------- 135

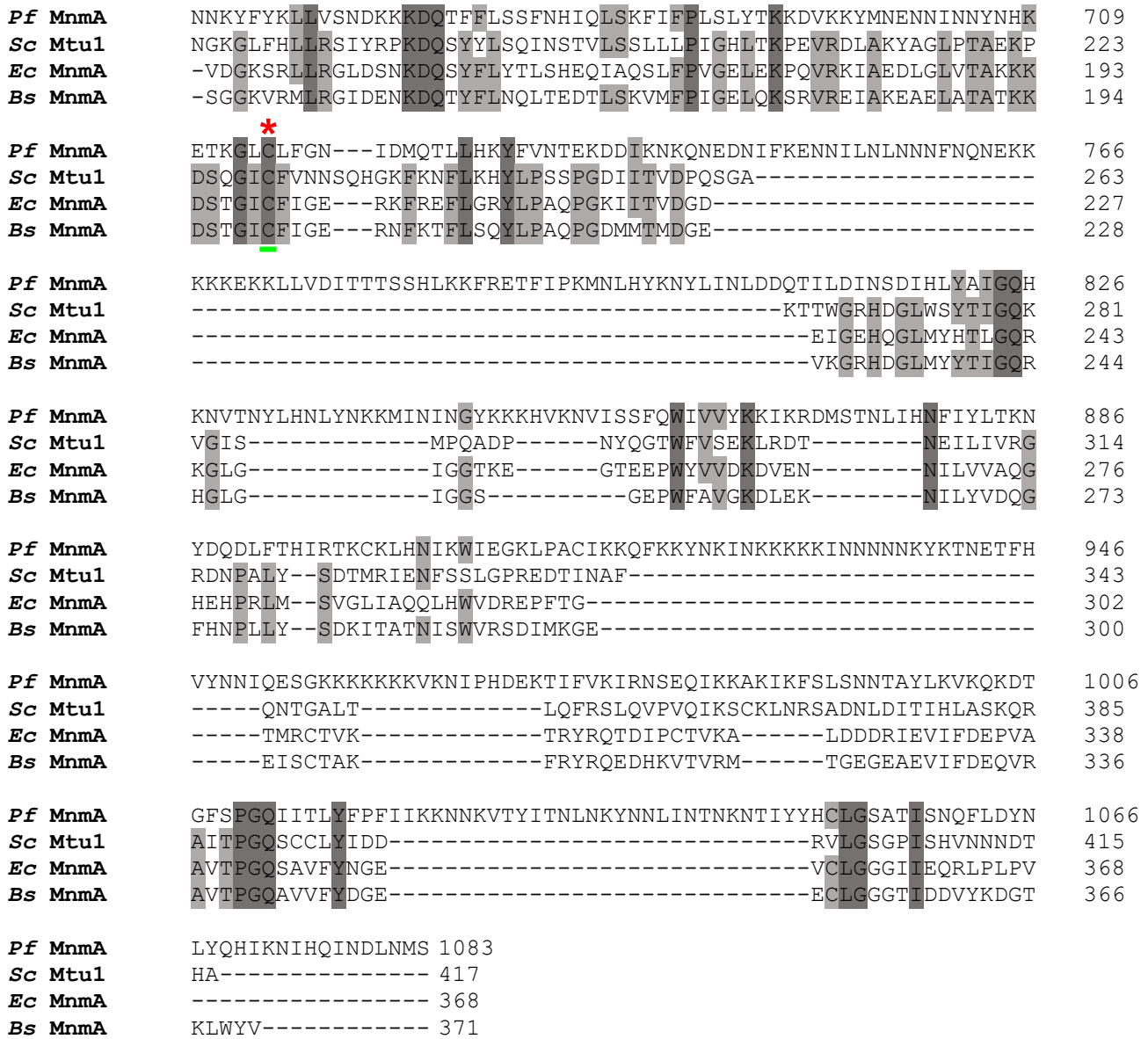

Figure 3- figure supplement 1

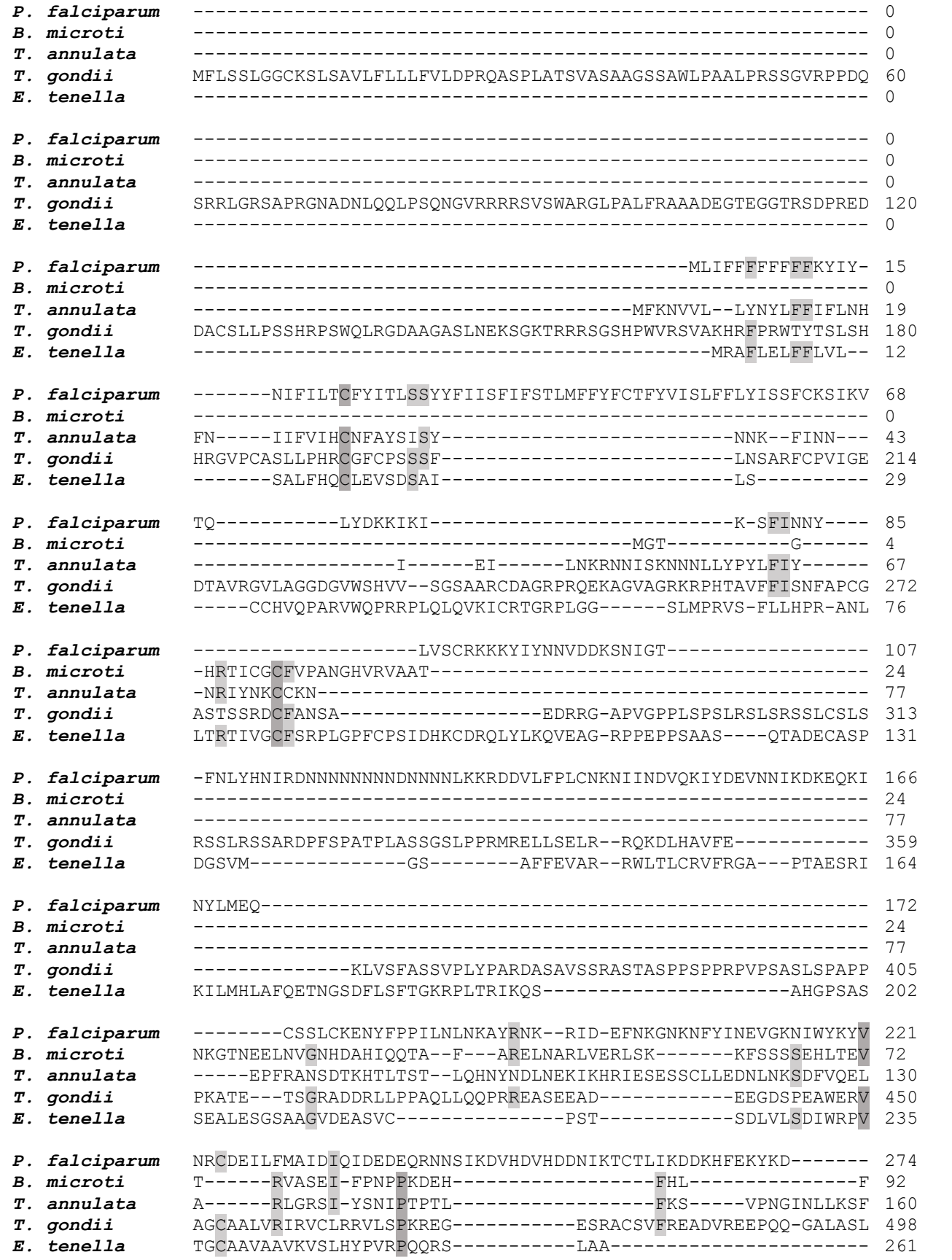
P. falciparum ---------- 0
B. microti ---------- 0
T. annulata ---------- 0
T. gondii MFLSSLGGCKSLSAVLFLLLFVLDPRQASPLATSVASAAGSSAWLPAALPRSSGVRPPDQ 60
E. tenella ---------- 0
P. falciparum ---------- 0
B. microti ---------- 0
T. annulata ---------- 0
T. gondii SRRLGRSAPRGNADNLQQLPSQNGVRRRRSVSWARGLPALFRAAADEGTEGGTRSDPRED 120
E. tenella ---------- 0
P. falciparum ----------MLIFFFFFFFKYIY- 15
B. microti ---------- 0
T. annulata ----------MFKNVVL--LYNYLFFIFLNH 19
T. gondii DACSLLPSSHRPSWQLRGDAAGASLNEKSGKTRRRSGSHPWVRSVAKHRFPRWTYTSLSH 180
E. tenella ----------MRAFLELFFLVL-- 12
P. falciparum -------NIFILTCFYITLSSYYFIISFIFSTLMFFYFCTFYVISLFFLYISSFCKSIKV 68
B. microti ---------- 0
T. annulata FN-----IIFVIHCNFAYSISY----------NNK--FINN--- 43
T. gondii HRGVPCASLLPHRCGFCPSSSF----------LNSARFCPVIGE 214
E. tenella -------SALFHQCLEVSDSAI----------LS---------- 29
P. falciparum TQ----------LYDKKIKI----------K-SFINNY---- 85
B. microti ----------MGT----------G------ 4
T. annulata ----------I------EI------LNKRNNISKNNNLLYPYLFIY------ 67
T. gondii DTAVRGVLAGGDGVWSHVV--SGSAARCDAGRPRQEKAGVAGRKRPHTAVFFISNFAPCG 272
E. tenella -----CCHVQPARVWQPRRPLQLQVKICRTGRPLGG------SLMPRVS-FLLHPR-ANL 76
P. falciparum ----------LVSCRKKKYIYNNVDDKSNIGT---------- 107
B. microti -HRTICGCFVPANGHVRVAAT---------- 24
T. annulata -NRIYNKCCKN---------- 77
T. gondii ASTSSRDCFANSA----------EDRRG-APVGPPLSPSLRSLSRSSLCSLS 313
E. tenella LTRTIVGCFSRPLGPFCPSIDHKCDRQLYLKQVEAG-RPPEPPSAAS----QTADECASP 131
P. falciparum -FNLYHNIRDNNNNNNNNDNNNNLKKRDDVLFPLCNKNIINDVQKIYDEVNNIKDKEQKI 166
B. microti ---------- 24
T. annulata ---------- 77
T. gondii RSSLRSSARDPFSPATPLASSGSLPPRMRELLSELR--RQKDLHAVFE---------- 359
E. tenella DGSVM----------GS--------AFFEVAR--RWLTLCRVFRGA---PTAESRI 164
P. falciparum NYLMEQ---------- 172
B. microti ---------- 24
T. annulata ---------- 77
T. gondii ----------KLVSFASSVPLYPARDASAVSSRASTASPPSPPRPVPSASLSPAPP 405
E. tenella KILMHLAFQETNGSDFLSFTGKRPLTRIKQS----------AHGPSAS 202
P. falciparum --------CSSLCKENYFPPILNLNKAYRNK--RID-EFNKGNKNFYINEVGKNIWYKYV 221
B. microti NKGTNEELNVGNHDAHIQQTA--F---ARELNARLVERLSK-------KFSSSSEHLTEV 72
T. annulata -----EPFRANSDTKHTLTST--LQHNYNDLNEKIKHRIESESSCLLEDNLNKSDFVQEL 130
T. gondii PKATE---TSGRADDRLLPPAQLLQQPRREASEEAD----------EEGDSPEAWERV 450
E. tenella SEALESGSAAGVDEASVC----------PST----------SDLVLSDIWRPV 235
P. falciparum NRCDEILFMAIDIQIDEDEQRNNSIKDVHDVHDDNIKTCTLIKDDKHFEKYKD------- 274
B. microti T------RVASEI-FPNPPKDEH----------FHL----------F 92
T. annulata A------RLGRSI-YSNIPTPTL----------FKS-----VPNGINLLKSF 160
T. gondii AGCAALVRIRVCLRRVLSPKREG----------ESRACSVFREADVREEPQQ-GALASL 498
E. tenella TGCAAVAAVKVSLHYPVRPQQRS----------LAA---------- 261

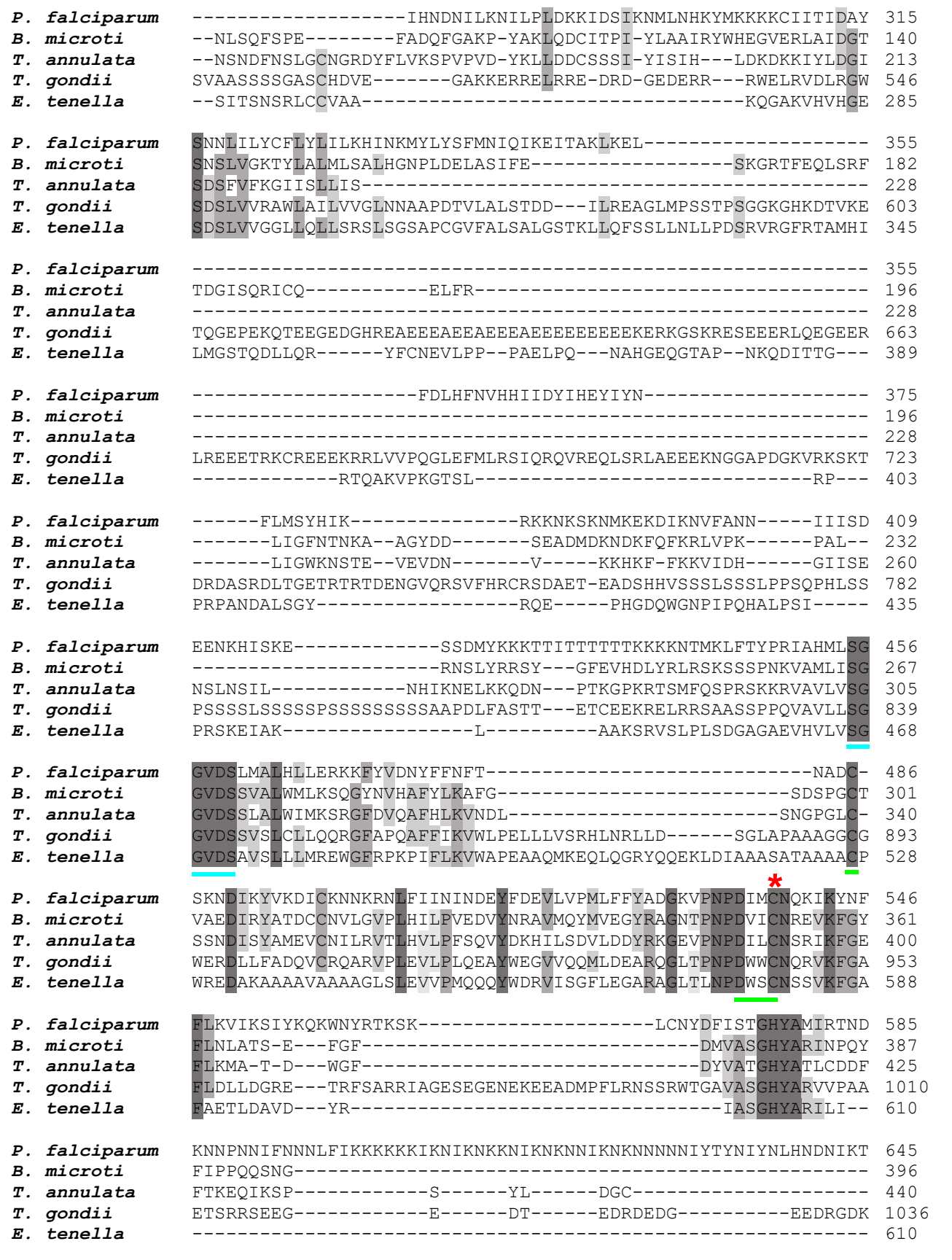
P. falciparum
B. microti
T. annulata
T. gondii
E. tenella

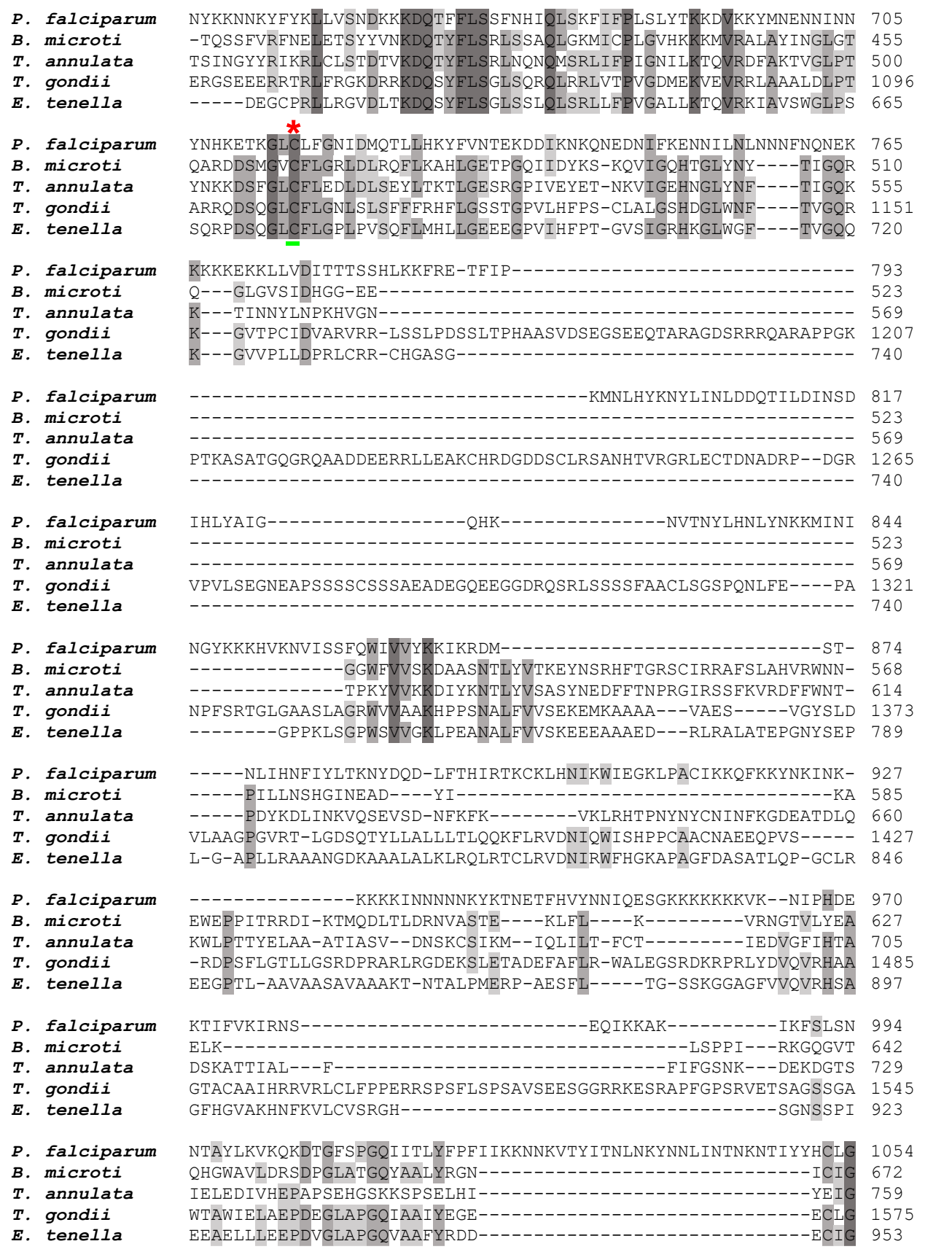
P. falciparum NYKKNNKYFYKLLVSNDKKKDQTFFLSSFNHIQLSKFIFPLSLYTKKDVKKYMNENNINN 705
B. microti -TQSSFVRFNELETSYYVNKDQTYFLSRLSSAQLGKMICPLGVHKKKMVRALAYINGLGT 455
T. annulata TSINGYYRIKRLCLSTDTVKDQTYFLSRLNQNQMSRLIFPIGNILKTQVRDFAKTVGLPT 500
T. gondii ERGSEEERRTRLFRGKDRRKDQSYFLSGLSQRQLRRLVTPVGDMEKVEVRRLAAALDLPT 1096
E. tenella -----DEGCPRLLRGVDLTKDQSYFLSGLSSLQLSRLLFPVGALLKTQVRKIAVSWGLPS 665
P. falciparum YNHKETKGLCLFGNIDMQTLLHKYFVNTEKDDIKNKQNEDNIFKENNILNLNNNFNQNEK 765
B. microti QARDDSMGVCFLGRLDLRQFLKAHLGETPGQIIDYKS-KQVIGQHTGLYNY----TIGQR 510
T. annulata YNKKDSFGLCFLEDLDLSEYLTKTLGESRGPIVEYET-NKVIGEHNGLYNF----TIGQK 555
T. gondii ARRQDSQGLCFLGNLSLSFFFRHFLGSSTGPVLHFPS-CLALGSHDGLWNF----TVGQR 1151
E. tenella SQRPDSQGLCFLGPLPVSQFLMHLLGEEEGPVIHFPT-GVSIGRHKGLWGF----TVGQQ 720
P. falciparum KKKKEKKLLVDITTTSSHLKKFRE-TFIP------------------------------ 793
B. microti Q---GLGVSIDHGG-EE--- 523
T. annulata K---TINNYLNPKHVGN--- 569
T. gondii K---GVTPCIDVARVRR-LSSLPDSSLTPHAASVDSEGSEEQTARAGDSRRRQARAPPGK 1207
E. tenella K---GVVPLLDPRLCRR-CHGASG------------------------------------ 740
P. falciparum ----------------------------------KMNLHYKNYLINLDDQTILDINSD 817
B. microti -- 523
T. annulata -- 569
T. gondii PTKASATGQGRQAADDEERRLLEAKCHRDGDDSCLRSANHTVRGRLECTDNADRP--DGR 1265
E. tenella -- 740
P. falciparum IHLYAIG------------------QHK---------------NVTNYLHNLYNKKMINI 844
B. microti -- 523
T. annulata -- 569
T. gondii VPVLSEGNEAPSSSSCSSSAEADEGQEEGGDRQSRLSSSSFAACLSGSPQNLFE----PA 1321
E. tenella -- 740
P. falciparum NGYKKKHVKNVISSFQWIVVYKKIKRDM----------------------------ST- 874
B. microti --------------GGWFVVSKDAASNTLYVTKEYNSRHFTGRSCIRRAFSLAHVRWNN- 568
T. annulata --------------TPKYVVKKDIYKNTLYVSASYNEDFFTNPRGIRSSFKVRDFFWNT- 614
T. gondii NPFSRTGLGAASLAGRWVVAAKHPPSNALFVVSEKEMKAAAA---VAES-----VGYSLD 1373
E. tenella --------GPPKLSGPWSVVGKLPEANALFVVSKEEEAAAED---RLRALATEPGNYSEP 789
P. falciparum -----NLIHNFIYLTKNYDQD-LFTHIRTKCKLHNIKWIEGKLPACIKKQFKKYNKINK- 927
B. microti -----PILLNSHGINEAD----YI--------------------------------KA 585
T. annulata -----PDYKDLINKVQSEVSD-NFKFK--------VKLRHTPNYNYCNINFKGDEATDLQ 660
T. gondii VLAAGPGVRT-LGDSQTYLLALLLTLQQKFLRVDNIQWISHPPCAACNAEEQPVS----- 1427
E. tenella L-G-APLLRAAANGDKAAALALKLRQLRTCLRVDNIRWFHGKAPAGFDASATLQP-GCLR 846
P. falciparum ---------------KKKKINNNNNKYKTNETFHVYNNIQESGKKKKKKKVK--NIPHDE 970
B. microti EWEPPITRRDI-KTMQDLTLDRNVASTE----KLFL----K---------VRNGTVLYEA 627
T. annulata KWLPTTYELAA-ATIASV--DNSKCSIKM--IQLILT-FCT---------IEDVGFIHTA 705
T. gondii -RDPSFLGTLLGSRDPRARLRGDEKSLETADEFAFLR-WALEGSRDKRPRLYDVQVRHAA 1485
E. tenella EEGPTL-AAVAASAVAAAKT-NTALPMERP-AESFL-----TG-SSKGGAGFVVQVRHSA 897
P. falciparum KTIFVKIRNS-------------------------EQIKKAK----------IKFSLSN 994
B. microti ELK---------------------------------------LSPPI---RKGQGVT 642
T. annulata DSKATTIAL---F-----------------------------FIFGSNK---DEKDGTS 729
T. gondii GTACAAIHRRVRLCLFPPERRSPSFLSPSAVSEESGGRRKESRAPFGPSRVETSAGSSGA 1545
E. tenella GFHGVAKHNFKVLCVSRGH-----------------------------SGNSSPI 923
P. falciparum NTAYLKVKQKDTGFSPGQIITLYFPFIIKKNNKVTYITNLNKYNNLINTNKNTIYYHCLG 1054
B. microti QHGWAVLDRSDPGLATGQYAALYRGN-------------------------ICIG 672
T. annulata IELEDIVHEPAPSEHGSKKSPSELHI-------------------------YEIG 759
T. gondii WTAWIELAEPDEGLAPGQIAAIYEGE-------------------------ECLG 1575
E. tenella EEAELLLEEPDVGLAPGQVAAFYRDD-------------------------ECIG 953

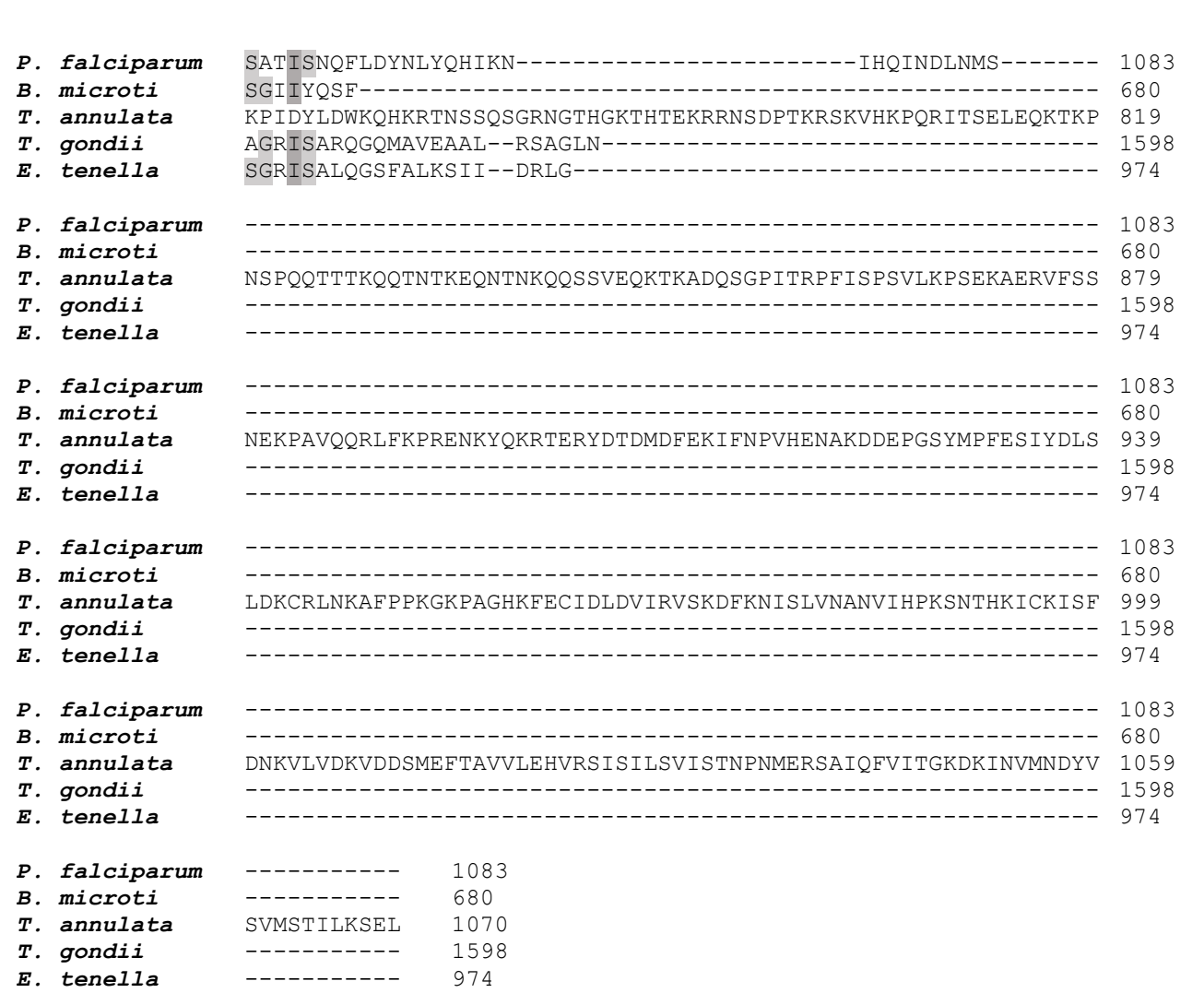

Figure 3- figure supplement 2

A

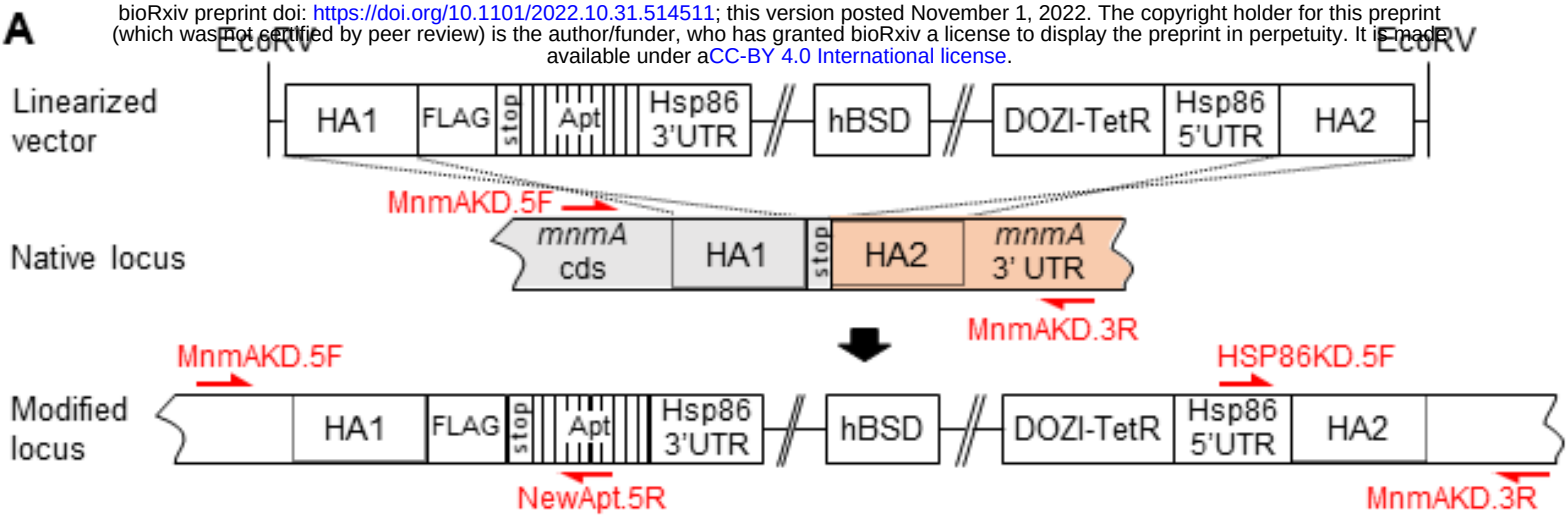

B

PCR reaction	Primer combination		Anticipated amplicon sizes (bp)	Parasite line
	Forward	Reverse		
Δ5'	MnmAKD.5F	NewApt.5R	800	*mnmA*-flag
Δ3'	HSP86KD.5F	MnmAKD.3R	596	
C	MnmAKD.5F	MnmAKD.3R	-	
Δ5'	MnmAKD.5F	NewApt.5R	-	PfMev (parental)
Δ3'	HSP86KD.5F	MnmAKD.3R	-	
C	MnmAKD.5F	MnmAKD.3R	1160	

C

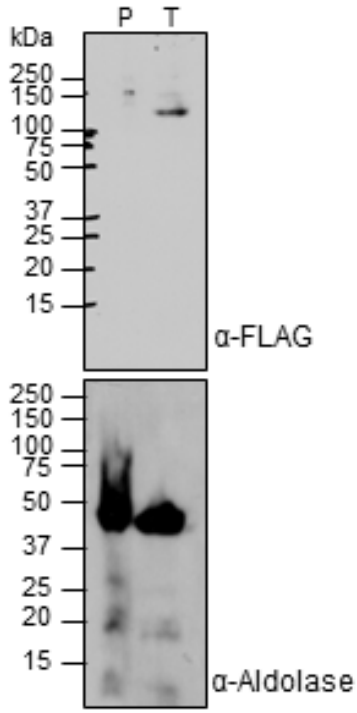

Figure 3- figure supplement 3

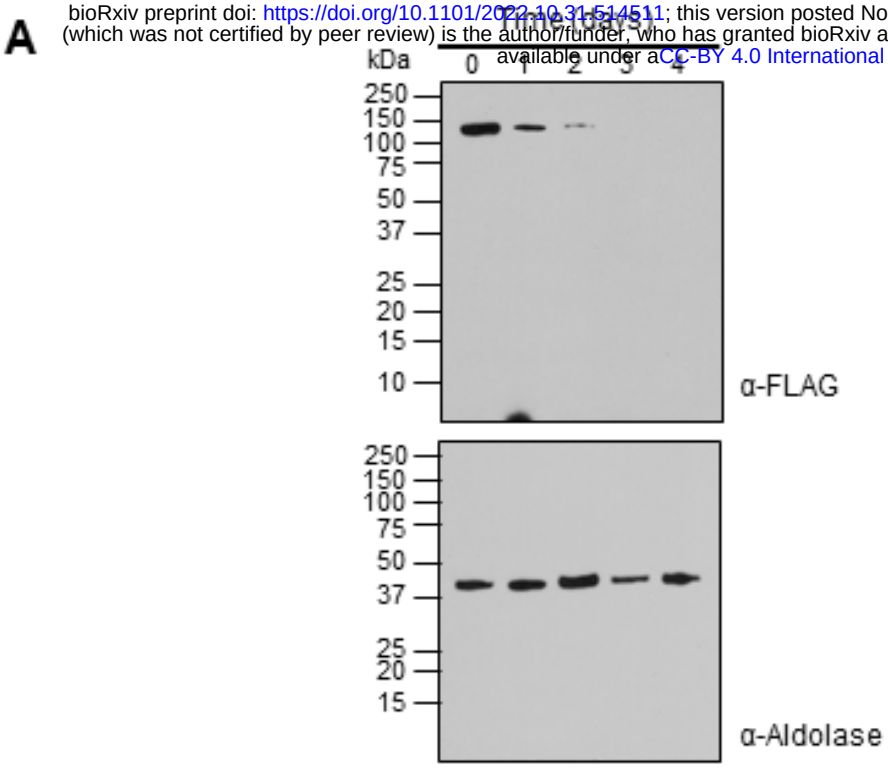

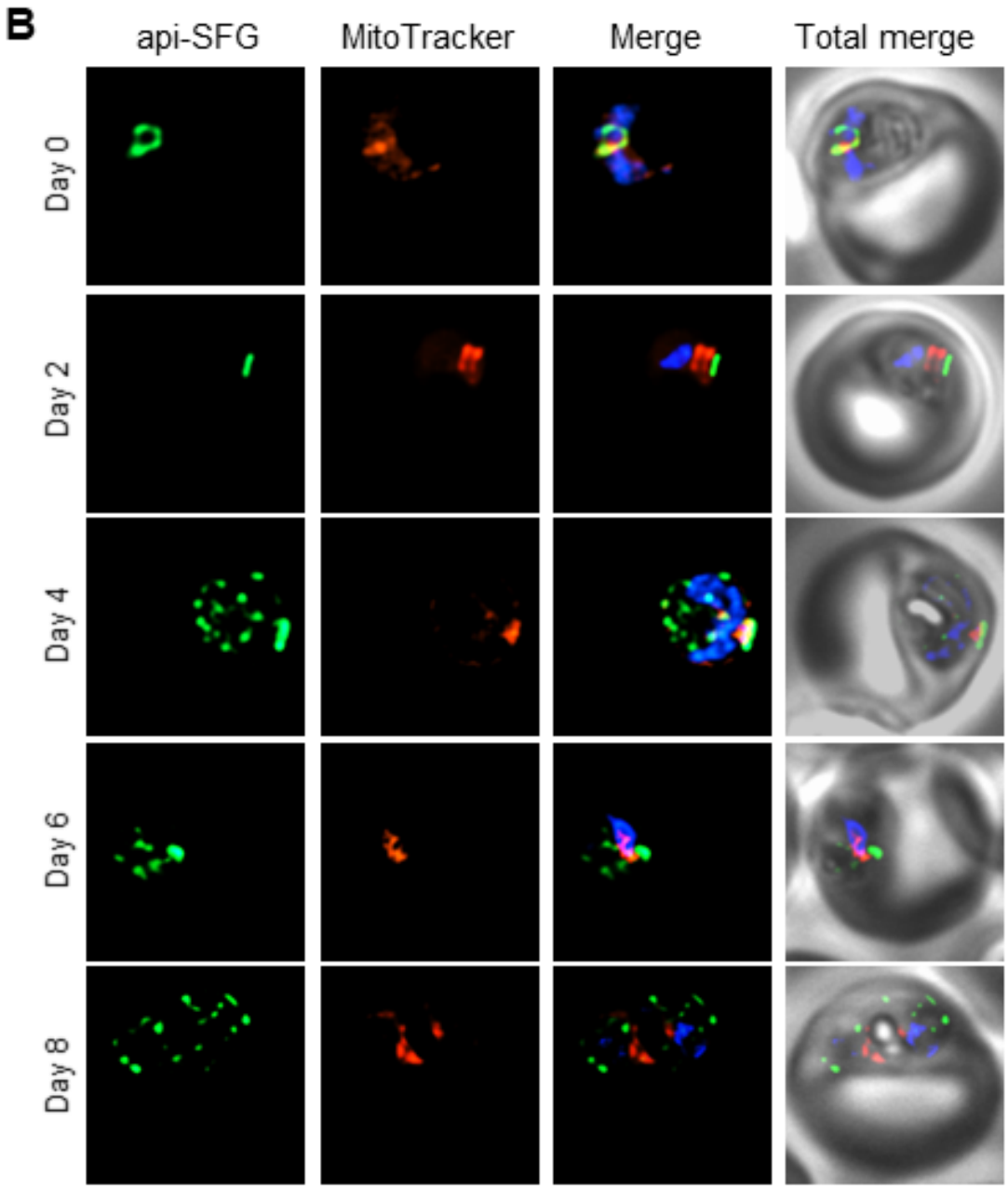

Figure 3-figure supplement 4

A

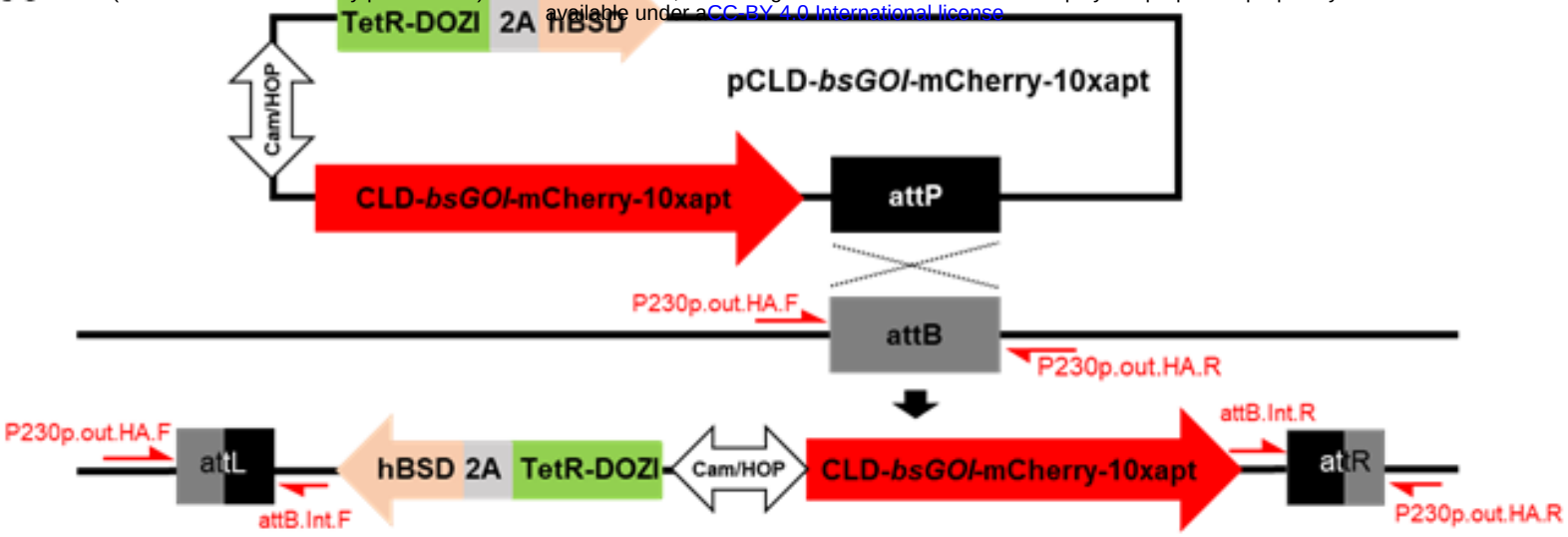

B

PCR reaction	Primer combination		Anticipated amplicon sizes (bp)	Parasite line
	Forward	Reverse		
attL	P230p.out.HA.F	attB.Int.F	642	*bsmnmA*⁺ */bsmnmA-yrvO*⁺
attR	attB.Int.R	P230p.out.HA.R	732	
attB	P230p.out.HA.F	P230p.out.HA.R	-	
attL	P230p.out.HA.F	attB.Int.F	-	PfMev^{attB} (parental)
attR	attB.Int.R	P230p.out.HA.R	-	
attB	P230p.out.HA.F	P230p.out.HA.R	1229	

Figure 4- figure supplement 1

Figure 4- figure supplement 2

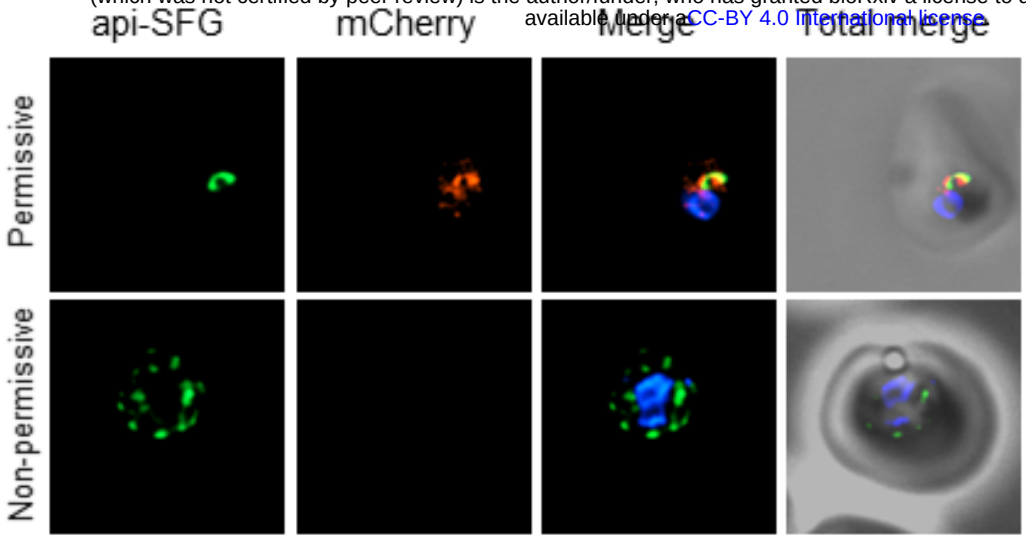

Figure 5- figure supplement 1

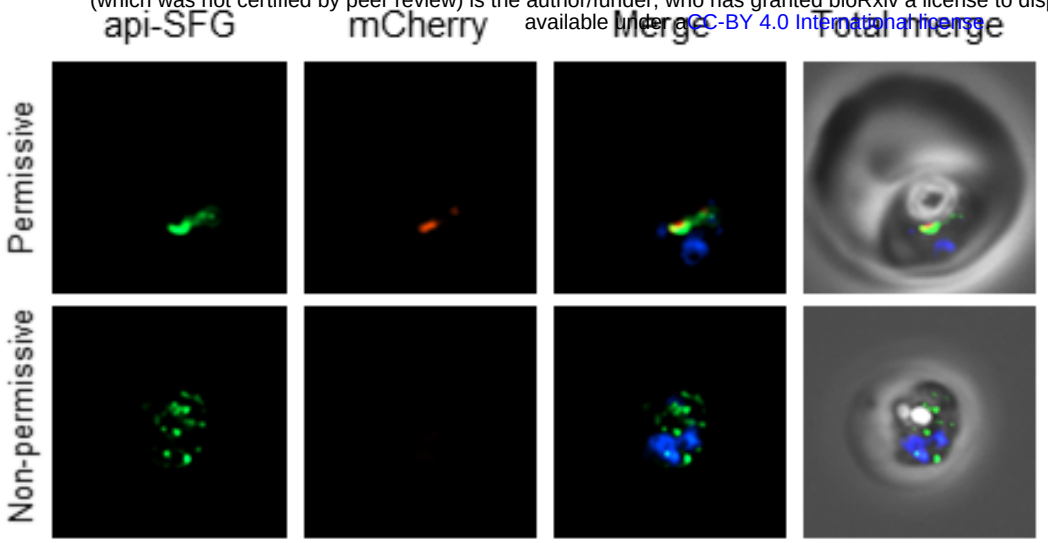

Figure 6- figure supplement 1

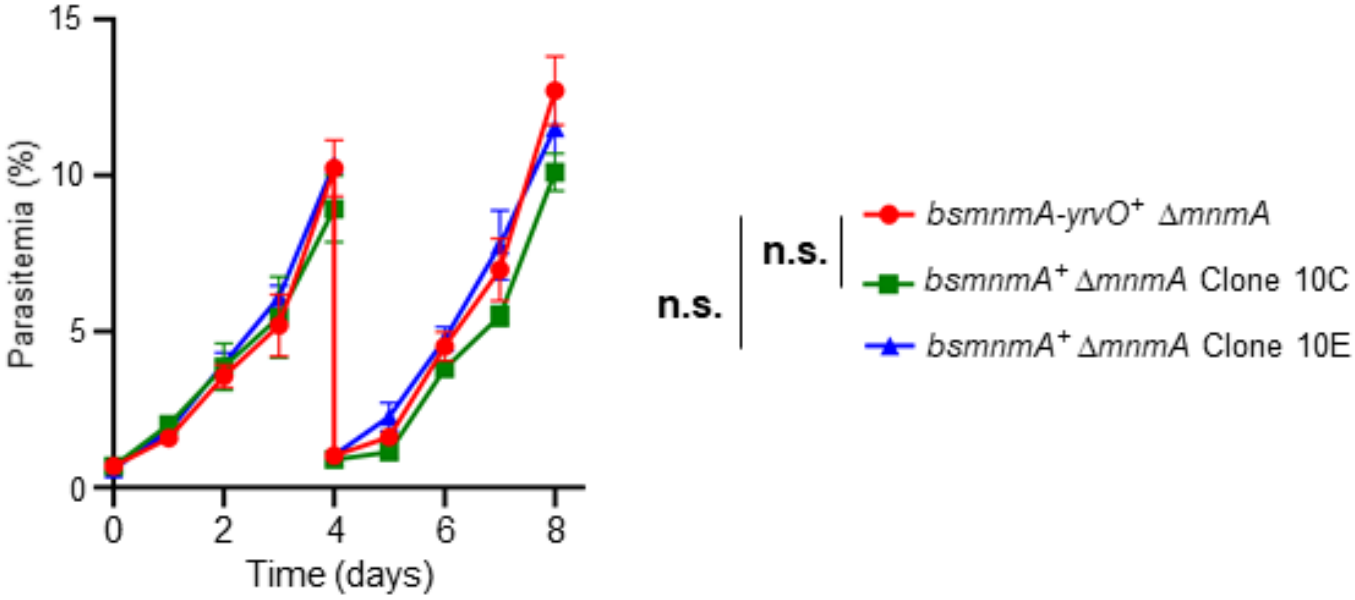

Figure 6- figure supplement 2